الجامعة الأردنيـــــة
كلية الدراسات العليا

التاريـــخ: / /

نموذج رقم (16)
اقرار والتزام بالمعايير الأخلاقية والأمانة العلمية وقوانين الجامعة الأردنية وأنظمتها وتعليماتها لطلبة الدكتوراة

أنا الطالب: رباب فايز عبدالفتاح تيم الرقم الجامعي: (9050289)

تخصص: العلوم الصيدلانية الكليـــــــــة: الصيدلة

عنوان الاطروحة:

DISCOVERY AND OPTIMIZATION OF NEW FRUCTOSE-1,6-BISPHOSPHATASE (FBPASE) INHIBITORS AS POTENTIAL ANTIDIABETIC AGENTS

اعلن بأنني قد التزمت بقوانين الجامعة الأردنية وأنظمتها وتعليماتها وقراراتها السارية المفعول المتعلقة باعداد اطروحات الدكتوراه عندما قمت شخصيا" باعداد اطروحتي وذلك بما ينسجم مع الأمانة العلمية وكافة المعايير الأخلاقية المتعارف عليها في كتابة الأطروحات العلمية. كما أنني أعلن بأن اطروحتي هذه غير منقولة أو مستلة من أطاريح أو كتب أو أبحاث أو أي منشورات علمية تم نشرها أو تخزينها في أي وسيلة اعلامية، وتأسيسا" على ما تقدم فانني أتحمل المسؤولية بأنواعها كافة فيما لو تبين غير ذلك بما فيه حق مجلس العمداء في الجامعة الأردنية بالغاء قرار منحي الدرجة العلمية التي حصلت عليها وسحب شهادة التخرج مني بعد صدورها دون أن يكون لي أي حق في التظلم أو الاعتراض أو الطعن بأي صورة كانت في القرار الصادر عن مجلس العمداء بهذا الصدد.

توقيع الطالب:............................ التاريخ: ٢٨ / ٤ / ٢٠١١

The University of Jordan

Authorization Form

I, Rabab Tayyem , authorize the University of Jordan to supply copies of my Thesis/ Dissertation to libraries or establishments or individuals on request, according to the University of Jordan regulations.

Signature:

Date: 28/04/2011

DISCOVERY AND OPTIMIZATION OF NEW FRUCTOSE-1,6-BISPHOSPHATASE (FBPASE) INHIBITORS AS POTENTIAL ANTIDIABETIC AGENTS

By:
Rabab Fayez Tayyem

Supervisor:
Dr. Mutasem Taha, Prof.

Co-Supervisor:
Dr. Mohammad Mubarak, Prof.

This Thesis was Submitted in Partial Fulfillment of the Requirements for the Doctor of Philosophy Degree in Pharmacy

Faculty of Graduate Studies
The University of Jordan

April, 2011

This Thesis (Discovery and Optimization of new Fructose-1,6-Bisphosphatase (FBPase) Inhibitors as Potential Antidiabetic Agents) was Successfully Defended and Approved on The 14th of April 2011.

Examination Committee	**Signature**
Dr. Mutasem Taha, Chairman Prof. of Medicinal Chemistry	------------------------------
Dr. Mohammad S. Mubarak, Member Prof. of Organic Chemistry	------------------------------
Dr. Imad Hamdan, Member Prof. of Pharmaceutical Analysis	------------------------------
Dr. Yasser Bustanji, Member Associate Prof. Biochemistry	------------------------------
Dr. Mohammad Hudaib, Member Associate Prof. Phytochemistry & Phytochemical Analysis	------------------------------
Dr. Ghassan Abusheikha, External Member Associate Prof. Medicinal Chemistry (Alzaytoonah University)	------------------------------

Dedication

To the pure soul of my Mother

To the merciful heart of my Father

To my beloved Brother and Sisters

Acknowledgements

First and foremost, I would like to express my sincere gratitude to my supervisor, Prof. Mutasem Taha and my co-supervisor Prof. Mohammad Mubarak for their guidance and support.

My deepest thanks are due to every member of the examination committee for their insightful discussion of my thesis work.

I acknowledge the valuable efforts made by Dr. Al Motasem Yousef during some critical times of my work.

I am indepted to Dr. Mohammad Khalil for his encouragement and inspiration.

My special thanks to the staff of Faculty of Pharmacy and Department of Chemisty for their kind assistance and endless cooperation.

To my colleuages in ACDIMA and King Hussein Cancer Center (KHCC), who kept motivating me to move forward.

For all of my friends … without you this would never have been possible.

LIST OF CONTENTS

LIST OF TABLES

LIST OF FIGURES

LIST OF ABBREVIATIONS

3D-QSAR	**three-dimensional quantitative structure activity analysis**
AMP	**Adenosine Monophosphate**
AUC	**Area Under the Curve**
CoMFA	**Comparative Moelcular Fiel Analysis**
CoMSIA	**Comparative Molecualr Similarity Index**
DAC	**Drug agrochemical**
DMSO	**Dimethyl Sulfoxide**
DTT	**Dithiothreitol**
EDTA	**Ethylenediaminetetraacetic acid**
FBPase	**Fructose-1,6-Bisphosphatase**
HBA	**Hydrogen Bond Acceptaor**
HBD	**Hydrogen Bond Donor**
Hbic	**Hydrophobic**
IC	**Inhibitory Concentration**
MS	**Mass spectroscopy**
NADP	**Nicotinamide adenine dinucleotide phosphate**
NCI	**National Cancer Institute**
NIDDM	**Noninsulin-dependent diabetes mellitus**
NMR	**Nuclear Magentic Resonance**
GNG	**Gluconeogenesis**
PDB	**Protein Databank**
RingArom	**Ring Aromatic**
ROC	**Receiver Operating Characteristic**
TLC	**Thin Layer Chrmoatography**
UV	**Ultra Violet**

DISCOVERY AND OPTIMIZATION OF NEW FRUCTOSE-1,6-BISPHOSPHATASE (FBPASE) INHIBITORS AS POTENTIAL ANTIDIABETIC AGENTS

By
Rabab Fayez Tayyem

Supervisor
Dr. Mutasem Taha, Prof.

Co-Supervisor
Dr. Mohammad Mubarak, Prof.

Abstract

Fructose-1,6-Bisphosphatase (FBPase) has been recently implicated in diabetes prompting several attempts to discover and optimize new FBPase inhibitors. Towards this end we explored the pharmacophoric space of 136 FBPase inhibitors using three diverse sets of inhibitors. This identified 520 pharmacophores that were subsequently clustered into 104 groups. Cluster centers were evaluated by receiver operating characteristic (ROC) curves analysis and correlation with bioactivities of collected compounds. Pharmacophore model Hypo1/7 illustrated the best combination of classification power (ROC-AUC) and correlation with bioactivity. Two other pharmacophores (Hypo2/1 and Hypo2/6) were found to be mergeable and their combined model (Hypo2-1/2-6) illustrated excellent ROC performance. We employed Hypo1/7and Hypo2-1/2-6 models to screen the national cancer institute (NCI) list of compounds. *In silico* mining identified 18 FBPase inhibitors out of which six were of sub-micromolar IC_{50} values. The resulting pharmacophores models and active *in silico* hits were used to guide the synthesis of several potent FBPase inhibitors out of which three were of sub-micromolar IC_{50} values.

1. Introduction

Noninsulin-dependent diabetes mellitus (NIDDM), also known as type II diabetes, results from a combination of insulin resistance at the target cells (liver, muscle and fat) and relative deficiency in the insulin production from the β-cells of pancreas (van Poelje *et al.*, 2007). The molecular basis of NIDDM is poorly understood, but whatever the pathogenesis behind this serious condition is, it always manifests itself by hyperglycemia. Hyperglycemia is caused by reduced entry of glucose into various tissues and increased release of glucose into the circulation by hepatic gluconeogenesis (Tsukada *et al.*, 2010). Therefore, reduction of the gluconeogenic rate in NIDDM should provide treatment for NIDDM patients (Iversen *et al.*, 1997).

Glycolysis and gluconeogenesis (GNG) are pathways involved in the degradation and synthesis of intracellular sugars, respectively. Although most enzymes are shared by the two pathways, fructose-6-phosphate kinase catalyzes the unidirectional phosphorylation of fructose 6-phosphate to fructose 1,6-bisphosphate in glycolysis. Fructose-1,6-bisphosphatase (D-fructose 1,6-bisphosphate 1-phosphohydrolase, FBPase) catalyzes the reverse reaction in gluconeogenesis, i.e., the hydrolysis of fructose 1,6-bisphosphate (Fru-1,6-P2) to fructose 6-phosphate (Fru-6-P) and inorganic phosphate (Xie *et al.*, 2010). Therefore FBPase is regarded as one of the key enzymes in gluconeogenesis (Rashid *et al.*, 2002).

FBPase is a homotetramer [subunit Mr = 37,000] with at least two quaternary states referred to as R (active state) and T (less active state). The amino acid sequence of the human liver F1,6BP was determined recently and was found to be approximately 90% identical to the porcine kidney enzyme. Each tetramer subunit has an allosteric AMP domain (residues 1-20) and a catalytic FBPase domain (residues 201-335), with the AMP-

binding site located approximately 28A^{o} away from the substrate binding site. X-ray structures of AMP, as well as AMP analogs, complexed to the allosteric binding pocket of human liver FBPase have been solved [Kurukulasuriya et al., 2003].

The number and nature of the divalent cations required in the human liver enzyme have not yet been fully investigated. One and two Mg^{2+} ions have been found in the human enzyme, and similar observations have also been reported for the porcine enzyme. The allosteric mechanism has also been investigated. The tetramer can be divided into two dimers, an upper dimer (two subunits) and a lower dimmer (two subunits). A 16-17" rotation of the lower dimer relative to the upper dimer has been described for the porcine FBPase upon binding of AMP to the allosteric binding pocket The unrotated form is called the R form and the rotated form is called the T form. The only structure reported of FBPase complexed with an allosteric inhibitor is AMP (porcine and human FBPase enzyme) [Iversen et al., 1997 and Hengming et al., 1990].

The normal function of the FBPase enzyme is to catalyze the hydrolysis of F1,6BP to F6P. This activity is induced by diabetes and starvation and is observed in diabetic rats. The level of FBPase can be normalized by insulin. However, similar information is not available from diabetic patients. FBPase is regulated directly by AMP and fructose-2,6-bisphosphate (F2,6BP), and indirectly by glucagon and insulin via phosphorylation. Inhibition of FBPase by AMP occurs at an allosteric site and is synergistic with F2,6BP inhibition. Hormonal control of F2,6BP synthesis and degradation regulates glycolysis and gluconeogenesis (GNG) through the modulation of fructose-1,6-kinase and F1,6BP [Kurukulasuriya et al., 2003].

Since fructose-l,6-bisphosphatase (FBPase) is the last specific enzyme in the gluconeogenic pathway, thus it plays a key role in the overall regulation of this pathway. FBPase enzyme is regulated (inhibited) by two endogenous ligands: fructose 2,6-bisphosphate and AMP (adenosine monophosphate). It is well established that fructose 2,6-bisphosphate is a competitive inhibitor of the substrate fructose 1,6-bisphosphate. The inhibition of FBPase activity by AMP is at an allosteric site and is synergistic with fructose-2,6-bisphosphate inhibition (Iversen *et al.*, 1997).

The fact that gluconeogenesis is implicated in NIDDM prompted continuous interest to develop new FBPase inhibitors (Tseukada *et al.*, 2010). However, although some FBPase inhibitors have been investigated in animal models, (van Poelje *et al.*, 2005) none were reported to succeed in clinical trials. Accordingly, there still room for the development of new FBPase inhibitors.

The main focus of recent efforts towards the development of new FBPase inhibitors concentrate on structure-based ligand design (Rudnitskaya *et al.*, 2010 and Heng *et al.*, 2010) and high throughput screening, with few ligand-based examples including 3D QSAR (e.g., CoMFA and CoMSIA) (Lan *et al.*, 2010). To date, several human FBPase X-ray complexes are documented in the Protein Data Bank (e.g., PDB codes: 1CNQ, 1D9Q, 1DBZ, 1FJ6, 1FJ9, 1KZ8, 1LBV, 1LBW, 1LBX, 1LBY, 1LBZ, 1LEV, 1Q9D, 1YXI, 1YYZ, 1YZ0, 2F3D, 2F3H, 2FHY, 2FIE with resolution range: 1.50 to 3.5 Å). However, although considered the most reliable structural information that can be used for drug design, crystallographic structures are limited by inadequate resolution (Beeley *et al.*, 2003) and crystallization-related artifacts of the ligand–protein complex (Klebe *et al*, 2006, Steuber *et al.*, 2006 and Stubbs *et al.,* 2002). Moreover, crystallographic structures

generally ignore structural heterogeneity related to protein anisotropic motion and discrete conformational substrates (DePristo *et al.*, 2004).

The continued interest in designing new FBPase inhibitors and lack of adequate ligand-based computer-aided drug discovery efforts combined with the drawbacks of structure-based design prompted us to explore the possibility of developing ligand-based three-dimensional (3D) pharmacophore (s). This approach avoids the pitfalls of structure-based techniques because it only focuses on common features among known ligands; furthermore, the pharmacophore model(s) can be used as 3D search queries to discover new FBPase inhibitory scaffolds.

We employed the HYPOGEN module from the CATALYST software package (Catalyst user manual, 2005) to construct plausible binding hypotheses for a diverse list of FBPase inhibitors (Wright *et al.,* 2001, Wright *et al.*, 2002 and Wright *et al*., 2003). Subsequently, pharmacophore models illustrated the best combination of classification power (ROC-AUC) and correlation with bioactivity. The optimal pharmacophores were subsequently used as 3D search queries to screen the national cancer institute (NCI) list of compounds and our *in-house* built structural database of established drugs and agrochemicals (DAC) for new FBPase inhibitory leads.

CATALYST models drug-receptor interaction using information derived only from the ligand structure. HYPOGEN identifies a 3D array of a maximum of five chemical features common to active training molecules, which provides a relative alignment for each input molecule consistent with their binding to a proposed common receptor site. The chemical features considered can be hydrogen bond donors and acceptors (HBDs and HBAs), aliphatic and aromatic hydrophobes (Hbic) and aromatic planes (RingArom). The

conformational flexibility of training ligands is modeled by creating multiple conformers, judiciously prepared to emphasize representative coverage over a specified energy range. CATALYST pharmacophores have been used as 3D queries for database searching (Van Drie *et al.*, 2003 and Poptodorov *et al.*, 2006).

2. Experimental

2.1. Molecular Modeling

2.1.1 Software and Hardware

The following software packages were utilized in the present research.

- CATALYST (Version 4.11), Accelrys Inc. (www.accelrys.com), USA.
- CERIUS2 (Version 4.10), Accelrys Inc. (www.accelrys.com), USA.
- CS ChemDraw Ultra 6.0, Cambridge Soft Corp. (http:// www.cambridgesoft.Com), USA.
- Discovery Studio 2.5, Accelrys Inc. (www.accelrys.com), USA.

Pharmacophore and QSAR modeling studies were performed using CATALYST (HYPOGEN module) and CERIUS2 software suites from Accelrys Inc. (San Diego, California, www.accelrys.com) installed on a Silicon Graphics Octane2 desktop workstation equipped with a dual 600 MHz MIPS R14000 processor (1.0 GB RAM) running the Irix 6.5 operating system. Structure drawing was performed employing ChemDraw Ultra 6.0 which was installed on a Pentium 4 PC.

2.1.2 Data Set

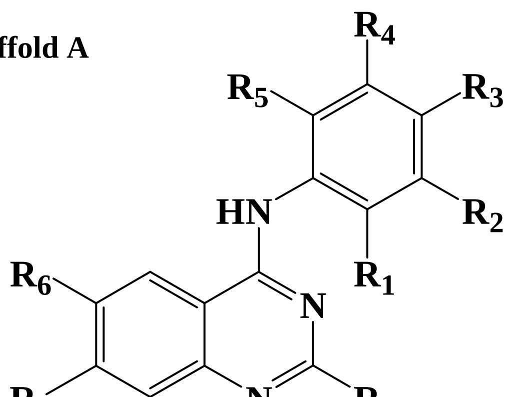
The structures of 136 FBPase inhibitors (**1-136**, Table1) were collected from recently published literature (Wright *et al.,* 2001, Wright *et al.*, 2002 and Wright *et al.*, 2003). Although the *in vitro* bioactivities of the collected inhibitors were gathered from three separate articles they were determined employing the same bioassay methodologies. The bioactivities were expressed as the concentrations of the test compounds that inhibited the

activity of FBPase by 50% (IC_{50}). The logarithm of measured IC_{50} (μM) values were used in the three-dimensional quantitative structure activity analysis (3D-QSAR), thus correlating the data linear to the free energy change.

In cases where the IC_{50} values of some compounds were expressed as being higher than 10 μM, we assumed that their IC_{50} values to be equal to 700 μM (4 logarithmic cycles away from the most potent inhibitor (i.e., **97**). These assumptions are necessary to allow pharmacophore modeling, statistical correlation. The logarithmic transformation of IC_{50} values should minimize any potential errors resulting from such assumptions.

The two-dimensional (2D) chemical structures of the inhibitors were sketched using ChemDraw Ultra and saved in MDL-molfile format. Subsequently, they were imported into CATALYST, converted into corresponding standard 3D structures and energy minimized to the closest local minimum using the molecular mechanics CHARMm force field implemented in CATALYST. The resulting 3D structures were utilized as starting conformers for CATALYST conformational analysis (Catalyst User Manual, 2005).

Scaffold A



Scaffold B

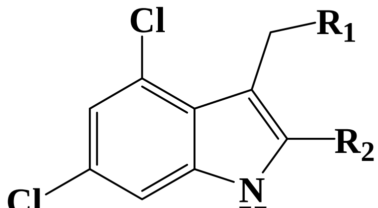


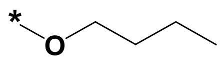
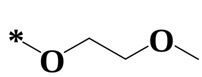
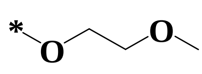
Figure 1: The chemical scaffolds of training compounds, the detailed structures are as in table 1.

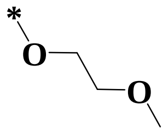
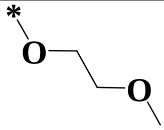
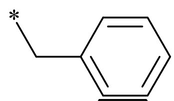
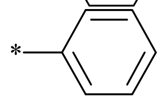
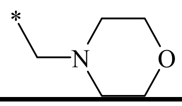
Scaffold A: substituted 4-aminoquinazoline derivatives **(1-102)**

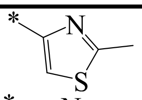
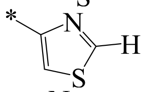
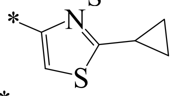
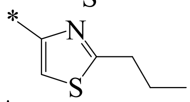
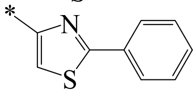
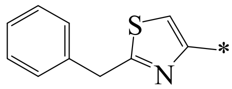
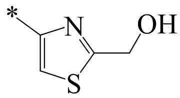
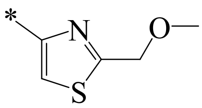
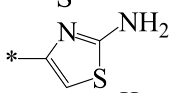
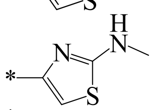
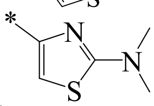
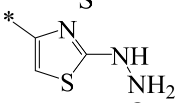
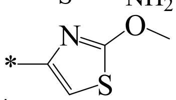
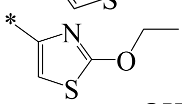
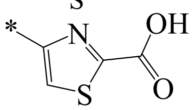
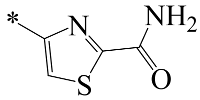
Scaffold B: substituted indole derivatives **(103-136)**

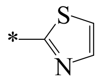
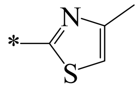
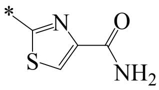
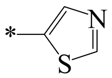
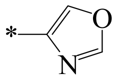
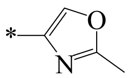
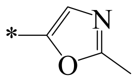
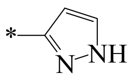
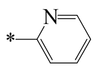
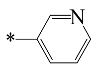
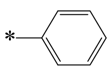
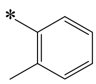
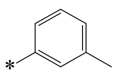
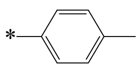
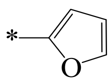
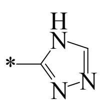
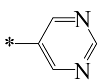
Table 1: Ligands used to build training Set

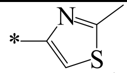
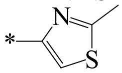
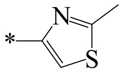
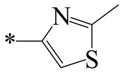
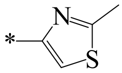
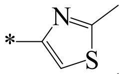
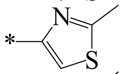
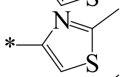
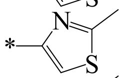
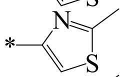
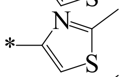
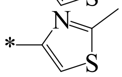
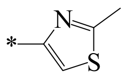
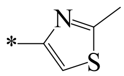
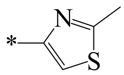
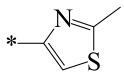
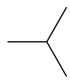
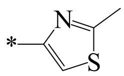
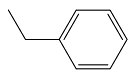
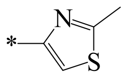
Cpd	R_1	R_2	R_3	R_4	R_5	R_6	R_7	R_8	IC_{50} (μM)
1	H	H	H	Cl	H	$-OCH_2CH_3$	$-OCH_2CH_3$	H	1.6
2	H	H	H	F	H	$-OCH_2CH_3$	$-OCH_2CH_3$	H	9.2
3	H	H	H	Br	H	$-OCH_2CH_3$	$-OCH_2CH_3$	H	1.7
4	H	H	H	I	H	$-OCH_2CH_3$	$-OCH_2CH_3$	H	2.1
5	H	H	H	C≡CH	H	$-OCH_2CH_3$	$-OCH_2CH_3$	H	2.4
6	H	H	H	CN	H	$-OCH_2CH_3$	$-OCH_2CH_3$	H	>10
7	H	H	H	H	H	$-OCH_2CH_3$	$-OCH_2CH_3$	H	>10
8	H	H	F	Cl	H	$-OCH_2CH_3$	$-OCH_2CH_3$	H	0.53

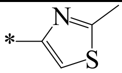
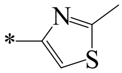
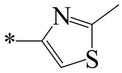
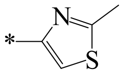
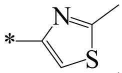
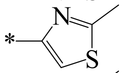
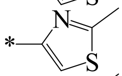
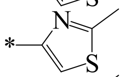
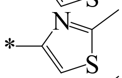
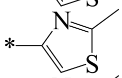
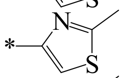
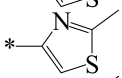
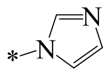
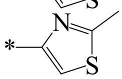
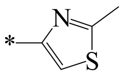
Cpd.	R_1	R_2	R_3	R_4	R_5	R_6	R_7	R_8	IC_{50} (µM)
9	H	$-CH_3$	Cl	H	H	$-OCH_2CH_3$	$-OCH_2CH_3$	H	>10
10	H	Cl	Cl	H	H	$-OCH_2CH_3$	$-OCH_2CH_3$	H	>10
11	H	Cl	H	H	H	$-OCH_3$	$-OCH_3$	H	1.3
12	H	Br	H	H	H	$-OCH_3$	$-OCH_3$	H	1.0
13	H	Br	H	H	H	$-OCH(CH_3)_2$	H	H	>10
14	H	Br	H	H	H		H	H	>10
15	H	Br	H	H	H		H	H	2.9
16	H	Br	H	H	H		$-OCH_3$	H	5.5

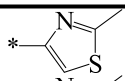
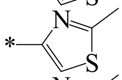
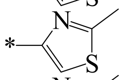
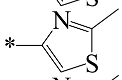
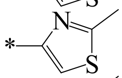
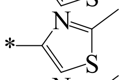
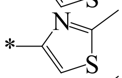
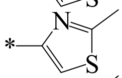
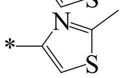
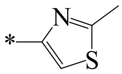
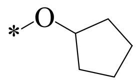
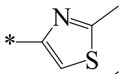
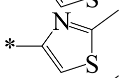
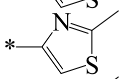
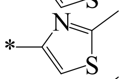
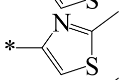
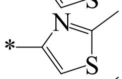
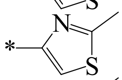
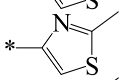
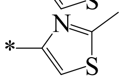
Cpd.	R_1	R_2	R_3	R_4	R_5	R_6	R_7	R_8	IC_{50} (μM)
17	H	Br	H	H	H			H	>10
18	H	-C≡CH	H	H	H	$-OCH_3$	$-OCH_3$	H	0.90
19	H	Br	H	H	H	$-NH_2$	Cl	H	>10
20	H	Br	H	H	H	H	$-CO_2H$	H	>10
21	H	Br	H	H	H	NO_2	Cl	H	>10
22	H	Br	H	H	H	NO_2	H_3CCH_2O-	H	3.6
23	H	Br	H	H	H	NO_2	$-OCH_3$	H	>10
24	H	Br	H	H	H	$-OCH_3$	$-OCH_3$	$-CH_3$	4.5
25	H	Br	H	H	H	$-OCH_3$	$-OCH_3$	$-N(CH_2CH_3)_2$	>10
26	H	Br	H	H	H	$-OCH_2CH_3$	$-OCH_2CH_3$		>10
27	H	Br	H	H	H	$-OCH_2CH_3$	$-OCH_2CH_3$		>10
28	H	Br	H	H	H	$-OCH_2CH_3$	$-OCH_2CH_3$	$-CH_2CH_3CHCH_3$	>10
29	H	Br	H	H	H	$-OCH_2CH_3$	$-OCH_2CH_3$	$-CH_2Cl$	>10
30	H	Br	H	H	H	$-OCH_2CH_3$	$-OCH_2CH_3$	$-CH_2SO_2CH_3$	>10
31	H	Br	H	H	H	$-OCH_2CH_3$	$-OCH_2CH_3$	$-CH_2N(CH_2CH_3)_2$	>10
32	H	Br	H	H	H	$-OCH_2CH_3$	$-OCH_2CH_3$		>10

Cpd	**R_1**	**R_2**	**R_3**	**R_4**	**R_5**	**R_6**	**R_7**	**R_8**	**IC_{50} (μM)**
33	H		H	H	H	$-OCH_2CH_3$	$-OCH_2CH_3$	H	0.64
34	H		H	H	H	$-OCH_2CH_3$	$-OCH_2CH_3$	H	0.39
35	H		H	H	H	$-OCH_2CH_3$	$-OCH_2CH_3$	H	0.83
36	H		H	H	H	$-OCH_2CH_3$	$-OCH_2CH_3$	H	>10
37	H		H	H	H	$-OCH_2CH_3$	$-OCH_2CH_3$	H	>10
38	H		H	H	H	$-OCH_2CH_3$	$-OCH_2CH_3$	H	>10
39	H		H	H	H	$-OCH_2CH_3$	$-OCH_2CH_3$	H	0.83
40	H		H	H	H	$-OCH_2CH_3$	$-OCH_2CH_3$	H	7.3
41	H		H	H	H	$-OCH_2CH_3$	$-OCH_2CH_3$	H	3.5
42	H		H	H	H	$-OCH_2CH_3$	$-OCH_2CH_3$	H	0.80
43	H		H	H	H	$-OCH_2CH_3$	$-OCH_2CH_3$	H	8.0
44	H		H	H	H	$-OCH_2CH_3$	$-OCH_2CH_3$	H	4.5
45	H		H	H	H	$-OCH_2CH_3$	$-OCH_2CH_3$	H	0.78
46	H		H	H	H	$-OCH_2CH_3$	$-OCH_2CH_3$	H	6.1
47	H		H	H	H	$-OCH_2CH_3$	$-OCH_2CH_3$	H	>10
48	H		H	H	H	$-OCH_2CH_3$	$-OCH_2CH_3$	H	0.93

Cpd.	R_1	R_2	R_3	R_4	R_5	R_6	R_7	R_8	IC_{50} (μM)
49	H		H	H	H	$-OCH_2CH_3$	$-OCH_2CH_3$	H	0.38
50	H		H	H	H	$-OCH_2CH_3$	$-OCH_2CH_3$	H	0.65
51	H		H	H	H	$-OCH_2CH_3$	$-OCH_2CH_3$	H	0.83
52	H		H	H	H	$-OCH_2CH_3$	$-OCH_2CH_3$	H	0.98
53	H		H	H	H	$-OCH_2CH_3$	$-OCH_2CH_3$	H	3.6
54	H		H	H	H	$-OCH_2CH_3$	$-OCH_2CH_3$	H	0.5
55	H		H	H	H	$-OCH_2CH_3$	$-OCH_2CH_3$	H	4.0
56	H		H	H	H	$-OCH_2CH_3$	$-OCH_2CH_3$	H	0.73
57	H		H	H	H	$-OCH_2CH_3$	$-OCH_2CH_3$	H	0.39
58	H		H	H	H	$-OCH_2CH_3$	$-OCH_2CH_3$	H	1.4
59	H		H	H	H	$-OCH_2CH_3$	$-OCH_2CH_3$	H	>10
60	H		H	H	H	$-OCH_2CH_3$	$-OCH_2CH_3$	H	>10
61	H		H	H	H	$-OCH_2CH_3$	$-OCH_2CH_3$	H	>10
62	H		H	H	H	$-OCH_2CH_3$	$-OCH_2CH_3$	H	>10
63	H		H	H	H	$-OCH_2CH_3$	$-OCH_2CH_3$	H	1.4
64	H		H	H	H	$-OCH_2CH_3$	$-OCH_2CH_3$	H	0.64
65	H		H	H	H	$-OCH_2CH_3$	$-OCH_2CH_3$	H	1.2

Cpd.	**R_1**	**R_2**	**R_3**	**R_4**	**R_5**	**R_6**	**R_7**	**R_8**	**IC_{50} (µM)**
66	H		H	CF_3	H	$-OCH_2CH_3$	$-OCH_2CH_3$	H	>10
67	H		F	H	H	$-OCH_2CH_3$	$-OCH_2CH_3$	H	0.61
68	H		Cl	H	H	$-OCH_2CH_3$	$-OCH_2CH_3$	H	5.3
69	H		H	H	F	$-OCH_2CH_3$	$-OCH_2CH_3$	H	0.48
70	H		H	H	Cl	$-OCH_2CH_3$	$-OCH_2CH_3$	H	1.7
71	H		F	H	F	$-OCH_2CH_3$	$-OCH_2CH_3$	H	>10
72	H		H	H	$-CH_3$	$-OCH_2CH_3$	$-OCH_2CH_3$	H	1.8
73	H		H	H	$-OCH_3$	$-OCH_2CH_3$	$-OCH_2CH_3$	H	0.99
74	H		H	H	$-OCH_2CH_3$	$-OCH_2CH_3$	$-OCH_2CH_3$	H	1.8
75	H		H	H	Br	$-OCH_2CH_3$	$-OCH_2CH_3$	H	>10
76	H		H	H	$-CH_2CH_3$	$-OCH_2CH_3$	$-OCH_2CH_3$	H	2.1
77	F		F	H	H	$-OCH_2CH_3$	$-OCH_2CH_3$	H	>10
78	H		H	H	H	$-OCH_2CH_3$	$-OCH_2CH_3$	$-CH_3$	1.0
79	H		H	H	H	$-OCH_2CH_3$	$-OCH_2CH_3$	$-CH_2CH_3$	1.5
80	H		H	H	H	$-OCH_2CH_3$	$-OCH_2CH_3$	$-CH_2CH_2CH_3$	1.4
81	H		H	H	H	$-OCH_2CH_3$	$-OCH_2CH_3$		5.0
82	H		H	H	H	$-OCH_2CH_3$	$-OCH_2CH_3$		>10
83	H		H	H	H	$-OCH_2CH_3$	$-OCH_2CH_3$	Cl	2.6

Cpd.	R_1	R_2	R_3	R_4	R_5	R_6	R_7	R_8	IC_{50} (μM)
84	H		H	H	H	$-OCH_2CH_3$	$-OCH_2CH_3$	$-CH_2Cl$	0.87
85	H		H	H	H	$-OCH_2CH_3$	$-OCH_2CH_3$	$-(CH_2)_2Cl$	1.0
86	H		H	H	H	$-OCH_2CH_3$	$-OCH_2CH_3$	$-(CH_2)_3Cl$	4.1
87	H		H	H	H	$-OCH_2CH_3$	$-OCH_2CH_3$	CF_3	>10
88	H	H	H	Br	H	$-OCH_2CH_3$	$-OCH_2CH_3$	$-CH_2Cl$	>10
89	H		H	H	H	$-OCH_2CH_3$	$-OCH_2CH_3$	$-CH_2OCH_3$	1.4
90	H		H	H	H	$-OCH_2CH_3$	$-OCH_2CH_3$	$-CH_2NH_2$	1.5
91	H		H	H	H	$-OCH_2CH_3$	$-OCH_2CH_3$	$-CH_2N(CH_3)_2$	2.0
92	H		H	H	H	$-OCH_2CH_3$	$-OCH_2CH_3$	$-CH_2NHCH_2CH_3$	6.0
93	H		H	H	H	$-OCH_2CH_3$	$-OCH_2CH_3$	$-CH_2N(CH_2)_4$	6.1
94	H		H	H	H	$-OCH_2CH_3$	$-OCH_2CH_3$	$-CH_2CH(CH_3)_2$	1.7
95	H		H	H	H	$-OCH_2CH_3$	$-OCH_2CH_3$	$-CH_2CO_2H$	0.96
96	H		H	H	H	$-OCH_2CH_3$	$-OCH_2CH_3$		0.77
97	H		H	H	H	$-OCH_2CH_3$	$-OCH_2CH_3$	$-CH_2CH_2NH_2$	0.22
98	H	$COCH_3$	H	H	H	$-OCH_2CH_3$	$-OCH_2CH_3$	H	>10
99	H	$COCH_2Br$	H	H	H	$-OCH_2CH_3$	$-OCH_2CH_3$	H	>10
100	H		H	H	H	$-OCH_2CH_3$	$-OCH_2CH_3$	$-CH_2SO_2CH_3$	2.1
101	H	H	H	Br	H	$-OCH_2CH_3$	$-OCH_2CH_3$	$-CH_2SO_2CH_3$	>10
102	H	H	H	Br	H	$-OCH_2CH_3$	$-OCH_2CH_3$	$-CH_2CH(CH_3)_2$	>10

Cpd.	R_1	R_2	R_3	R_4	R_5	R_6	R_7	R_8	IC_{50} (μM)
103	H		H	H	H	H	H	H	>10
104	H		H	H	H	$-OCH_3$	$-OCH_3$	H	4.4
105	H		H	H	H	$-OCH_3$	$-OCH_2CH_3$	H	3.4
106	H		H	H	H	$-OCH_3$	$-OCH_2CH_2CH_3$	H	5.6
107	H		H	H	H	$-OCH_3$	$-OCH_2(CH_3)_2$	H	2.3
108	H		H	H	H	$-OCH_3$	$-OCH_2CH_2CH_3$	H	>10
109	H		H	H	H	$-OCH_3$	$-OCH(CH_3)_3$	H	1.3
110	H		H	H	H	$-OCH_3$	$-OCHCH_3CH_2CH_3$	H	>10
111	H		H	H	H	$-OCH_3$	$-OCH_2CH_2OCH_3$	H	>10
112	H		H	H	H	$-OCH_3$		H	>10
113	H		H	H	H	$-OCH_2CH_3$	$-OCH_3$	H	1.2
114	H		H	H	H	$-OCH_2(CH_3)_2$	$-OCH_3$	H	>10
115	H		H	H	H	$-OCH_2CH_2CH_3$	$-OCH_3$	H	>10
116	H		H	H	H	$-OCH_2CH_2OCH_3$	$-OCH_3$	H	>10
117	H		H	H	H	$-OCH_2CH_3$	$-OCH_2CH_2CH_3$	H	1.0
118	H		H	H	H	$-OCH_2CH_3$	$-OCH_2(CH_3)_2$	H	0.42
119	H		H	H	H	$-OCH_2CH_3$	$-OCH_2CH_3$	H	>10
120	H		H	H	H	$-OCH_2CH_2O$		H	>10
121	H		H	H	H	CH=CH-CH=CH		H	>10

Cpd.	R_1	R_2	IC_{50} (μM)
122	$-CH_2CO_2H$	$-CO_2H$	2.5
123	$-CH_2CONH_2$	$-CO_2H$	2.2
124	$-CH_2CON(CH_3)_2$	$-CO_2H$	1.7
125	$-CH_2CONHOH$	$-CO_2H$	1.5
126	$-CH_2CO_2CH_3$	$-CO_2H$	7.0
127	$-CH_2CH_2OH$	$-CO_2H$	2.7
128	$-CH_2CO_2H$	$-CONH_2$	>10
129	$-CH_2CO_2H$	$-CON(CH_3)_2$	>10
130	$-CH_2CO_2H$	$-CONHOH$	>10
131	$-CH_2CO_2H$	$-CO_2CH_2CH_3$	>10
132	$-CH_2CO_2H$	$-CH_2OH$	>10
133	$-CH_2CO_2H$	$-CO_2H$	>10
134	$-CO_2H$	$-CO_2H$	>10
135	$-(CH_2)_2CO_2H$	$-CO_2H$	1.0
136	$-(CH_2)_3CO_2H$	$-CO_2H$	1.2

2.1.3 Conformational Analysis

The molecular flexibilities of the collected compounds were taken into account by considering each compound as a collection of conformers representing different areas of the conformational space accessible to the molecule within a given energy range. Accordingly, the conformational space of each inhibitor (**1-136**, Figure 1 and Table 1) was explored adopting the “best conformer generation” option within CATALYST (Catalyst User

Manual, 2005) based on the generalized CHARMm force field implemented in the program. Default parameters were employed in the conformation generation procedure of training compounds and screened libraries (NCI and DAC), i.e., a conformational ensemble was generated with an energy threshold of 20 kcal/mol from the local minimized structure at which has the lowest energy level and a maximum limit of 250 conformers per molecule (Catalyst User Manual, 2005).

2.1.4 Pharmacophoric Hypotheses Generation

All 136 molecules with their associated conformational models were regrouped into a spreadsheet The biological data of the inhibitors were reported with an "Uncertainty" value of 3, which means that the actual bioactivity of a particular inhibitor is assumed to be situated somewhere in an interval ranging from one-third to three-times the reported bioactivity value of that inhibitor (Fischer, 1966 and Sutter *et al.*, 2000). Subsequently, three structurally diverse training subsets: sets **I**, **II** and **III** in Table 2, respectively were carefully selected from the collection for pharmacophore modeling. Typically, CATALYST requires informative training sets that include at least 16 compounds of evenly spread bioactivities over at least three and a half logarithmic cycles. Lesser training lists could lead to chance correlation and thus faulty models.

Table 2: Training subsets employed in exploring the pharmacophoric space of FBPase inhibitors.

Subsets	Most active[a]	Moderate active	Least active[b]
I	**1**, **78**, **94**, **95**, **96**, **124**, **135**, **136**	**2**, **85**, **91**, **90**, **122**, **123**, **126**	**13**, **14**, **20**, **134**
II	**42**, **49**, **52**, **56**, **57**, **63**, **69**, **96**	**2**, **4**, **5**, **123**	**13**, **131**, **132**, **128**
III	**3**, **8**, **18**, **11**, **12**	**2**, **43**, **55**, **87**, **92**	**13**, **36**, **37**, **61**, **119**, **133**

[a,b]Potency categories as defined by equations (A) and (B).

The selected training sets were utilized to conduct 52 modeling runs to explore the pharmacophoric space of FBPase inhibitors (Table 3). The exploration process included altering interfeature spacing parameter (100 and 300 picometers) and the maximum number of allowed features in the resulting pharmacophore hypotheses, i.e., they were allowed to vary from 4 to 5 for first and second runs and from 5 to 5 for third and fourth runs of each training set, as shown in Table 3.

Pharmacophore modeling employing CATALYST proceeds through three successive phases: the constructive phase, subtractive phase and optimization phase (see CATALYST Modeling Algorithm) (Kurogi *et al*., 2001 and Catalyst User Manual, 2005).

Table 3: Training sets and CATALYST run parameters employed for exploring FBPase pharmacophoric space

Run Number	Training set[a]	Number of compounds	Selected features[b]	Max-Min Features[c]	Spacing[d]
1		19	HBA (2-4), HBD (0-2), HBic (1-3), RingArom (0-1)	4-5	100
2		19	HBA (2-4), HBD (0-2), HBic (1-3), RingArom (0-1)	4-5	300
3		19	HBA (2-4), HBD (0-2), HBic (1-3), RingArom (0-1)	5-5	100
4		19	HBA (2-4), HBD (0-2), HBic (1-3), RingArom (0-1)	5-5	300
5		19	HBA (1-4), HBD (0-2), HBic (1-3), RingArom (0-1)	4-5	100
6		19	HBA (1-4), HBD (0-2), HBic (1-3), RingArom (0-1)	4-5	300
7		19	HBA (1-4), HBD (0-2), HBic (1-3), RingArom (0-1)	5-5	100
8		19	HBA (1-4), HBD (0-2), HBic (1-3), RingArom (0-1)	5-5	300
9		19	HBA(2-2), HBic (1-3), RingArom (0-1)	5-5	100
10		19	HBA(2-2), HBic (1-3), RingArom (0-1)	5-5	300
11	**I**	19	HBA (2-4), HBD (0-2), HBic (1-3), RingArom (0-1), ExVol (0-10)	4-5	100
12		19	HBA (2-4), HBD (0-2), HBic (1-3), RingArom (0-1), ExVol (0-10)	4-5	300
13		19	HBA (2-4), HBD (0-2), HBic (1-3), RingArom (0-1), ExVol (0-10)	5-5	100
14		19	HBA (2-4), HBD (0-2), HBic (1-3), RingArom (0-1), ExVol (0-10)	5-5	300
15		19	HBA (1-4), HBD (0-2), HBic (1-3), RingArom (0-1), ExVol (0-10)	4-5	100
16		19	HBA (1-4), HBD (0-2), HBic (1-3), RingArom (0-1), ExVol (0-10)	4-5	300
17		19	HBA (1-4), HBD (0-2), HBic (1-3), RingArom (0-1), ExVol (0-10)	5-5	100
18		19	HBA (1-4), HBD (0-2), HBic (1-3), RingArom (0-1), ExVol (0-10)	5-5	300
19		19	HBA(2-2), HBic (1-3), RingArom (0-1), ExVol (0-10)	5-5	100
20		19	HBA(2-2), HBic (1-3), RingArom (0-1), ExVol (0-10)	5-5	300
21		16	HBA (2-4), HBD (0-2), HBic (1-3), RingArom (0-1)	5-5	100
22		16	HBA (2-4), HBD (0-2), HBic (1-3), RingArom (0-1)	5-5	300
23		16	HBA (2-4), HBD (0-2), HBic (1-3), RingArom (0-1)	4-5	100
24		16	HBA (2-4), HBD (0-2), HBic (1-3), RingArom (0-1)	4-5	300
25		16	HBA (1-4), HBD (0-2), HBic (1-3), RingArom (0-1)	5-5	100
26		16	HBA (1-4), HBD (0-2), HBic (1-3), RingArom (0-1)	5-5	300
27	**II**	16	HBA (1-4), HBD (0-2), HBic (1-3), RingArom (0-1)	4-5	100
28		16	HBA (1-4), HBD (0-2), HBic (1-3), RingArom (0-1)	4-5	300
29		16	HBA (2-4), HBD (0-2), HBic (1-3), RingArom (0-1), ExVol (0-10)	5-5	100
30		16	HBA (2-4), HBD (0-2), HBic (1-3), RingArom (0-1), ExVol (0-10)	5-5	300
31		16	HBA (2-4), HBD (0-2), HBic (1-3), RingArom (0-1), ExVol (0-10)	4-5	100
32		16	HBA (2-4), HBD (0-2), HBic (1-3), RingArom (0-1), ExVol (0-10)	4-5	300
33		16	HBA (1-4), HBD (0-2), HBic (1-3), RingArom (0-1), ExVol (0-10)	5-5	100

Run Number	Training set[a]	Number of compounds	Selected features[b]	Max-Min Features[c]	Spacing[d]
34	III	16	HBA (1-4), HBD (0-2), HBic (1-3), RingArom (0-1), ExVol (0-10)	5-5	300
35		16	HBA (1-4), HBD (0-2), HBic (1-3), RingArom (0-1), ExVol (0-10)	4-5	100
36		16	HBA (1-4), HBD (0-2), HBic (1-3), RingArom (0-1), ExVol (0-10)	4-5	300
37		16	HBA (2-4), HBD (0-2), HBic (1-3), RingArom (0-1)	4-5	100
38		16	HBA (2-4), HBD (0-2), HBic (1-3), RingArom (0-1)	4-5	300
39		16	HBA (2-4), HBD (0-2), HBic (1-3), RingArom (0-1)	5-5	100
40		16	HBA (2-4), HBD (0-2), HBic (1-3), RingArom (0-1)	5-5	300
41		16	HBA (1-4), HBD (0-2), HBic (1-3), RingArom (0-1)	4-5	100
42		16	HBA (1-4), HBD (0-2), HBic (1-3), RingArom (0-1)	4-5	300
43		16	HBA (1-4), HBD (0-2), HBic (1-3), RingArom (0-1)	5-5	100
44		16	HBA (1-4), HBD (0-2), HBic (1-3), RingArom (0-1)	5-5	300
45		16	HBA (2-4), HBD (0-2), HBic (1-3), RingArom (0-1), ExVol (0-10)	4-5	100
46		16	HBA (2-4), HBD (0-2), HBic (1-3), RingArom (0-1), ExVol (0-10)	4-5	300
47		16	HBA (2-4), HBD (0-2), HBic (1-3), RingArom (0-1), ExVol (0-10)	5-5	100
48		16	HBA (2-4), HBD (0-2), HBic (1-3), RingArom (0-1), ExVol (0-10)	5-5	300
49		16	HBA (1-4), HBD (0-2), HBic (1-3), RingArom (0-1), ExVol (0-10)	4-5	100
50		16	HBA (1-4), HBD (0-2), HBic (1-3), RingArom (0-1), ExVol (0-10)	4-5	300
51		16	HBA (1-4), HBD (0-2), HBic (1-3), RingArom (0-1), ExVol (0-10)	5-5	100
52		16	HBA (1-4), HBD (0-2), HBic (1-3), RingArom (0-1), ExVol (0-10)	5-5	300

[a]Training subsets as in Table 2.
[b]HBA: Hydrogen Bond Acceptor, HBD: Hydrogen Bond Donor, RingArom: Ring Aromatic, Hbic: Hydrophobic, ExVol: Exclusion Volumes. Numbers in brackets refer to the allowed ranges of corresponding features in each pharmacophore modeling run.
[c]Max-Min refers to the allowed range of pharmacophoric features in each model.
[d]Spacing refers to the maximum interfeature distance in picometers. Other parameters were set to their default values.

2.1.5 Assessment of the Generated Hypotheses

When generating hypotheses, CATALYST attempts to minimize a cost function consisting of three terms: Weight cost, Error cost and Configuration cost (see CATALYST Cost Analysis in Assessment of Generated Binding Hypotheses). An additional approach to assess the quality of CATALYST-HYPOGEN pharmacophores is to cross-validate them

using the Cat-Scramble program implemented in CATALYST. This validation procedure is based on Fischer's randomization test. In this validation test; we selected a 95% confidence level, which instruct CATALYST to generate 19 random spreadsheets by the Cat-Scramble command. Subsequently, CATALYST-HYPOGEN is challenged to use these random spreadsheets to generate hypotheses using exactly the same features and parameters used in generating the initial unscrambled hypotheses. Success in generating pharmacophores of comparable cost criteria to those produced by the original unscrambled data reduces the confidence in the training compounds and the unscrambled original pharmacophore models (Catalyst User Manual, 2005 and Fischer *et al.*, 1966). Based on Fischer randomization criteria; all pharmacophores exceeded the 85% significance threshold for subsequent processing (clustering).

2.1.6 Clustering of the Generated Pharmacophore Hypotheses

The successful models (520) were clustered into 104 groups utilizing the hierarchical average linkage method available in CATALYST. Subsequently, the highest-ranking representatives, as judged based on their significance F-values, were selected to represent their corresponding clusters in subsequent modeling. Table 4 shows information about representative pharmacophores including their pharmacophoric features, success criteria and differences from corresponding null hypotheses. The table also shows the corresponding Cat. Scramble confidence levels for each representative pharmacophore.

2.1.7 Addition of Exclusion Volumes

To account for the steric constrains of the binding pocket we decided to decorate Hypo2-1/2-6 with exclusion volumes employing Hip-Hop-Refine module of CATALYST. Hip-Hop-Refine uses inactive training compounds to construct excluded volumes that resemble

the steric constrains of the binding pocket It identifies spaces occupied by the conformations of inactive compounds and free from active ones. These regions are then filled with excluded volumes (Catalyst User Manual, 2005). Since each pharmacophore resembles separate binding mode, it was decided to select the three separate training subsets for constructing appropriate exclusion spheres

In Hip-Hop-Refine the user defines how many molecules must map completely or partially the particular hypothesis via the Principal and Maximum Omitted Features (MaxOmitFeat) parameters. Active compounds are normally assigned MaxOmitFeat parameter of zero and principal value of 2 to instruct the software to consider all their chemical moieties in pharmacophore modeling and to fit them against all the pharmacophoric features of a particular hypothesis. On the other hand, inactive compounds are allowed to miss one (or two) features by assigning them a MaxOmitFeat of 1 (or 2) and principal value of zero.

We decided to consider 10 μM as an appropriate activity/inactivity threshold. Accordingly, inhibitors of IC_{50} values < 10 μM were regarded as ''actives'' and were assigned principal and MaxOmitFeat values of 2 and 0, respectively, On the other hand, inhibitors of IC_{50} > 10 μM were considered inactive and were assigned principal values of zero (Catalyst User Manual, 2005). However, each inactive compound was carefully evaluated to assess whether its low potency is attributable to missing one or more pharmacophoric features, i.e., compared to active compounds, or related to possible steric clashes within the binding pocket, or due to both factors and accordingly the MaxOmitFeat parameter was set to 1 or 2. Hip-Hop-Refine was configured to allow a maximum of 100 exclusion spheres to be added to the generated pharmacophoric hypotheses.

Table 8 shows the training compounds employed in this step and their corresponding principal and MaxOmitFeat parameters.

2.1.8 Receiver Operating Characteristic (ROC) Curve Analysis

Selected pharmacophore models (i.e., Hypo1/7 and Hypo 2-1/2-6) were validated by assessing their abilities to selectively capture diverse FBPase active compounds from a large testing list of actives and decoys.

The testing list was prepared as described by Verdonk and co-workers (Verdonk *et al.*, 2004). Briefly, decoy compounds were selected based on three basic one-dimensional (1D) properties that allow the assessment of distance (D) between two molecules (e.g., i and j): (1) the number of hydrogen-bond donors (NumHBD); (2) number of hydrogen-bond acceptors (NumHBA) and (3) count of nonpolar atoms (NP, defined as the summation of Cl, F, Br, I, S and C atoms in a particular molecule). For each active compound in the test set, the distance to the nearest other active compound is assessed by their Euclidean Distance (Eq. (4)):

$$D(i,j)=\sqrt{(NumHBD_i - NumHBD_j)^2 + (NumHBA_i - NumHBA_j)^2 + (NP_i - NP_j)^2} \quad ....(4)$$

The minimum distances are then averaged over all active compounds (Dmin). Subsequently, for each active compound in the test set, around 30 decoys were randomly chosen from the ZINC database (Irwin *et al.*, 2005). The decoys were selected in such a way that they did not exceed Dmin distance from their corresponding active compound.

To diversify active members in the list, we excluded any active compound having zero distance ($D(i,j)$) from other active compound(s) in the test set Active testing compounds

were defined as those possessing FBPase affinities ranging from 0.22 to >10 μM. The test set included 32 active compounds and 1110 ZINC decoys.

The test set (1142 compounds) was screened by each particular pharmacophore employing the "Best flexible search" option implemented in CATALYST, while the conformational spaces of the compounds were generated employing the "Fast conformation generation option" implemented in CATALYST. Compounds missing one or more features were discarded from the hit list.

The ROC curve analysis describes the sensitivity (Se or true positive rate, Eq. (5)) for any possible change in the number of selected compounds (n) as a function of (1-Sp). Sp is

$$Se = \frac{Number\ of\ Selected\ Actives}{Total\ Number\ of\ Actives} = \frac{TP}{TP + FN} \quad \ldots\ldots\ldots\ldots\ldots\ldots\ldots\ldots (5)$$

defined as specificity or true negative rate (Eq. (6)). (Veber *et al.,* 2002 and Irwin *et al.,* 2005).

$$Sp = \frac{Number\ of\ Discarded\ Inactives}{Total\ Number\ of\ Inactives} = \frac{TN}{TN + FP} \quad \ldots\ldots\ldots\ldots\ldots\ldots\ldots\ldots (6)$$

where, TP is the number of active compounds captured by the virtual screening method (true positives), FN is the number of active compounds discarded by the virtual screening method, TN is the number of discarded decoys (presumably inactives), while FP is the number of captured decoys (presumably inactive) (Lipinski *et al.*, 2001 and Kirchmair *et al.,* 2008).

If all molecules scored by a virtual screening (VS) protocol with sufficient discriminatory power are ranked according to their score (i.e., fit values), starting with the best-scored

molecule and ending with the molecule that got the lowest score, most of the actives will have a higher score than the decoys. Since some of the actives will be scored lower than decoys, an overlap between the distribution of active molecules and decoys will occur, which will lead to the prediction of false positives and false negatives (Irwin *et al*., 2005, Triballeau *et al.,* 2005 and Kirchmair *et al.,* 2008). The selection of one score value as a threshold strongly influences the ratio of actives to decoys and therefore the validation of a VS method. The ROC curve method avoids the selection of a threshold by considering all Se and Sp pairs for each score threshold (Kirchmair *et al.,* 2008). A ROC curve is plotted by setting the score of the active molecule as the first threshold. Afterwards, the number of decoys within this cutoff is counted and the corresponding Se and Sp pair is calculated. This calculation is repeated for the active molecule with the second highest score and so forth, until the scores of all actives are considered as selection thresholds.

The ROC curve representing ideal distributions, where no overlap between the scores of active molecules and decoys exists, proceeds from the origin to the upper-left corner until all the actives are retrieved and Se reaches the value of 1. In contrast to that, the ROC curve for a set of actives and decoys with randomly distributed scores tends towards the Se = 1-Sp line asymptotically with increasing number of actives and decoys (Jacobsson *et al*., 2003, Triballeau *et al*., 2005 and Kirchmair *et al*., 2008). The success of a particular virtual screening workflow can be judged from the following criteria (shown in Table 4):

1) Area under the ROC curve (AUC). (Triballeau *et al.,* 2005 and Kirchmair *et al.,* 2008). In an optimal ROC curve an AUC value of 1 is obtained; however, random distributions cause an AUC value of 0.5. Virtual screening that performs better than a random discrimination of actives and decoys retrieve an AUC value between 0.5 and 1, whereas an

AUC value lower than 0.5 represents the unfavorable case of a virtual screening method that has a higher probability to assign the best scores to decoys than to actives (Triballeau *et al*., 2005 and Kirchmair *et al*., 2008).

2) Overall Accuracy (ACC): describes the percentage of correctly classified molecules by the screening protocol (Eq. (7)). Testing compounds are assigned a binary score value of zero (compound not captured) or one (compound captured) (Jacobsson *et al*., 2003, Triballeau *et al*., 2005 and Kirchmair *et al*., 2008).

$$ACC = \frac{TP + TN}{N} = \frac{A}{N}.Se + \left(1 - \frac{A}{N}\right).Sp \quad \ldots\ldots\ldots\ldots\ldots\ldots\ldots (7)$$

where, N is the total number of compounds in the testing database, A is the number of true actives in the testing database.

3) Overall specificity (SPC): describes the percentage of discarded inactives by the particular virtual screening workflow. Inactive test compounds are assigned a binary score value of zero (compound not captured) or one (compound captured) regardless to their individual fit values (Jacobsson *et al*., 2003, Triballeau *et al*., 2005 and Kirchmair *et al*., 2008).

4) Overall True Positive Rate (TPR or overall sensitivity): describes the fraction percentage of captured actives from the total number of actives. Active test compounds are assigned a binary score value of zero (compound not captured) or one (compound captured) regardless to their individual fit values (Jacobsson *et al*., 2003, Triballeau *et al*., 2005 and Kirchmair *et al*., 2008).

5) Overall False Negative Rate (FNR or overall percentage of discarded actives): describes the fraction percentage of active compounds discarded by the virtual screening method. Discarded active test compounds are assigned a binary score value of zero (compound not captured) or one (compound captured) regardless to their individual fit values (Jacobsson *et al*., 2003, Triballeau *et al*., 2005 and Kirchmair *et al*., 2008).

2.1.8 *In Silico* Screening for New FBPase Inhibitors

The Hypo1/7 and sterically-refined version of Hypo 2-1/2-6 were employed as 3D search queries to screen two 3D flexible structural databases: NCI and DAC. The screening was done employing the "Best Flexible Database Search" option implemented within CATALYST. NCI hits were filtered according to Lipinski's and Veber's (Lipinski *et al.*, 2001 and Veber *et al.*, 2002) rules. Remaining hits were fitted against the pharmacophores using the "best fit" option within CATALYST.

2.2 *In vitro* Experimental Studies

2.2.1 Materials

All of the chemicals used in these experiments were of reagent grade and obtained from commercial suppliers. NCI samples were kindly provided by the national cancer institute and were of purity >95%.

- Recombinant Human FBPase (Abnova, Taiwan)
- Glucose-6-phosphate dehydrogenase (Sigma, USA)
- phosphoglucose isomerase (Sigma, USA)
- water for bioanalysis (Sigma, USA)

- AMP (Sigma, USA)
- Fructose-1,6-Phosphate (Sigma, USA)
- Tris Buffer (Sigma, USA)
- $MgCl_2$ (Sigma, USA)
- EDTA (Sigma, USA)
- DTT (Sigma, USA)
- NADP (Sigma, USA)
- DMSO for bioanalysis (Sigma, USA)

2.2.2 Preparation of hit compounds for *in vitro* assay

The tested compounds were provided as dry powders in variable quantities (5 mg to 500 mg). They were initially dissolved in DMSO to give stock solutions of 0.02 M. Subsequently, they were diluted to the required concentrations with deionized water for enzymatic assay.

2.2.3 Quantification of FBPase activity in a spectrophotometric assay

The FBPase activity was quantified by coupled enzyme assay procedure to measure the released inorganic phosphate. 100 mM Tris (12.1 g/L), 2 mM $MgCl_2$ (2 ml of 1 M/L), 0.05 mM EDTA (0.1 ml of 500 mM/L), 1 mM DTT (154 mg/L), 0.2 mM NADP (170mg/L), pH ~ 7.4. For each 75 µl of the prepared reaction mix, 2 µl of Glucose-6-phosphate Dehydrogenase, 2 µl of Phosphoglucose Isomerase, 1 µl of FPBase enzymes and 10 µl of the inhibitor were added. Aliquots were left to stand at room temperature for around 3 min,

the reaction was initiated by adding 10 µl of 10 mM Fru 1,6-P2 (final concentration 100 µM), and the reaction rate was determined by comparing the slopes of tested compounds relative to the slope of the positive controls. Percantage was calculated as percent of remaining activity (Eq.1).

Slope of inhibited enzyme activity/slope of uninhibited enzyme activity x 100 = % remaining activity of inhibited enzyme ………………….……………………………… (1)

Blank was prepared as above except 10 µl of distilled water was used instead of inhibitor solution. The enzymatic reaction rate was determined spectrophotomertically at λ_{max} 340 nm using a plate reader (Bio-Tek instruments ELx 800, USA).

Inhibition of FBPase was calculated as percent activity of the uninhibited FBPase control. AMP was used as standard inhibitor, while negative controls were prepared by adding the substrate without the FBPase enzyme.

2.3. Synthesis of the Optimized Hits

2.3.1 Materials

- Sodium carbonate, Min. 99.5%, Sigma-Aldrich, (USA).
- Triethaylamine (TEA), Sigma-Aldrich, (USA).
- Acetone, Min. 99.5%, was purchased from TEDIA Company (USA).
- Aniline, Min. 99%, From MERCK, (Germany).
- 3-Nitroaniline, From Riedel-de Haën, (Germany).
- 4-Nitroaniline, From Riedel-de Haën (Germany).
- *p*- Anisidine, Min. 99%, From Sigma-Aldrich, (USA).
- Resorcinol (Benzene -1, 3-diol), 99-100.5%, Laboratory Rasayan.

- 1, 3 -Phenylene diamine, Min. 98%, From MERCK, (Germany).
- 2-Methylaniline Min. 99%, From MERCK, (Germany).
- 3-Methylaniline Min. 99%, From MERCK, (Germany).
- 4-Methylaniline Min. 99%, From MERCK, (Germany).
- 3-Methoxy-4-methyl-aniline,Sigma-Aldrich, (USA)
- 4-Methoxyaniline, Sigma-Aldrich, (USA).
- 4-Methoxy-aniline (p-anisidine), Min. 98%, From Fluka, (Switzerland).
- 3-Methoxy-aniline (o-anisidine), Min. 98%, From Fluka, (Switzerland).
- Benzoyl chloride, Min. 99%, From MERCK, (Germany).
- 4-Methyl-benzoyl chloride, Min. 98%, Sigma-Aldrich, (USA).
- 4- Nitro-benzoyl chloride, Min. 98%, From MERCK, (Germany).
- 3- Nitro-benzoyl chloride, Min. 98%, From Acros, (USA).
- *p*-toluenesulfonyl chloride, Min. 99%, Sigma-Aldrich, (USA).
- Pyridine, 99.8%, Sigma-Aldrich, (USA).
- Stuart scientific electro-thermal melting point apparatus.

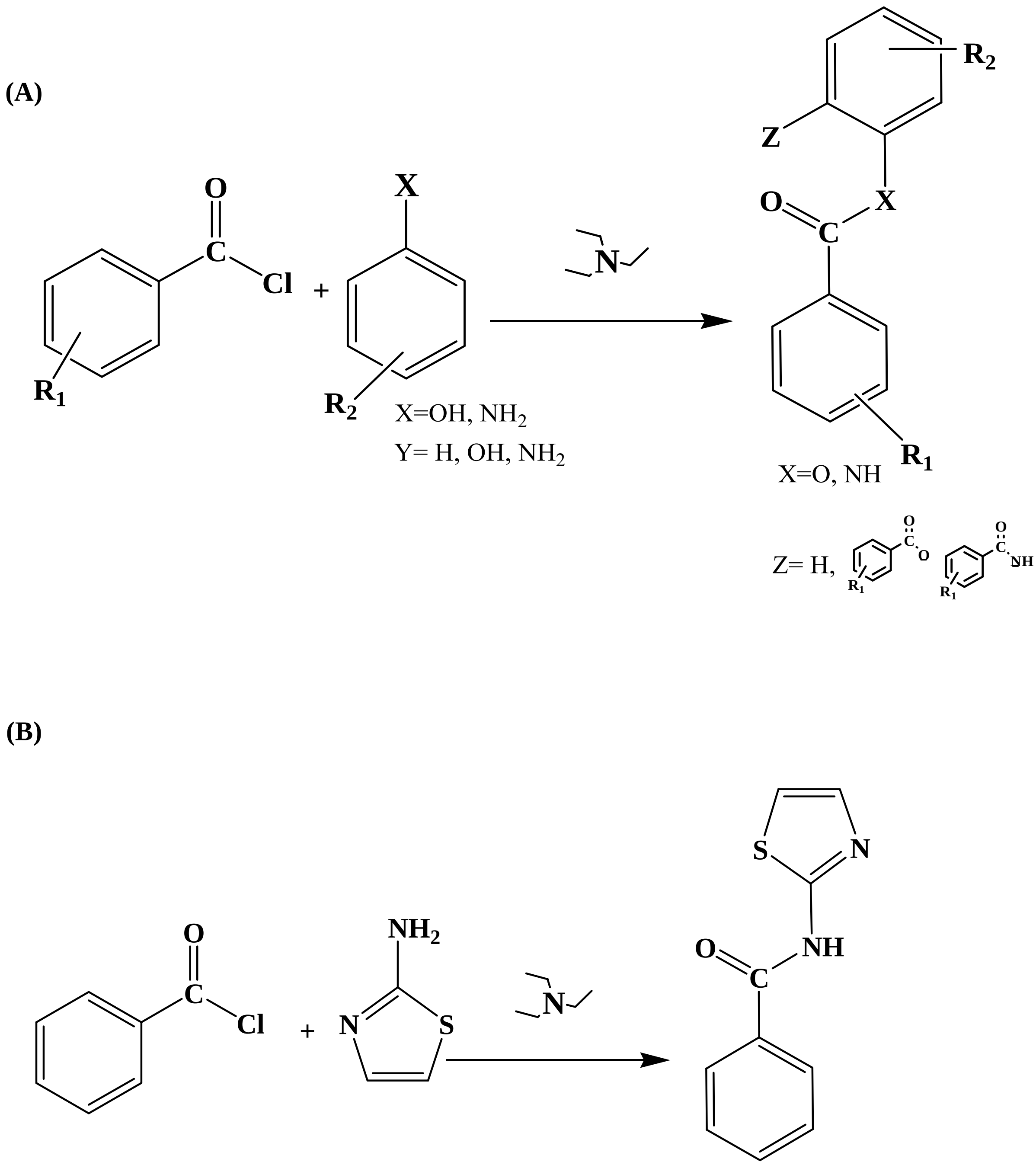
2.3.2 General Methods

Melting points were measured using Gallenkampf melting point apparatus and are uncorrected. ^{1}H NMR and ^{13}C NMR spectrums were collected on a Bruker NMR400 spectrometer. High resolution mass spectrometry was performed using LC Mass Bruker Apex-IV mass spectrometer utilizing an electrospray interface. Infrared spectra were recorded using Shimadzu IR Affinity-1 spectrophotometer. The samples were analyzed as KBr pellets. Analytical thin layer chromatography (TLC) was carried out using pre-coated aluminum plates and visualized by UV light (at 254 and/or 360 nm). Elemental analysis

was performed using EuroVector elemental analyzer. Chemicals and solvents were used without further purification.

General Method

To a magnetically-stirred, ice-bathed, solution of the substituted phenol derivative, aniline, heterocyclic amine or aryl alkyl amine (1 equiv) and triethylamine (2 equiv) in anhydrous acetone (50 mL), benzoyl chloride derivative (2 equiv) was added. The solution was stirred at room temperature until completion (as revealed by TLC). The reaction mixture was quenched by slow addition into sufficient 5% aqueous sodium bicarbonate. The precipitated crude amide (or ester) products were purified by recrystallization from acetone/water (Scheme 1).

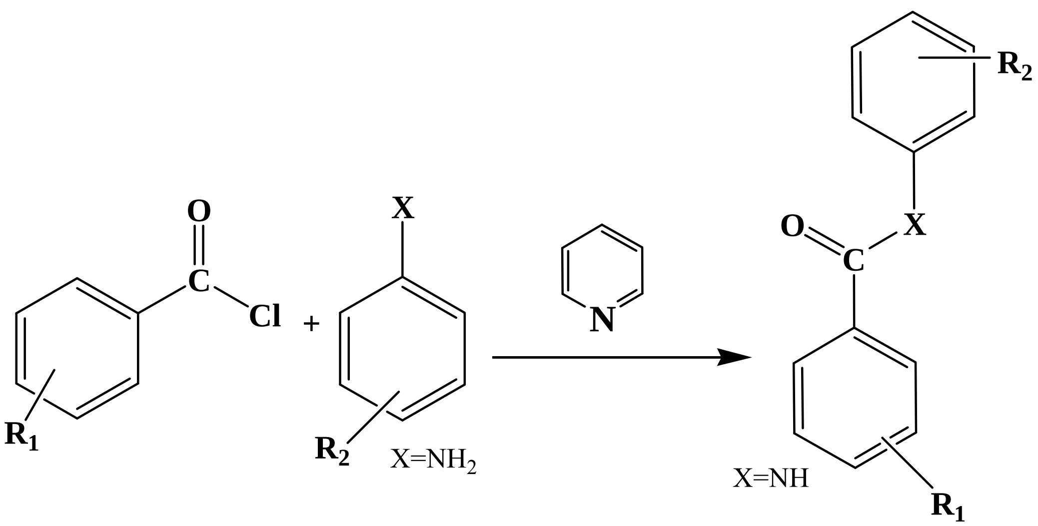


Scheme 1: Synthesis of acyl amide or ester, **(A)** substituted alkyl amine or ester derivatives, **(B)** aminothiazole derivative.

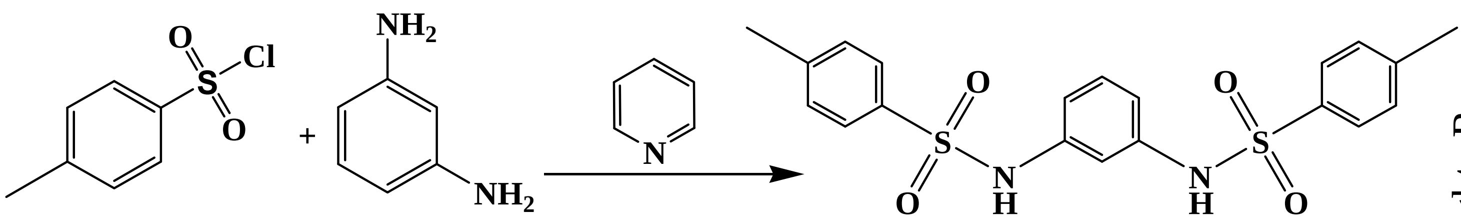
Method B

To a magnetically-stirred solution of the substituted aniline (or aryl alkyl amine) in dry pyridine (50 mL), benzoyl chloride (or sulfonylchloride) derivative (1.5 equiv) was added. The solution was refluxed until completion (as revealed by TLC). The reaction mixture was quenched by addition of water (200 ml). The precipitated crude amide and sulfonamide products were subsequently washed with methanol (Scheme 2).

(A)



(B)



Scheme 2: Synthesis of **(A)** acyl amide and **(B)** acyl sulfonamide

3. Results and Discussion

CATALYST enables automatic pharmacophore construction by using a collection of molecules with activities ranging over a number of orders of magnitude. CATALYST pharmacophores (hypotheses) explain the variability of bioactivity with respect to the geometric localization of the chemical features present in the molecules used to build it. The pharmacophore model consists of a collection of features necessary for the biological activity of the ligands arranged in 3D space (e.g., hydrogen bond acceptors and donors, hydrophobic regions, etc…). Different hypotheses were generated for a series of FBPase inhibitors. A total of 136 compounds were used in this study (Figure 1) (Wright *et al.*, 2001, Wright *et al.*, 2002 and Wright *et al*., 2003). Three training subsets were selected from the collection (Table 3). Each subset consisted of inhibitors of wide structural diversity. The biological activity in the training subsets spanned from 3.5 to 4.0 orders of magnitude.

3.1 Data Mining and Conformational Coverage

The literature was surveyed to collect many reported structurally diverse FBPase inhibitors (**1-136**, see Table 1 and the 2D structures of the inhibitors were imported into CATALYST and converted automatically into 3D single conformer representations.

The conformational space of each inhibitor was extensively sampled utilizing the poling algorithm employed within the CONFIRM module of CATALYST (Catalyst user Manual, 2005). Conformational coverage was performed employing the "Best" module to ensure extensive sampling of conformational space. Pharmacophore generation and pharmacophore-based search procedures are known for their sensitivity to inadequate

conformational sampling within the training compounds prompting our extensive conformational sampling (Sheridan *et al.*, 2002).

3.2 Exploration of FBPase Pharmacophoric Space

The fact that we have an informative list of 136 FBPase inhibitors of evenly spread bioactivities over more than 3.5 orders of magnitude, prompted us to employ CATALYST-HYPOGEN to identify possible pharmacophoric binding modes assumed by FBPase inhibitors (Wright *et al.,* 2001, Wright *et al.*, 2002 and Wright *et al*., 2003).

HYPOGEN implements an optimization algorithm that evaluates large number of potential binding models for a particular target through fine perturbations to hypotheses that survived the constructive and subtractive phases of the modeling algorithm.

3.3 Pharmacophoric Hypotheses Generation

The extent of the evaluated pharmacophoric space is reflected by the configuration (Config.) cost calculated for each modeling run. It is generally recommended that the Config. cost of any HYPOGEN run not to exceed 17 (corresponding to 2 (Beeley *et al.*, 2003) hypotheses to be assessed by CATALYST) to guarantee thorough analysis of all models. The size of the investigated pharmacophoric space is a function of training compounds, selected input chemical features and other CATALYST control parameters (Sutter *et al.,* 2000).

Restricting the extent of explored pharmacophoric space should improve the efficiency of optimization via allowing effective evaluation of limited number of pharmacophoric models. On the other hand, rigorous restrictions imposed on the pharmacophoric space

might reduce the possibility of discovering optimal pharmacophoric hypotheses, as they might occur outside the “boundaries” of the pharmacophoric space.

Therefore, we decided to explore the pharmacophoric space of FBPase inhibitors under reasonably imposed "boundaries" through 52 HYPOGEN automatic runs and employing three carefully selected training subsets: subsets **I-III** in Table 2. The training compounds in these subsets were selected in such away to guarantee maximal 3D diversity and continuous bioactivity spread over more than 3.5 logarithmic cycles. We gave special emphasis to the 3D diversity of the most active compounds in each training subset (Table 2) because of their significant influence on the extent of the evaluated pharmacophoric space during the constructive phase of HYPOGEN algorithm (Catalyst User Manual, 2005).

During the constructive phase, CATALYST generates common conformational alignments among the mostactive training compounds. Only molecular alignments based on a maximum of five chemical features are considered. The program identifies a particular compound as being within the most active category if it satisfies Eq. (2)

(MAct -UncMAct)-(Act=UncAct) > 0.0 …………………………………………...……. (2)

where ‘MAct’ is the activity of the most active compound in the training set, ‘Unc’ is the uncertainty of the compounds and ‘Act’ is the activity of the training compounds (Table 1).

In the subsequent subtractive phase, CATALYST eliminates some hypotheses that fit inactive training compounds. A particular training compound is defined as being inactive if it satisfies Eq. (3)

Log(Act) - log(MAct) > BS……………………..……. ………………………………..(3)

where, 'BS' is the bioactivity spread (equals 3.5 by default, Table 1).

However, in the optimization phase, CATALYST applies fine perturbations in the form of vectored feature rotation, adding new feature and/or removing a feature, to selected hypotheses that survived the subtractive phase, in an attempt to find new models of enhanced bioactivity/mapping correlations. CATALYST selects the highest-ranking models (10 by default) and presents them as the optimal pharmacophore hypotheses resulting from the particular automatic modeling run.

Guided by our rationally restricted pharmacophoric exploration concept, we restricted the software to explore pharmacophoric models incorporating from one (or two) to four HBA, zero to two HBD, one to three Hbic, and from zero to one RingArom features instead of the default range of zero to five, as shown in Table 3. Furthermore, we instructed HYPOGEN to explore only 4- and 5-featured pharmacophores, i.e., ignore models of lesser number of features in order to further narrow the investigated pharmacophoric space and to represent the feature-rich nature of known FBPase ligands (as shown in Table 3).

In each run, the resulting binding hypotheses were automatically ranked according to their corresponding "total cost" value, which is defined as the sum of error cost, weight cost and configuration cost (see Assessment of the Generated Hypotheses). (Catalyst user Manual, 2005) Error cost provides the highest contribution to total cost and it is directly related to the capacity of the particular pharmacophore as 3D-QSAR model, i.e., in correlating the molecular structures to the corresponding biological responses (Catalyst User manual, 2005) HYPOGEN also calculates the cost of the null hypothesis, which presumes that there is no relationship in the data and that experimental activities are normally distributed about

their mean. Accordingly, the greater the difference from the null hypothesis cost (residual cost, Table 4) the more likely that the hypothesis does not reflect a chance correlation.

Table 4: Success criteria of representative pharmacophore hypotheses (cluster centers).

N	Run[a]	Hypotheses[b]	Features	Config. cost	Total cost	Null Hypothesis	Residual Cost[c]	R[d]	F-stat[f]	Cat. Scramble
1		6[g,h]	2x HBA, Hbic, RingArom	16.68	91.44	115	23.56	0.91	4.7	95%
2	1	8	2x HBA, Hbic, RingArom	16.68	91.97	115	23.03	0.92	6.53	95%
3		9	3x HBA, Hbic	16.68	92.56	115	22.44	0.9	5.94	95%
4	2	1	3x HBA, Hbic	14.98	87.74	115	27.26	0.93	6.99	95%
5		3	3x HBA, Hbic	14.98	88.56	115	26.44	0.94	6.09	95%
6	3	1	2x HBA, 3x Hbic	13.18	84.62	115	30.38	0.95	3.37	95%
7		3	2x HBA, 3x Hbic	13.18	88.18	115	26.82	0.9	6.27	95%
8	4	8	2x HBA, 3x Hbic	10.08	90.51	115	24.49	0.84	11.5	95%
9	5	6	2x HBA, HBD, Hbic	17.81	92.28	115	22.72	0.92	1.24	95%
10		9	2x HBA, HBD, Hbic	17.81	92.65	115	22.35	0.92	4.19	95%
11		1	2x HBA, HBD, Hbic	16.47	89.64	115	25.36	0.94	4.18	95%
12		4	2x HBA, HBD, Hbic	16.47	92.78	115	22.22	0.89	1.24	95%
13	6	5	HBA, HBD, Hbic	16.47	92.97	115	22.03	0.92	0.26	95%
14		7	HBA, HBD, 2x Hbic	16.47	94.65	115	20.35	0.88	8.41	95%
15		9	HBA, HBD, 2x Hbic	16.47	95.27	115	19.73	0.87	1.34	95%
16	7	4	2x HBA, 3x Hbic	14.7	94.31	115	20.69	0.84	1.77	95%
17		9	2x HBA, 3x Hbic	14.7	97.94	115	17.06	0.81	7.74	95%
18	9	9	2x HBA, 3x Hbic	24.79	108.2	115	6.76	0.81	11.8	95%
19	6	10	HBA, HBD, 2x Hbic	16.47	95.39	115	19.61	0.86	0.64	95%
20	8	10	HBA, Hbic, RingArom	11.72	93.46	115	21.54	0.82	5.06	95%
21		2	2x HBA, HBD, Hbic, 5 ExVol	16.7	88.75	115	26.25	0.97	9.17	95%
22	1	7	2x HBA, 2x Hbic, 3 ExVol	16.7	90.91	115	24.09	0.91	7.69	95%
23		8	3x HBA, Hbic, 3 ExVol	16.7	91.39	115	23.61	0.91	5.19	95%
24	2	4	3x HBA, Hbic, 4 ExVol	15	85.49	115	29.51	0.96	8.26	95%
25		6	2x HBA, Hbic, RingArom, 4 ExVol	15	85.6	115	29.4	0.96	4.71	95%
26	4	4	2x HBA, 3x Hbic, 2 ExVol	10.08	85.04	115	29.96	0.91	2.94	95%
27		5	2x HBA, 3x Hbic, 3 ExVol	10.08	85.22	115	29.78	0.92	12.4	95%

N	Run[a]	Hypotheses[b]	Features	Config. cost	Total cost	Null Hypothesis	Residual Cost[c]	R[d]	F-stat[f]	Cat. Scramble
28	5	9	2x HBA, HBD, Hbic, 2 ExVol	17.83	93.79	115	21.21	0.89	6.71	95%
29	6	2	2x HBA, Hbic, RingArom	16.49	94.73	115	20.27	0.86	4.66	95%
30		3	HBA, HBD, 2x Hbic	16.49	95.48	115	19.52	0.86	1.23	95%
31		1	2x HBA, 3x Hbic, 5 ExVol	14.7	83.52	115	31.48	0.97	1.28	95%
32	7	5	HBA, 3x Hbic, RingArom	14.7	93.2	115	21.8	0.86	5.03	95%
33		6	HBA, 3x Hbic, RingArom, 1 ExVol	14.7	94.06	115	20.94	0.85	3.00	95%
34	8	6	HBA, 3x Hbic, RingArom, 2 ExVol	11.72	90	115	25	0.85	3.02	95%
35		9	2x HBA, 3x Hbic	11.72	93.81	115	21.19	0.82	8.3	95%
36	10	2	2x HBA, 3x Hbic, 1 ExVol	21.69	90.9	115	24.1	0.96	5.98	95%
37		7	2x HBA, 3x Hbic, 3 ExVol	21.69	95.79	115	19.21	0.91	5.44	95%
38	2	10	2x HBA, HBD, Hbic, 4 ExVol	15	86.06	115	28.94	0.95	5.06	95%
39	6	10	2x HBA, 2x Hbic, 2 ExVol	16.49	98.07	115	16.93	0.83	12.73	95%
40	8	10	HBA, HBD, 3x Hbic, 2 ExVol	11.72	93.84	115	21.16	0.83	5.79	95%
41	1	8	2x HBA, 3x Hbic	14.64	84.09	111	26.87	0.87	4.62	95%
42	3	8	3x HBA, Hbic	17.22	86.17	111	24.79	0.9	5.39	95%
43	4	5	2x HBA, HBD, Hbic	15.3	82.24	111	28.72	0.89	3.47	95%
44	5	5	HBA, 3x Hbic, RingArom	16.13	88.34	111	22.62	0.83	2.63	95%
45		4	HBA, HBD, 3x Hbic	14.5	80.67	111	30.29	0.9	5.04	95%
46	6	6	HBA, 3x Hbic, RingArom	14.5	84.28	111	26.68	0.86	3.76	95%
47		9	HBA, HBD, 3x Hbic	14.5	84.61	111	26.35	0.86	4.36	95%
48		1	2x HBA, 3x Hbic	18.33	87.76	111	23.2	0.86	4.71	95%
49		2	HBA, HBD, 2x Hbic	18.33	88.3	111	22.66	0.89	0.28	95%
50	7	4	HBA, 3x Hbic, RingArom	18.33	88.77	111	22.19	0.86	5.36	95%
51		7	HBA, 2x HBD, Hbic	18.33	89.01	111	21.95	0.87	1.8	95%
52		9	HBA, 3x Hbic	18.33	89.16	111	21.8	0.86	0.32	95%
53		2	HBA, HBD, Hbic, RingArom	17.22	79.44	111	31.52	0.94	4.18	95%
54	8	4	HBA, HBD, 2x Hbic	17.22	81.92	111	29.04	0.91	7.26	95%
55		5	2x HBA, Hbic	17.22	82.8	111	28.16	0.9	6.8	95%
56	2	10	2x HBA, 3x Hbic	11.48	82.55	111	28.41	0.85	7.95	90%

N	Run[a]	Hypotheses[b]	Features	Config. cost	Total cost	Null Hypothesis	Residual Cost[c]	R[d]	F-stat[f]	Cat. Scramble
57	1	1	2x HBA, 3x Hbic, 8 ExVol	14.64	74.18	111	36.78	0.96	5.56	90%
58		**7**	**2x HBA, 3x Hbic, 8 ExVol**	**14.64**	**82.47**	**111**	**28.49**	**0.88**	**11.74**	**90%**
59	3	3	2x HBA, HBD, Hbic, 4 ExVol	15.33	77.13	111	33.83	0.95	5.28	90%
60		4	2x HBA, HBD, Hbic, 4 ExVol	15.33	79.44	111	31.52	0.94	2.98	90%
61	4	1	2x HBA, 2x Hbic, 7 ExVol	17.24	79.4	111	31.56	0.95	4.5	75%
62		8	2x HBA, HBD, Hbic, 4 ExVol	17.24	84.76	111	26.2	0.93	7.42	90%
63	5	9	HBA, HBD, 3x Hbic, 4 ExVol	18.35	86.98	111	23.98	0.87	8.92	90%
64	6	1	HBA, HBD, Hbic, RingArom, 4 ExVol	17.24	78.53	111	32.43	0.94	4.4	90%
65		4	HBA, 2x Hbic, RingArom, 6 ExVol	17.24	78.87	111	32.09	0.96	10.07	95%
66	7	3	HBA, HBD, 2xHbic, 5 ExVol	18.35	83.13	111	27.83	0.91	6.44	90%
67		6	HBA, HBD, Hbic, RingArom,	18.35	84	111	26.96	0.9	4.98	90%
68		7	2x HBA, Hbic, RingArom, 5 ExVol	18.35	84.49	111	26.47	0.9	2.4	90%
69		9	HBA, 2x HBD, Hbic, 4 ExVol	18.35	85.43	111	25.53	0.9	1.04	90%
70	8	3	HBA, HBD, 3x Hbic, 1 ExVol	14.5	83.77	111	27.19	0.87	1.13	90%
71	4	10	HBA, HBD, Hbic, RingArom, 4 ExVol	17.24	85.62	111	25.34	0.87	0.71	90%
72	6	10	HBA, HBD, 2x Hbic, 4 ExVol	17.24	81.6	111	25.34	0.92	4.11	95%
73	1	2	2x HBA, 3x Hbic	13.74	85.44	115	29.56	0.84	3.48	95%
74	2	2	2x HBA, 3x Hbic	11.12	81.08	108	26.92	0.85	9.19	95%
75	4	1	2x HBA, 3x Hbic	8.74	74.63	108	33.37	0.89	5.09	95%
76		8	2x HBA, 3x Hbic	8.74	85.19	108	22.81	0.79	8.03	95%
77		9	2x HBA, 3x Hbic	8.74	85.78	108	22.22	0.77	2.87	95%
78	5	2	HBA, 3x Hbic, RingArom	15.97	87.12	108	20.88	0.84	6.75	95%
79		7	2x HBA, 3x Hbic	15.97	89.16	108	18.84	0.82	4.75	95%
80	6	6	2x HBA, 2x Hbic	13.95	87.67	108	20.33	0.82	6.67	95%
81		9	2x HBA, 3x Hbic	13.95	87.96	108	20.04	0.81	6.12	95%
82	7	9	2x HBA, 3x Hbic	14.57	89.87	108	18.13	0.83	1.98	95%
83	8	2	2x HBA, 3x Hbic	12.15	81.33	108	26.67	0.86	5.16	95%
84		4	HBA, 3x Hbic, RingArom	12.15	82.57	108	25.43	0.85	8.35	95%
85		5	HBA, 3x Hbic, RingArom	12.15	83.47	108	24.53	0.84	2.63	95%

N	Run[a]	Hypotheses[b]	Features	Config. cost	Total cost	Null Hypothesis	Residual Cost[c]	R[d]	F-stat[f]	Cat. Scramble
86	2	10	2x HBA, Hbic, RingArom	11.12	87.56	108	20.44	0.79	3.48	95%
87	5	10	HBA, 3x Hbic, RingArom	16	91.21	108	16.79	0.79	4.83	95%
88	6	10	HBA, 3x Hbic, RingArom	13.95	88.63	108	19.37	0.8	5.08	95%
89	1	1	2x HBA, Hbic, 8 ExVol	14.06	73.89	108	34.11	0.97	1.04	95%
90		9	2x HBA, Hbic, RingArom, 4 ExVol	14.06	86.76	108	21.24	0.82	3.57	95%
91	2	2	2x HBA, Hbic, 6 ExVol	11.61	76.67	108	31.33	0.91	5.39	95%
92		8	2x HBA, Hbic, RingArom, 2 ExVol	11.61	84.29	108	23.71	0.83	9.45	95%
93	5	1	HBA, 3x Hbic, RingArom, 9 ExVol	15.97	73.66	108	34.34	0.97	8.15	95%
94		6	HBA, 2x Hbic, RingArom, 1 ExVol	15.97	86.39	108	21.61	0.86	0.14	95%
95		8	2x HBA, 3x Hbic, 3 ExVol	15.97	87.76	108	20.24	0.84	3.79	95%
96		9	2x HBA, 3x Hbic, 3 ExVol	15.97	88.48	108	19.52	0.82	4.84	95%
97	6	5	HBA, 3x Hbic, RingArom, 2 ExVol	13.95	85.24	108	22.76	0.84	9.04	95%
98		7	HBA, 3x Hbic, RingArom, 2 ExVol	13.95	85.51	108	22.49	0.84	4.04	95%
99	7	2	2x HBA, 3x Hbic, 5 ExVol	14.57	85.05	108	22.95	0.85	3.39	95%
100		4	2x HBA, 3x Hbic, 1 ExVol	14.57	88.29	108	19.71	0.81	10.38	95%
101		9	HBA, HBD, 3x Hbic, 2 ExVol	14.57	89.33	108	18.67	0.8	3.13	95%
102	8	6	HBA, 3x Hbic, RingArom, 7 ExVol	12.15	77.2	108	30.8	0.9	3.51	95%
103		9	HBA, HBD, 3x Hbic, 3 ExVol	12.15	79.01	108	28.99	0.89	3.73	95%
104	1	10	2x HBA,2x Hbic, 1 ExVol	14.06	87.97	108	20.03	0.84	3.34	95%

[a]Correspond to runs in Table 3, [b]High ranking representative hypotheses (in their corresponding clusters, see section 4.1.6). [c]Difference between total cost and the cost of the corresponding null hypotheses. [d]Correlation coefficients between pharmacophore-based bioactivity estimates and bioactivities of corresponding training compound (subsets in Table 2. [e]Correlation coefficients between pharmacophore-based bioactivity estimates and bioactivities of all collected compounds. [f]Fisher statistic calculated based on the linear regression between the fit values of all collected inhibitors(**1-13**6, Table1 1) against pharmacophore hypothesis (employing the "best fit" option and equation (C)) and their respective inhibitory bioactivities (log (1/IC_{50}) values). [g]Ranking of hypotheses is as generated by CATALYST in each automatic run. [h]Bolded pharmacophores appeared in the best ROC analyses.

An additional validation technique based on Fisher's randomization test (Fisher *et al.,* 1966) was recently introduced into CATALYST: Cat. Scramble (Catalyst User Manual, 2005). In this test the biological data and the corresponding structures are scrambled several times and the software is challenged to generate pharmacophoric models from the randomized data. The confidence in the parent hypotheses (i.e., generated from unscrambled data) is lowered proportional to the number of times the software succeeds in generating binding hypotheses from scrambled data of apparently better cost criteria than the parent hypotheses (see Assessment of the Generated Hypotheses) (Sutter *et al.,* 2000, Catalyst User Manual, 2005 and, Poptodorov *et al.*, 2006).

Eventually, 520 pharmacophore models emerged from 52 automatic HYPOGEN runs, out of which 508 models illustrated Cat. scramble confidence levels ≥ 85%. These successful models were clustered and their best representatives (104 models, Table 4. Clustering of the Generated Pharmacophore Hypotheses) were subsequently evaluated by receiver-operating characteristic curve (ROC) analyses and correlation between fit values and bioactivities (F-values) among collected compounds (**1-136**, Table 1), as in Table 5.

Table 5: ROC curve analysis criteria for pharmacophores and their sterically- refined versions

N	Pharmacophore Model	ROC[a]-AUC[b]	ACC[c]	SPC[d]	TPR[e]	FNR[f]	F-VALUE
1	Hypo1/6	74.25%	96.46%	97.59%	65.63%	2.41%	4.7
2	Hypo1/8	77.99%	96.46%	96.33%	100.00%	3.67%	6.53
3	Hypo1/9	76.56%	96.46%	96.44%	96.88%	3.56%	5.94
4	Hypo2/1	63.98%	96.46%	97.13%	78.13%	2.87%	6.99
5	Hypo2/3	68.78%	96.46%	96.79%	87.50%	3.21%	6.09
6	Hypo3/1	76.51%	96.46%	97.25%	75.00%	2.76%	3.37
7	Hypo3/3	77.33%	96.46%	97.36%	71.88%	2.64%	6.27
8	Hypo4/8	84.12%	96.46%	96.79%	87.50%	3.21%	11.5
9	Hypo5/6	60.94%	96.46%	97.47%	68.75%	2.53%	1.24
10	Hypo5/9	63.91%	96.46%	97.59%	65.63%	2.41%	4.19
11	Hypo6/1	77.17%	96.46%	98.97%	28.13%	1.03%	4.18
12	Hypo6/4	67.86%	96.46%	98.85%	31.25%	1.15%	1.24
13	Hypo6/5	76.95%	96.46%	98.62%	37.50%	1.38%	0.26
14	Hypo6/7	75.23%	96.46%	97.02%	81.25%	2.99%	8.41
15	Hypo6/9	86.41%	96.46%	99.08%	25.00%	0.92%	1.34
16	Hypo4/7	74.16%	96.46%	97.47%	68.75%	2.53%	1.77
17	Hypo7/9	74.95%	96.46%	97.70%	62.50%	2.30%	7.74
18	Hypo9/9	79.29%	96.46%	96.67%	90.63%	3.33%	11.8
19	Hypo6/10	82.74%	96.46%	98.97%	28.13%	1.03%	0.64
20	Hypo8/10	80.72%	96.46%	97.47%	68.75%	2.53%	5.06
21	Hypo1/2	67.05%	96.13%	96.47%	87.50%	3.53%	9.17
22	Hypo1/7	77.83%	96.13%	96.10%	96.88%	3.90%	7.69
23	Hypo1/8	55.53%	92.54%	92.19%	96.88%	7.81%	5.19
24	Hypo2/4	69.36%	96.00%	97.66%	56.25%	2.34%	8.26
25	Hypo2/6	75.91%	95.69%	96.34%	81.25%	3.66%	4.71
26	Hypo4/4	77.62%	96.46%	97.82%	59.38%	2.18%	2.94

N	Pharmacophore Model	ROC[a]-AUC[b]	ACC[c]	SPC[d]	TPR[e]	FNR[f]	F-VALUE
27	Hypo4/5	84.69%	96.46%	97.13%	78.13%	2.87%	12.4
28	Hypo5/9	52.36%	99.12%	99.49%	57.14%	0.51%	6.71
29	Hypo6/2	71.49%	96.46%	97.47%	68.75%	2.53%	4.66
30	Hypo6/3	86.77%	96.46%	98.97%	28.13%	1.03%	1.23
31	Hypo7/1	80.74%	96.46%	98.16%	50.00%	1.84%	1.28
32	Hypo7/5	87.32%	93.71%	93.71%	93.75%	6.29%	5.03
33	Hypo7/6	81.70%	96.46%	97.36%	71.88%	2.64%	3
34	Hypo8/6	83.31%	96.46%	97.70%	62.50%	2.30%	3.02
35	Hypo8/9	77.85%	96.46%	96.90%	84.38%	3.10%	8.3
36	Hypo10/2	58.58%	61.20%	98.77%	1.94%	1.23%	5.98
37	Hypo10/7	77.33%	96.46%	97.36%	71.88%	2.64%	5.44
38	Hypo2/10	54.56%	96.46%	96.56%	93.75%	3.44%	5.06
39	Hypo6/10	74.41%	94.75%	94.64%	96.88%	5.36%	12.73
40	Hypo8/10	77.97%	93.68%	96.62%	50.00%	3.38%	5.79
41	Hypo1/8	78.85%	96.46%	96.90%	84.38%	3.10%	4.62
42	Hypo3/8	75.18%	96.46%	96.44%	96.88%	3.56%	5.39
43	Hypo4/5	68.60%	96.46%	96.44%	96.88%	3.56%	3.47
44	Hypo5/5	72.77%	96.46%	97.70%	62.50%	2.30%	2.63
45	Hypo6/4	81.01%	96.46%	97.02%	81.25%	2.99%	5.04
46	Hypo6/6	78.70%	96.46%	97.25%	75.00%	2.76%	3.76
47	Hypo6/9	80.16%	96.46%	97.59%	65.63%	2.41%	4.36
48	Hypo7/1	85.39%	96.46%	98.28%	46.88%	1.72%	4.71
49	Hypo7/2	84.63%	96.46%	98.28%	46.88%	1.72%	0.28
50	Hypo7/4	82.25%	96.46%	98.16%	50.00%	1.84%	5.36
51	Hypo7/7	61.00%	64.87%	97.78%	4.10%	2.22%	1.8
52	Hypo7/9	72.50%	94.22%	94.83%	84.38%	5.17%	0.32
53	Hypo8/2	89.23%	95.05%	96.59%	65.63%	3.41%	4.18

N	Pharmacophore Model	ROC[a]-AUC[b]	ACC[c]	SPC[d]	TPR[e]	FNR[f]	F-VALUE
54	Hypo8/4	72.88%	94.86%	95.09%	90.63%	4.92%	7.26
55	Hypo8/5	64.43%	96.46%	96.44%	96.88%	3.56%	6.8
56	Hypo2/10	80.13%	96.46%	96.56%	93.75%	3.44%	7.95
57	Hypo1/1	83.59%	96.46%	97.82%	59.38%	2.18%	5.56
58	**Hypo1/7**	**87.53%**	**96.46%**	**98.28%**	**46.88%**	**1.72%**	**11.74**
59	Hypo 3/3	64.07%	96.46%	97.02%	81.25%	2.99%	5.28
60	Hypo3/4	67.34%	96.46%	96.90%	84.38%	3.10%	2.98
61	Hypo4/1	80.67%	96.46%	96.44%	96.88%	3.56%	4.5
62	Hypo4/8	72.39%	96.46%	97.13%	78.13%	2.87%	7.42
63	Hypo5/9	84.18%	96.46%	98.39%	43.75%	1.61%	8.92
64	Hypo6/1	75.92%	96.46%	97.70%	62.50%	2.30%	4.4
65	Hypo6/4	82.26%	96.46%	96.33%	100.00%	3.67%	10.07
66	Hypo7/3	75.84%	96.46%	97.82%	59.38%	2.18%	6.44
67	Hypo7/6	69.60%	96.46%	96.90%	84.38%	3.10%	4.98
68	Hypo7/7	76.82%	96.46%	96.90%	84.38%	3.10%	2.4
69	Hypo7/9	82.01%	96.46%	98.97%	28.13%	1.03%	1.04
70	Hypo8/3	78.38%	96.46%	97.36%	71.88%	2.64%	1.13
71	Hypo4/10	77.35%	96.46%	96.67%	90.63%	3.33%	0.71
72	Hypo6/10	78.50%	96.46%	97.25%	75.00%	2.76%	4.11
73	Hypo1/2	86.26%	93.56%	93.33%	96.88%	6.67%	3.48
74	Hypo2/2	64.46%	98.84%	98.83%	100.00%	1.17%	9.19
75	Hypo4/1	73.44%	95.21%	100.00%	0.00%	0.00%	5.09
76	Hypo4/8	80.09%	94.50%	94.36%	96.88%	5.64%	8.03
77	Hypo4/9	77.69%	98.27%	98.24%	100.00%	1.76%	2.87
78	Hypo5/2	80.50%	95.05%	96.58%	65.63%	3.42%	6.75
79	Hypo5/7	0.00%	100.00%	100.00%	0.00%	0.00%	4.75
80	Hypo6/6	59.87%	98.61%	99.40%	42.86%	0.60%	6.67

N	Pharmacophore Model	ROC[a]-AUC[b]	ACC[c]	SPC[d]	TPR[e]	FNR[f]	F-VALUE
81	Hypo6/9	65.44%	98.89%	100.00%	0.00%	0.00%	6.12
82	Hypo7/9	69.88%	98.85%	99.83%	14.29%	0.17%	1.98
83	Hypo8/2	83.73%	94.73%	96.21%	68.00%	3.79%	5.16
84	Hypo8/4	83.22%	93.38%	93.57%	90.63%	6.43%	8.35
85	Hypo8/5	88.73%	99.18%	99.17%	100.00%	0.83%	2.63
86	Hypo2/10	87.58%	92.91%	92.36%	100.00%	7.64%	3.48
87	Hypo5/10	100.00%	100.00%	100.00%	100.00%	0.00%	4.83
88	Hypo6/10	87.16%	95.58%	96.67%	72.00%	3.33%	5.08
89	Hypo1/1	66.79%	96.46%	96.79%	87.50%	3.21%	1.04
90	Hypo1/9	75.82%	96.46%	96.44%	96.88%	3.56%	3.57
91	Hypo2/2	59.85%	96.46%	96.44%	96.88%	3.56%	5.39
92	Hypo2/8	68.26%	97.18%	97.27%	93.94%	2.73%	9.45
93	Hypo5/1	81.24%	96.46%	97.13%	78.13%	2.87%	8.15
94	Hypo5/6	74.25%	96.46%	96.33%	100.00%	3.67%	0.14
95	Hypo5/8	74.02%	95.02%	95.08%	93.75%	4.92%	3.79
96	Hypo5/9	0.00%	100.00%	100.00%	0.00%	0.00%	4.84
97	Hypo6/5	77.38%	98.86%	98.85%	100.00%	1.15%	9.04
98	Hypo6/7	60.82%	96.46%	99.31%	18.75%	0.69%	4.04
99	Hypo7/2	53.96%	96.46%	100.00%	0.00%	0.00%	3.39
100	Hypo7/4	79.44%	96.46%	97.02%	81.25%	2.99%	10.38
101	Hypo7/9	81.28%	96.46%	97.36%	71.88%	2.64%	3.13
102	Hypo8/6	79.42%	96.12%	97.19%	69.70%	2.81%	3.51
103	Hypo8/9	82.10%	96.36%	97.05%	78.13%	2.96%	3.73
104	Hypo1/10	72.18%	96.46%	96.33%	100.00%	3.67%	3.34

[a]**ROC**: receiver operating characteristic curve.
[b]**AUC**: area under the curve.
[c]**ACC**: overall accuracy.
[d]**SPC**: overall specificity.
[e]**TPR**: overall true positive rate.

In ROC analysis, the ability of a particular pharmacophore model to correctly classify a list of compounds as actives or inactives is indicated by the area under the curve (AUC) of the corresponding ROC as well as other parameters, namely, overall accuracy, overall specificity, overall true positive rate and overall false negative rate (see Receiver Operating Characteristic Curve Analysis for more details) (Verdonek *et al*., 2004, Irwin *et al.,* 2005 and Kirchmair *et al.,* 2008). Table 5 shows the ROC results of representative pharmacophores, while Figure 2 shows the ROC results of Hypo1/7 and merged Hypo2-1/2-6 together with the ROC behavior of its component models and optimally sterically-refined Hypo2-1/2-6.

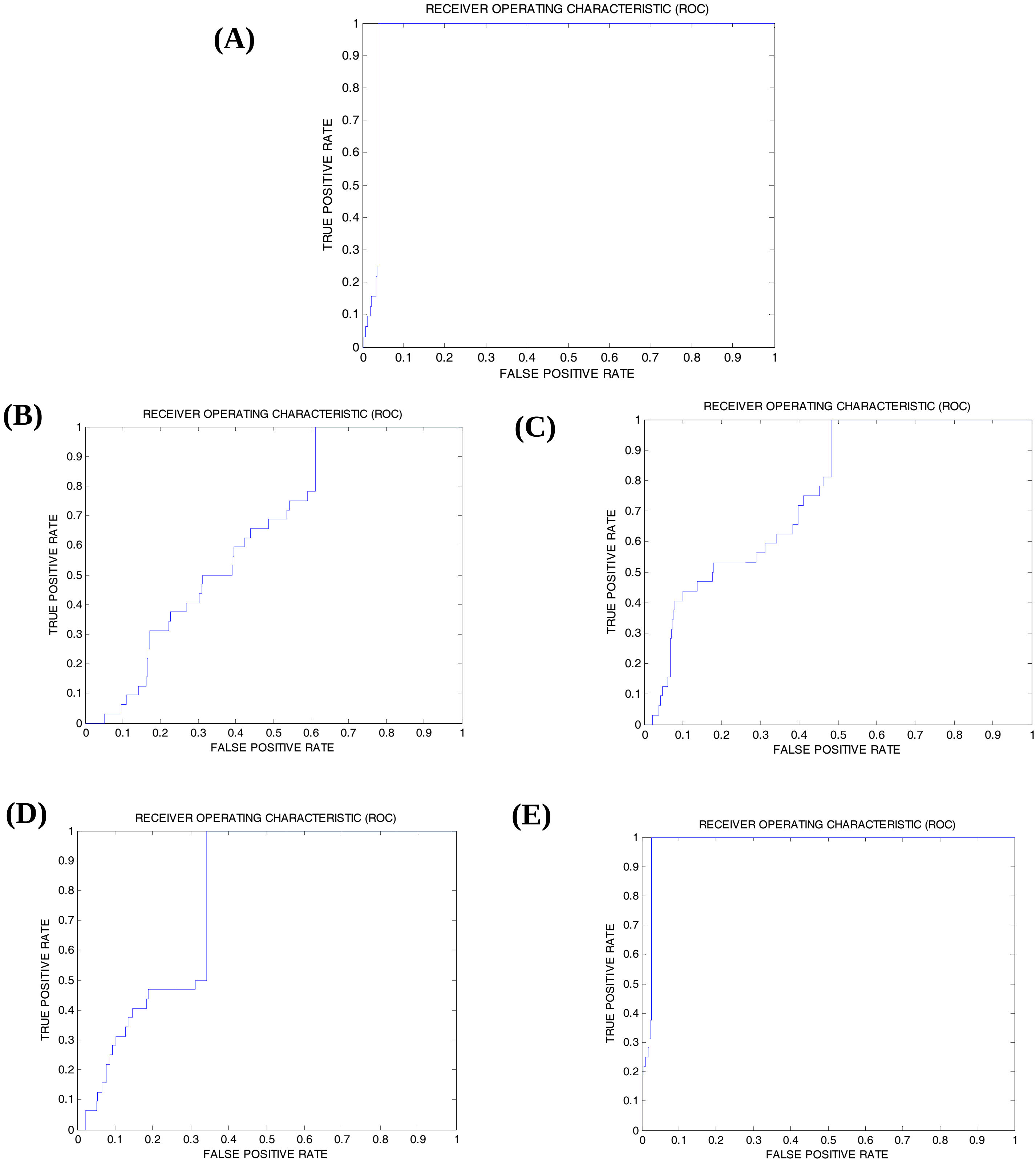


Figure 2: ROC curves of: **(A)** Hypo1/7, **(B)** Hypo1/2 **(C)** Hypo2/6, **(D)** Merged-Hypo21/26, **(E)** Sterically-Refined Merged Hypo2-1/2-6

Careful evaluation of Table 5 shows that model Hypo1/7 (generated in run 58 in Table 4) combined best ROC-AUC (Figure 2) and F-value (Table 5) prompting us to select this model as the best candidate for subsequent *in silico* screening. Furthermore, close scrutiny of the 104 representative models shows that two models, namely, Hypo2/1 and Hypo2/6, share three pharmacophoric features (types and positions) prompting us to merge them in a single pharmacophore model (Hypo2-1/2-6), as shown in figure 4. The new merged model was found to possess superior ROC-AUC compared to the original hypotheses (i.e., 77.5% compared to 64 % and 75.9 %, respectively). The ROC-AUC of the merged model Hypo2-1/2-6 was further improved by addition of exclusion spheres. Gradual addition of exclusion spheres enhanced the ROC-AUC of the merged model from 77.5% to become 98% upon addition of 50 exclusion spheres (Table 6), prompting us to use this sterically refined hybrid model as a second model for *in silico* search. Table 7 shows the X, Y and Z corrdinates of the optimal models employed for *in silico* search.

Table 6: ROC analyses of hybrid model Hypo2-1/2-6 and its sterically-refined versions

Pharmacophore Model	ROC-AUC	ACC	SPC	TPR	FNR
Hypo2-1/2-6	77.38%	96.46%	98.16%	50.00%	1.84%
Hypo2-1/2-6 (10 ExVol[a])	91.21%	96.46%	98.39%	43.75%	1.61%
Hypo2-1/2-6 (20 ExVol[a])	92.81%	96.46%	98.51%	40.63%	1.49%
Hypo2-1/2-6 (30 ExVol[a])	94.66%	96.46%	98.51%	40.63%	1.49%
Hypo2-1/2-6 (40 ExVol[a])	92.81%	96.46%	98.51%	40.63%	1.49%
Hypo2-1/2-6 (50 ExVol[a])	97.95%	96.46%	98.62%	37.50%	1.38%

[a]Exclusion spheres added *via* HipHop-Refine module of CATALYST.

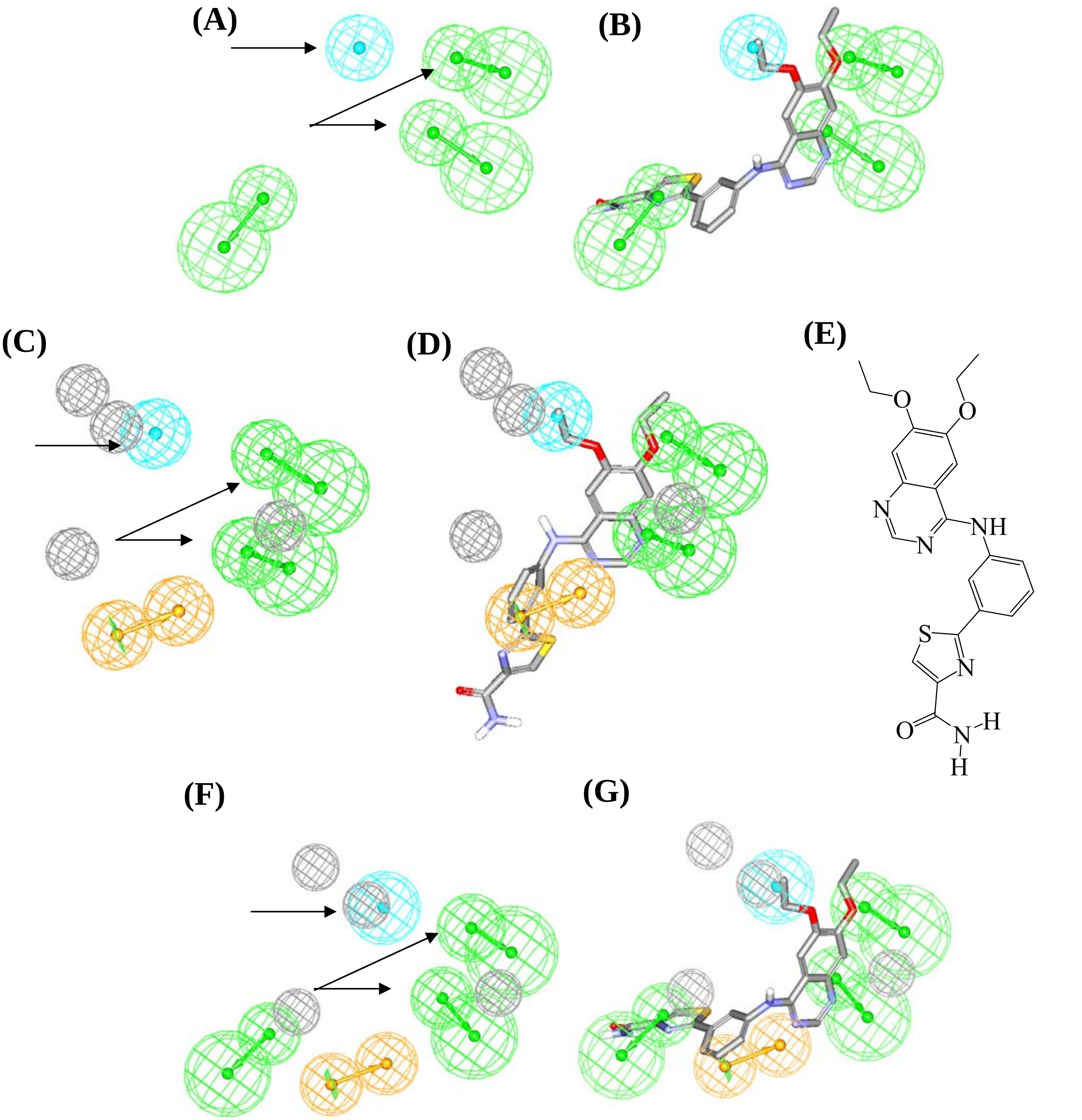


Figure 3 (A), (C) and **(F)** show the pharmacophoric features of Hypo2/1, Hypo2/6 and merged Hypo2-1/2-6, respectively, HBA as green vectored spheres, Hbic as blue spheres, and RingArom as orange vectored spheres. Arrows point to common features between Hypo2/1and Hypo2/6 allowing pharmacophore merging. **(B), (D)** and (**G**) show Hypo2/1, Hypo2/6 and merged Hypo2-1/2-6, respectively, fitted against **48** (IC_{50} = 0.93 μM, table1), **(E)** chemical structure of **48**.

Table 7: Pharmacophoric features and corresponding weights, tolerances and 3D coordinates of Hypo1/7 and Hypo2-1/2-6.

Model	Definition		Chemical Features						
			HBA		**HBA**		**Hbic**	**Hbic**	**Hbic**
Hypo1/7[a]	Weights		1.80		1.80		1.80	1.80	1.80
	Tolerances		1.6	2.2	1.6	2.2	1.6	1.6	1.6
	Coordinates	X	5.406	3.254	2.482	1.725	-0.034	3.79	1.35
		Y	4.945	3.596	1.502	3.467	0.432	-0.717	-3.411
		Z	9.021	10.618	2.54	4.677	2.257	3.922	0.91

Model	Definition										
			HBA		**HBA**		**HBA**		**Hbic**	**RingArom**	
Hypo21/26[b]	Weights		2.7		2.7		2.7		2.43	2.43	
	Tolerances		2.2	1.6	2.374	1.741	1.6	2.2	1.871	1.6	1.6
	Coordinates	X	-6.212	-5.609	-1.688	-1.865	-12.232	-15.074	-3.628	-9.921	-12.402
		Y	5	2.969	3.234	1.03	1.531	0.632	-2.219	1.288	0.462
		Z	-3.82	-1.696	-3.07	-1.06	4.033	4.365	2.573	-1.697	-0.227

[a]Hypo1/7: the 7th pharmacophore hypothesis generated in the 1st HYPOGEN run (Table 4).
[b]Hypo2-1/2-6: the merged pharmacophore hypothesis generated from the 2nd HYPOGEN run (Table 4).

3.4 Addition of Exclusion Volumes

Although ligand-based pharmacophores can probe ligand/macromolecule recognition and are useful as 3D search queries, they suffer from a major drawback: They lack steric constrains necessary to define the size of the binding pocket This liability renders pharmacophoric models rather promiscuous in some cases (Fischer *et al.,* 1966). This trend was particularly apparent with the hybrid model Hypo2-1/2-6. Therefore, we decided to complement this pharmacophore with exclusion spheres employing the HipHop-Refine module implemented within CATALYST (Catalyst User Manual, 2005). Excluded volumes resemble sterically inaccessible regions within the binding site (see Addition of Exclusion Volumes) (Clement *et al.,* 2000). A structurally diverse training subset was selected for HipHop-Refine-based addition of exclusion spheres on Hypo2-1/2-6, as in Table 8.

Table 8**: Hip-Hop steric refinement list for merged Hypo2-1/2-6**

Compound	Principal Value	MaxOmitFeat
6	0	0
7	0	2
8	2	0
10	0	1
12	2	1
13	0	1
14	0	2
17	0	2
20	0	0
21	0	2
23	0	2
25	0	2
26	0	2
27	0	2
28	0	2
29	0	2
31	0	2
35	2	1
36	0	0
45	2	1
48	2	1
49	2	0
50	2	1
51	2	1
56	2	0
57	2	1
65	2	0
67	2	1
69	2	1
70	2	0
71	0	2
73	2	1
78	2	0
84	2	1
85	2	1
90	2	0
95	2	1
96	2	1
97	2	1
113	2	1
117	2	1
118	2	0
119	0	0
120	0	0
121	0	0
133	0	0

The training compounds were selected in such away that the bioactivities of weakly active compounds are explainable by steric clashes within the binding pocket However, to identify the optimal number of exclusion spheres, we decided to explore the effect of increasing number of exclusion spheres on the ROC curves of the corresponding pharmacophoric sterically-refined variations. We noticed that the ROC-AUC increased with increasing number of exclusion spheres until it plateaued at 98% corresponding to 50 or more exclusion spheres. Table 3 summarizes the results of the exploration process. Figure 4 shows the sterically refined version of Hypo2-1/2-6 and how it fits one of the potent training compounds.

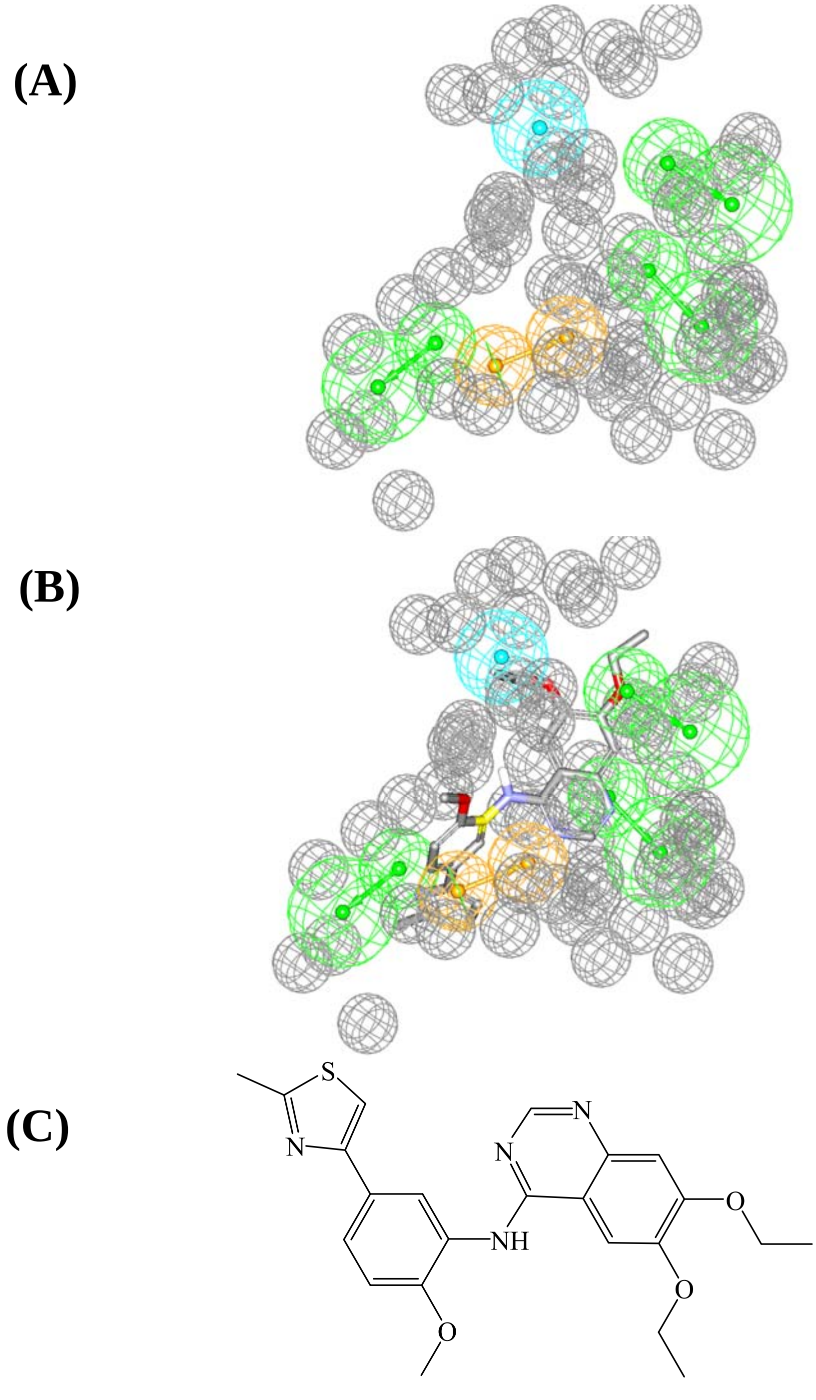


Figure 4: **(A)** Shows sterically refined Hypo2-1/2-6, **(B)** Sterically-refined Hypo2-1/2-6 co-crystallized with **48**, and **(C)** Chemical Structure of **48**.

3.5 Comparison of Pharmacophore Model with the Allosteric Binding Site of FBPase

To further emphasize the validity of our pharmacophore modeling approach, we compared a crystallographic structure of FBPase (code: 2FIX, resolution 3.50 Å) complexed with a potent ligand (PDB code: **870**, IC_{50} = 0.57 μM) with the way this ligand maps Hypo1/7. Figure 5 shows the chemical structure of the ligand and compares its FBPase complex with how it maps Hypo1/7 employing rigid mapping, i.e., fitting the ligand's bound state against the pharmacophore without conformational adjustments.

(A)

(B)

(C)

(D)

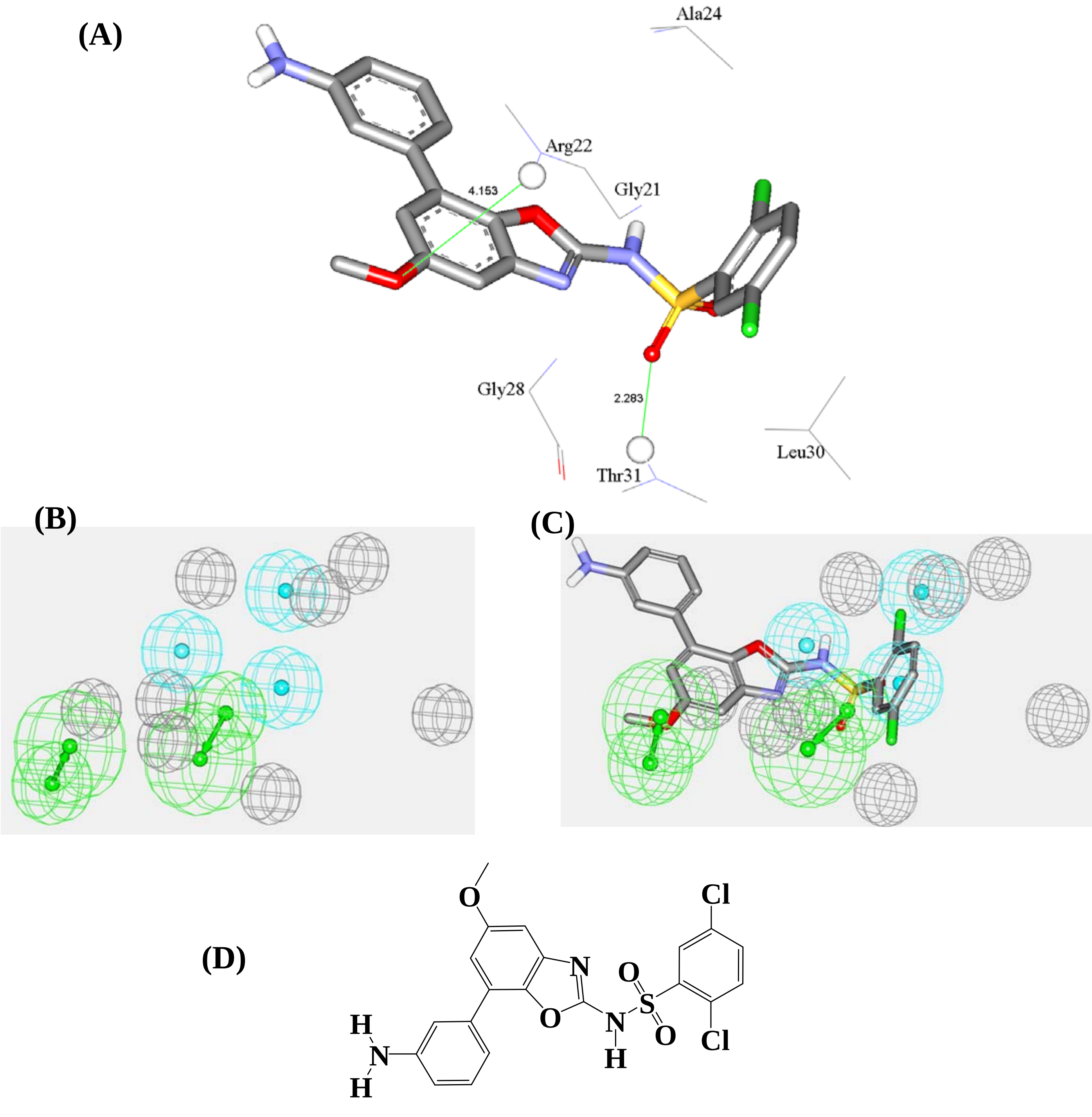


Figure 5: (A) Co-crystal structure of FBPase (code: 2FIX, resolution 3.50 Ǻ) complexed with potent FBPase inhibitor (PDB code: **870**, IC_{50} = 0.57 μM). **(B)** Pharmacophoric features of Hypo1/7: HBA as green vectored spheres, Hbic as blue spheres, **(C)** Hypo1/7 fitted against **870** employing rigid mapping (i.e., without allowing conformational flexibility), **(D)** Chemical structure of **870.**

Furthermore, we compared another FBPase co-crystallized complex (code: 2FIE, resolution 2.81 Å) with the pharmacophoric features of the hybride pharmacophore Hypo2-1/2-6 and the way it maps the corresponding complexed ligand (A74, IC_{50} = 3.5 μM), as shown in Figure 6. Hydrogen bonding interactions connecting the SO_2 of the ligand with the amidic NH atoms of Leu30 (via bridging water molecule) and Thr31 (Figure 6 A) correlate with fitting the SO_2 functionality against two HBA features in Hypo2-1/2-6 (Figure 6 C). Similarly, mapping the ligand's pyridyl nitrogen against HBA feature in Hypo2-1/2-6 (Figure 6 C) seems consistent with hydrogen-bonding interaction tying this nitrogen with the amidic carbonyl of Thr27 via a bridging water molecule (H_2O108, Figure 6 A). In the same context, mapping the chloro substituent of the ligand against Hbic feature in Hypo2-1/2-6 (Figure 6 C) agrees with hydrophobic interactions connecting this group with the adjacent methyl of Ala24 (Figure 6 A). Finally, the suboptimal mapping of the benzoxazole ring of the ligand against a RingArom feature in Hypo2-1/2-6 (Figure 6 C) agrees with stacking this aromatic ring against the hydrophobic linker of Arg22 (propylene, Figure 6A). Mapping the aromatic methoxy against HBA in Hypo1/7 corresponds to hydrogen-bonding connecting the aromatic methoxy of the ligand the NH of Arg22 (Figure 6 A and C). Similarly mapping the SO_2 of the ligand against HBA feature in Hypo1/7 agrees with Hydrogen-bonding connecting the ligand's sulfone group with the peptidic NH of Thr31 (Figure 6 A and C). On the other hand, mapping the dichlorobenzene fragment of the ligand against two Hbic features seems to correspond to placing this fragment within a hydrophobic pocket comprised of the side chains of Ala24, Gly21 and Leu30 in the crystallographic complex (Figure 6 A and C). Finally, mapping part of the oxazole ring of the ligand against Hbic feature encodes for hydrophobic interactions connecting the carbon of this fragment with the methyl side chain of Gly21 (Figure 6 A and 6 C).

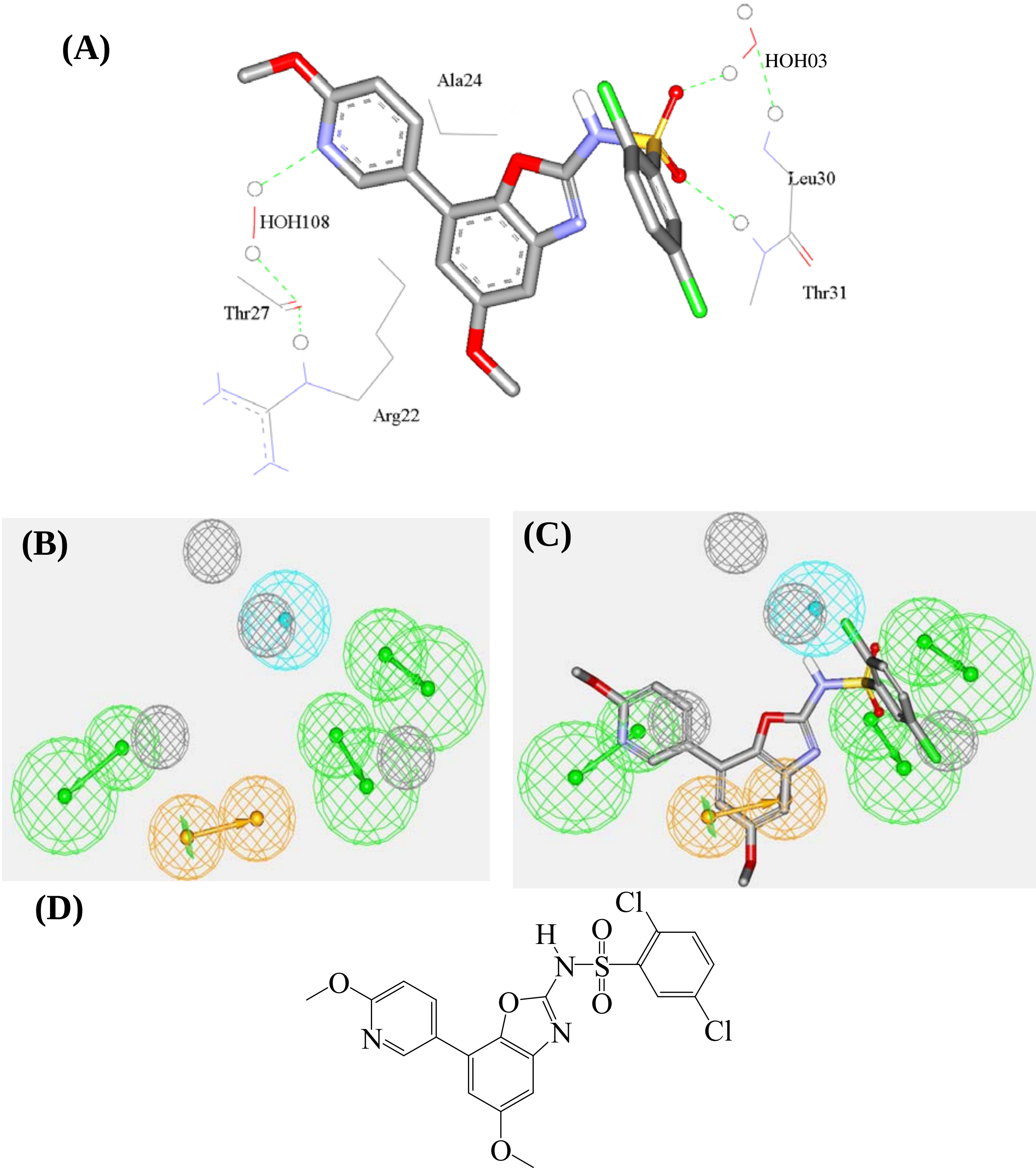


Figure 6: **(A)** Co-crystalline structure of FBPase (PDB code: 2FIE, resolution 2.81 Å) complexed with potent ligand (PDB code: **A74**, IC_{50} = 3.5 μM, table 1) (Gum *et al.*, 2006). **(B)** Pharmacophoric features of merged Hypo2-1/2-6: HBA as green vectored spheres, Hbic as blue spheres, RingArom as vectored orange spheres, **(C)** Hypo2-1/2-6 fitted against **A74**, **(D)** Chemical structure of **A74**

Clearly from the above discussion, Hypo1/7 and Hypo2-1/2-6 represent two valid binding modes assumed by ligands within FBPase. Furthermore, these models point to limited number of critical interactions required for high ligand-FBPase affinity in each of the binding modes. In contrast, crystallographic complexes reveal many bonding interactions without highlighting critical ones.

3.6 *In-Silico* Screening and Subsequent *In vitro* Evaluation

Hypo1/7 and sterically-refined Hypo2-1/2-6 were employed as 3D search queries against the NCI library (238,819 structures) using the "Best Flexible Database Search" option implemented within CATALYST. Compounds that have their chemical groups spatially overlap (map) with corresponding features of the particular pharmacophoric model were captured as hits. Table 9 summarizes the numbers of captured hits by sterically-refined versions of the pharmacophores.

Table 9: Numbers of captured hits by sterically-refined versions of Hypo1/7 and Sterically-Refined Hypo2 1/2-6

		Pharmacophore models	
3D Database[a]	**Post screening filtering[b]**	**Hypo1/7**	**Sterically-Refined Hypo2-1/2-6**
NCI	**Before**	**602**	**999**
	After	**365**	**103**

[a]NCI: national cancer institute list of available compounds (238,819 structures),
[b]Using Lipinski's and Veber's rules.

NCI hits were filtered based on Lipinski's and Veber's rules (Lipinski *et al.*, 2001 and Veber *et al.*, 2002). Enforcing some kind of drug-likeness pre-filters on virtual hits should help in finding hits more amenable for subsequent optimization into leads.

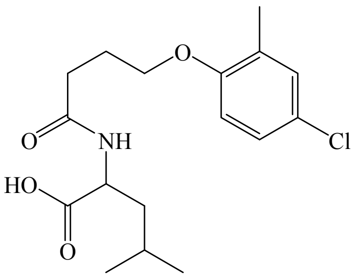
Surviving hits were fitted against Hypo1/7 and Hypo2-1/2-6. Hits exhibiting summation of fit against both models ≥ 3.0 were evaluated *in vitro* against human recombinant FBPase. The bioassay is an established enzyme coupled assay that measures the amount of inorganic phosphate released by the activity of human FBPase (Lanzetta *et al*., 2006) To validate our bioassay settings, we determined the IC_{50} value of standard inhibitor AMP under the same conditions. Our conditions determined the IC_{50} value of AMP to be 12.3 µM, which is close to the reported literature value of 25 µM (determined by UV spectrophotmetry).

Initially, hits were screened at 10 µM concentrations, subsequently; compounds of FBPase inhibitory percentages ≥ 60% at 10 µM were further assessed to determine their IC_{50} values. Table 10 and Figure show active hits and their corresponding estimated and experimental FBPase bioactivities. Figure shows the dose-response curves of active hits.

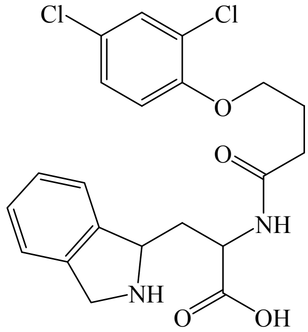
Table 10: Experimental bioactivities of high-ranking hit molecules.

Hits[a]		**Best Fit values[b]**		**Experimental anti-FBPase Bioactivities**	
Compound	**NCI code**	**Hypo1/7**	**Sterically-Refined Hypo2-1/2-6**	**%Inhibition at 10 μM**	**IC_{50} (μM)[c,d]**
137	NCI00 16760	5.05	4.33	60	2.44 (0.97)[e]
138	NCI00 16768	5.11	4.52	67	5.88 (1.00)[f]
139	NCI00 81750	4.62	0.00	NA[g]	
140	NCI00 90952	5.76	0.00	77	3.46 (1.00)[f]
141	NCI0 134227	7.85	0.00	37	ND[h]
142	NCI0 143140	8.95	0.41	87	0.33 (1.00)[f]
143	NCI0 187542	0.00	5.90	81	3.80 (1.00)[f]
144	NCI0 204387	8.43	0.00	100	0.15 (0.99)[e]
145	NCI0 208708	5.48	0.00	74	2.23 (0.96)[e]
146	NCI0 211543	6.41	0.00	100	0.25 (0.97)[e]
147	NCI0 292941	0.00	6.33	100	0.70 (0.94)[e]
148	NCI0 318214	5.51	6.98	NA[g]	
149	NCI0 371439	3.41	0.00	76	0.32 (1.00)[f]
150	NCI0 403576	5.40	0.00	100	1.65 (1.00)[f]
151	NCI0 409025	2.45	6.53	69	6.02 (1.00)[f]
152	NCI0 518963	6.98	0.00	87	0.90 (0.96)[e]
153	NCI0 610648	4.55	4.33	NA[g]	
	AMP[i]	----	----	12.3 (0.99)[f]	

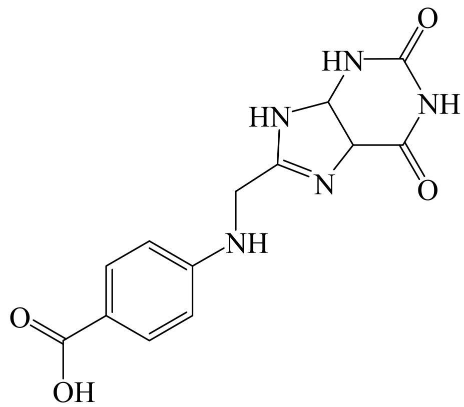
[a]Chemical structures shown in figure 6. [b]Fit values calculated against respective hypotheses using equation (D, [c]Experimental IC_{50} values determined at 10, 1, and 0.1 μM inhibitor concentrations, [d]Values in brackets represent the correlation coefficients of the corresponding dose-response curve, [e]dose-response data were against linear function. [f]Fitting was performed using Graph Pad Prism (version5.04) via fitting against sigmoidal dose-inhibition model, [g]not active (NA), [h]not determined (ND), [i]Adenosine Monophospahe (AMP) standard inhibitor



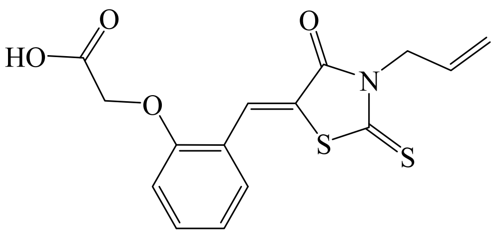
137



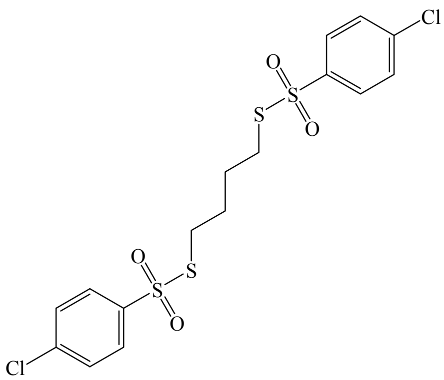
138



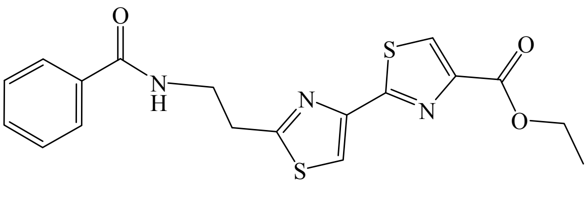
139



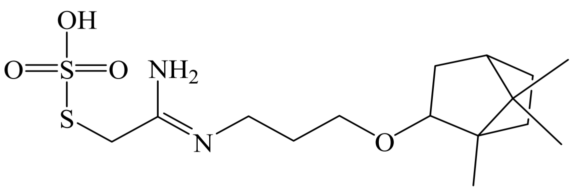
140



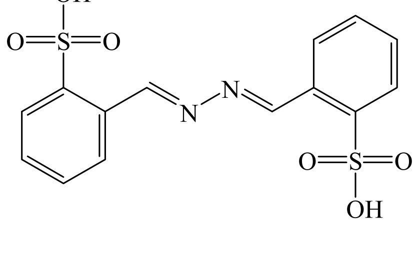
141



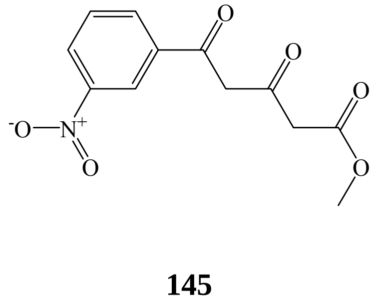
142



143

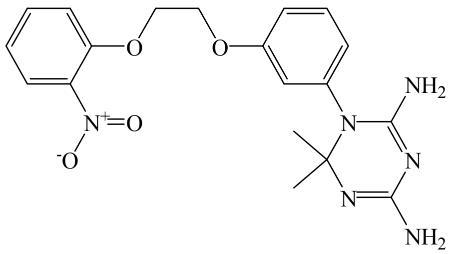


144

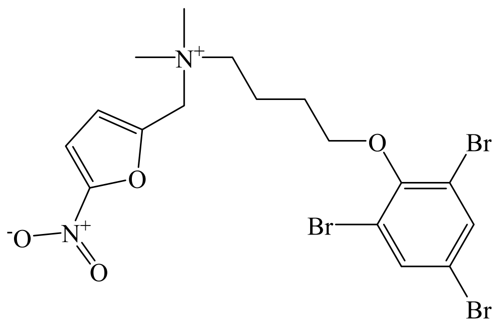


145

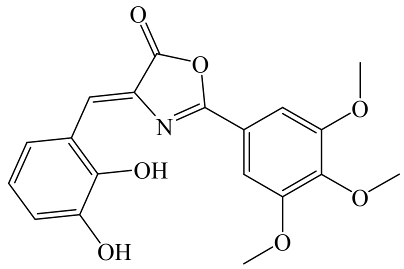
Figure 7: Chemical structure of active hits



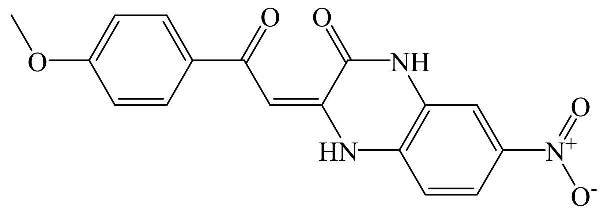
146



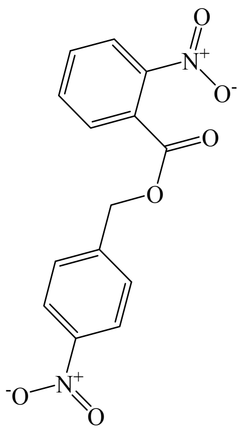
147



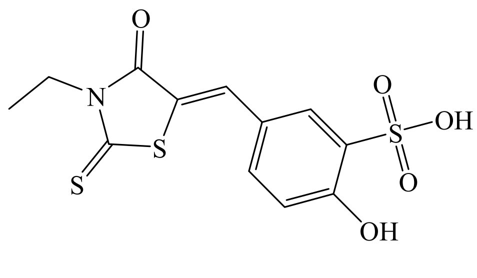
148



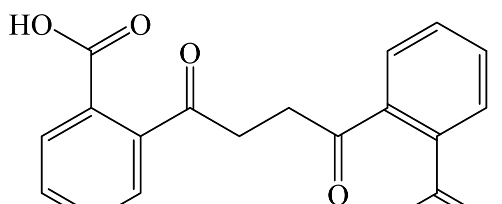
149



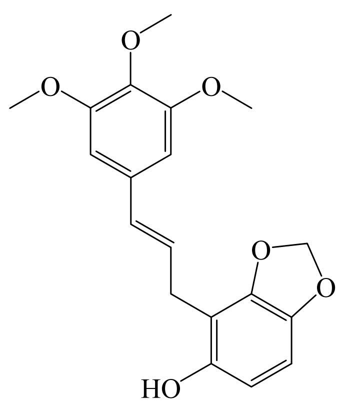
150



151



152



153

Figure 8: Chemical structure of active hits

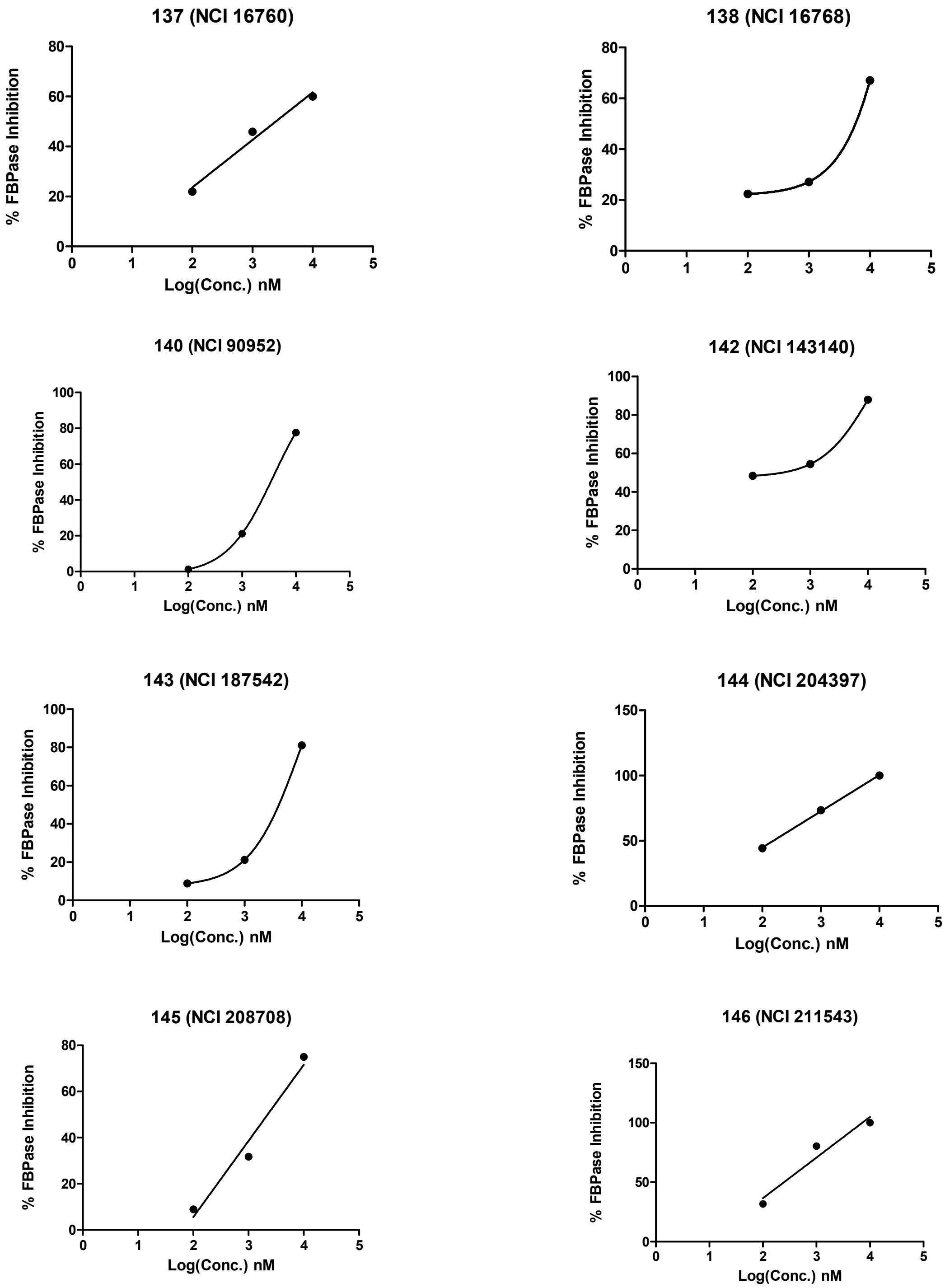


Figure 8: Dose-response plots of active hits: **137**, **138**, **139**, **140**, **141**, **142**, **143**, **145**, **146**, **147**, **148**, **149**, **150**, **151**, **152** and **153**. Data fitting was performed using GraphPad Prism (version 5.04) via fitting against linear and sigmoidal dose-inhibition model.

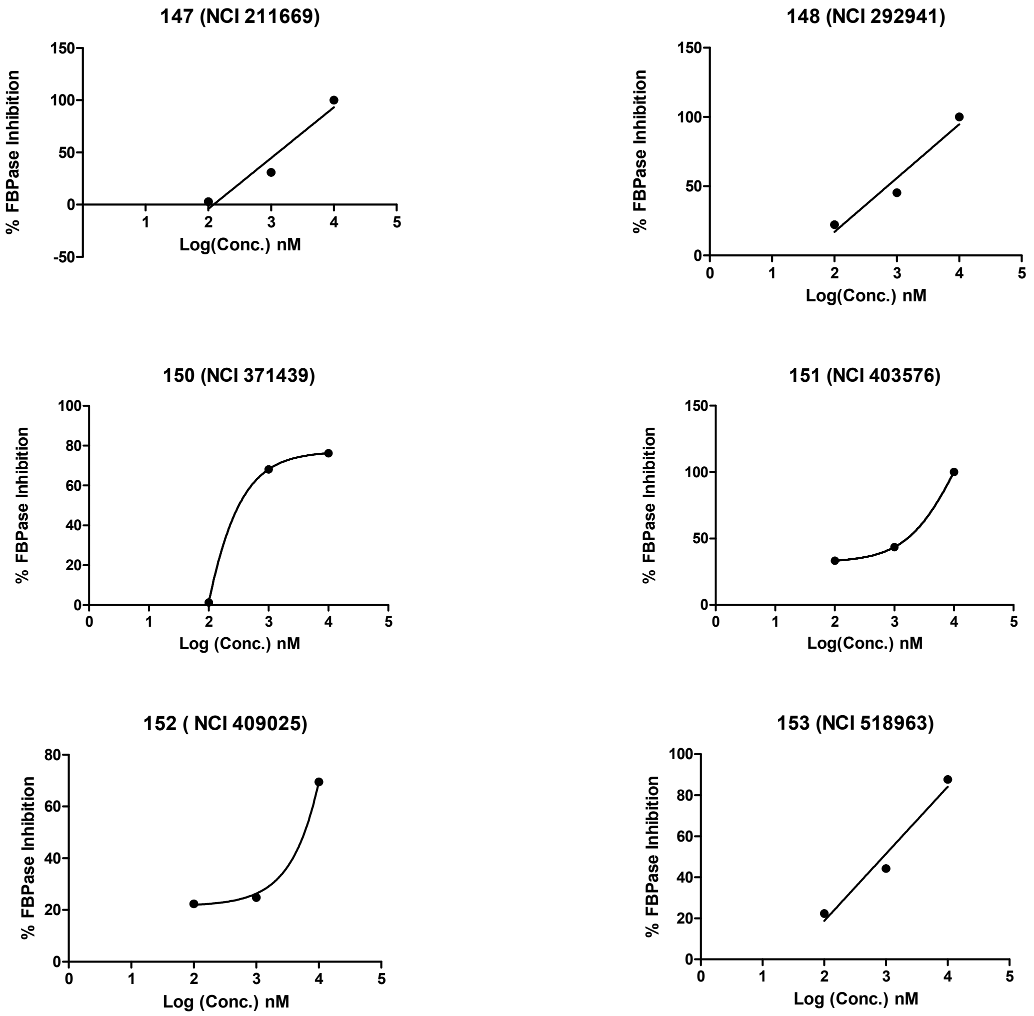


Figure 9: Dose-response plots of active hits: **137**, **138**, **139**, **140**, **141**, **142**, **143**, **144, 145**, **146**, **147**, **148**, **149**, **150**, **151**, **152** and **153**. Data fitting was performed using GraphPad Prism (version 5.04) via fitting against linear and sigmoidal dose-inhibition models.

Clearly from the table and figures, *in vitro* testing showed that 13 NCI high-ranking hits possess submicromolar to low micromolar inhibitory profiles against FBPase, while the rest were found weakly active or inactive.

3.7 Pharmacophore-Guided Synthesis of Novel FBPase inhibitors

Clearly, both optimal pharmacophores, i.e., Hypo2-1/2-6 and Hypo1/7, share opposing hydrogen-bonding terminals (HBAs) separated by hydrophpobic linker regions. This trend can be clearly seen in potent hits captured by our in silico screening protocol, e.g., **144**

(IC_{50}=0.15μM), **150** (IC_{50}=1.65μM) and **152** (IC_{50}=0.9μM). These facts prompted us to explore a set of aryl amides substituted with opposing hydrogen-bond forming regions as potential inhibitors of FBPase.

Amides combine two advantages: (i) facile preparation, and (ii) accessibility to diverse functionalization necessary to satisfy the feature-rich nature of optimal pharmacophores. Accordingly, we prepared 20 amide analogues and tested their bioactivities against FBPase. Table 10 shows the prepared compounds and their experimental bioactivities. The bis-*p*-nitro-phenyl-*m*-phenylene diamide derivative **164** (Table 10) was the most potent with IC_{50} value 1.16 μM. Figure 9 shows how **164** fits the optimal pharmacophore models Hypo2-1/2-6 and Hypo1/7, while Table 10 shows the structures of the prepared compounds, their fit values against both models as well as their bioacitivites against FBPase.

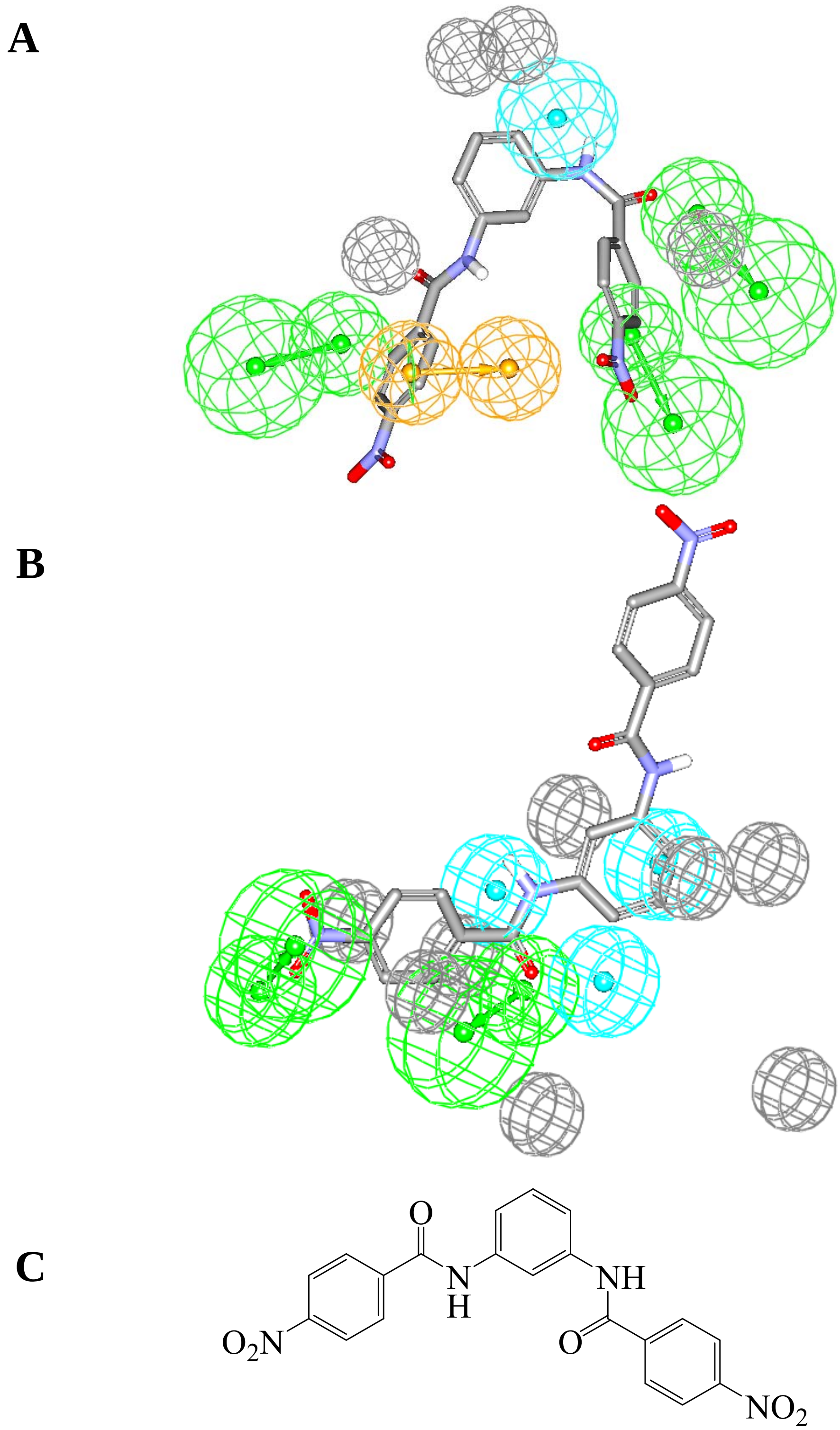


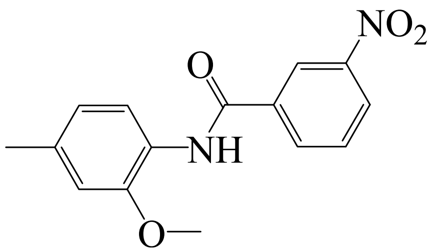
Figure 9: Fitting the most potent synthetic derivative **164** (IC_{50} = 1.16 μM) against **(A)** Hypo1/7, and **(B)** Hypo2-1/2-6, **(C)** The chemical structure of **164**.

Unfortunately, only 4 prepared compounds illustrated micromolar IC_{50} values. The rest were inactive. We believe this behavior is either because the prepared compounds lacked the opposing hydrogen-bond forming regions, e.g., **156**, **165**, **169**, **170**, **171**, or because the separating distances between these regions is suboptimal, e.g., **154**, **155**, **157**, **158**, **159**, **160**, **161**, **162**, **166**.

Syntheses were performed via coupling several anilines or phenol derivatives with acid chlorides or sulfonamides, as outlined in Schemes 1 and 2. The reactions were either performed at room temperature in acetone to give the mono-amide, diamide or diester substituted derivatives (**155-164**, **167-172**) 22.3-86.8 % yields, or refluxed in pyridine (**166**, **173-174**), 49-86% yields.

The following compounds were prepared according to general procedure:

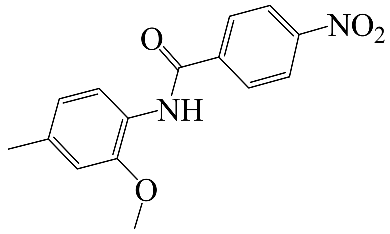
N-(2-Methoxy-4-methyl-phenyl)-3-nitro-benzamide (154)



This compound was prepared from *m*-nitrobenzoyl chloride (3.66 g, 20 mmol) and 3-Methoxy-4-methyl-aniline (1.35 g, 10 mmol) to yield **154** as yellow powder (2.23 g, 80%); mp 95–96 ^oC; IR (KBr): ν_{max} = 3400, 1680, 1580, 1530 cm^{-1}, ^{1}H-NMR (DMSO-d_6): δ = 2.23 (s, 3H, CH_3), 3.76 (s, 3H, OCH_3), 6.97 (m, 2H), 7.45 (s, 1H), 7.79 (t, 1H), 8.38 (ddd, J_1 = 7.84, J_2 = 1.44, J_3 = 1.41 Hz, 2H), 8.72 (d, J = 1.79, 1H), 9.88 (s, 1H, CONH).; ^{13}C NMR (75 MHz, DMSO-d6): δ = 20.75 (CH_3), 56.24 (OCH_3), 111.93 (CH), 124.08 (CH), 126.02 (CH), 126.43 (CH), 127.08 (CH), 129.51 (CH), 129.57 (C), 140.77 (C), 149.62 (C), 150.34 (C), 164.06 (C=O) ppm. HRMS-FAB m/z $[M + Na]^+$ calcd for $C_{15}H_{14}N_2O_4$:

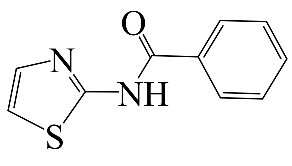
285.08753, found: 285.08808. Anal. Calcd for $C_{15}H_{13}N_2O_4$: C: 62.93, H: 4.93 N: 9.79 found: C: 60.29, H: 4.37, N: 9.42.

N-(2-Methoxy-4-methyl-phenyl)-4-nitro-benzamide (155)



This compound was prepared from *p*-nitrobenzoyl chloride (3.66 g, 20 mmol) and 2-Methoxy-4-methyl-aniline (1.35 g, 10 mmol) to yield **155** as yellow powder (1.49 g, 53%); mp 151-157°C; IR (KBr): ν_{max} = 3350, 1700, 1580-1560, 1540 cm^{-1}, ^{1}H-NMR (DMSO-d_6): δ = 2.23 (s, 3H, CH_3), 3.76 (s, 3H, OCH_3), 6.97 (t, , J_1 = 2.19, J_2 = 8.59 Hz, 2H), 7.51 (s, 1H), 8.15 (d, *J* = 8.58 Hz, 2H), 8.33 (d, *J* = 8.65 Hz, 2H), 8.58 (d, 1H), 8.72 (d, 2H), 9.76 (s, 1H, CONH).;^{13}C NMR (75 MHz, DMSO-d6): δ = 20.69 (CH_3), 56.18 (OCH_3), 111.95 (CH), 122.895 (CH), 126.50 (CH), 126.55 (CH), 127.18 (CH), 130.67 (CH), 134.40 (C), 136.51 (C), 148.28 (C), 150.65 (C), 163.66 (C=O) ppm. HRMS-FAB m/z $[M + Na]^+$ calcd for $C_{15}H_{14}N_2O_4$: 285.08753, found: 285.08808. Anal. Calcd for $C_{15}H_{13}N_2O_4$: C: 62.93, H:4.93 N: 9.79 found: C: 62.61, H: 4.32, N: 9.54.

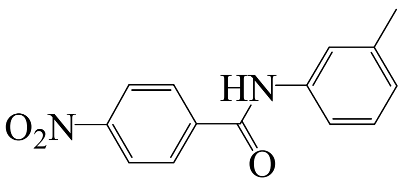
N-Thiazol-2-yl-benzamide (156)



This compound was prepared from benzoyl chloride (3.66 g, 20 mmol) and 2-aminothiazole (3.66 g, 20 mmol) to yield **156** as white crystals (0.85 g, 24.13%); Mp 146-

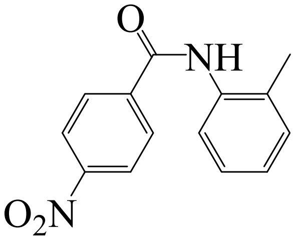
152 °C. IR (KBr): ν_{max} = 1700, 1540 cm^{-1}, ^{1}H-NMR (DMSO-d_6): δ = 7.24 (s, 2H), 7.48 (m, 3H), 8.05 (m, 2H), 12.60 (s, 1H, CONH).^{13}C-NMR (DMSO-d_6): δ = 114.34 (CH), 128.63 (CH), 129.06 (CH), 132.677 (C), 133.01 (CH), 138.08 (CH), 159.25 (C), 165.58 (C). HRMS (EIMS) *m/z*: calcd. for $C_{10}H_7N_2OS$ [M - H]$^+$ 203.02901, found 203.02846. Anal. Calcd. for $C_{10}H_8N_2OS$: C, 58.80; H, 3.95; N, 13.72, Found: C, 59.68; H, 3.22; N, 139.95%

4-Nitro-N-*m*-tolyl-benzamide (157)



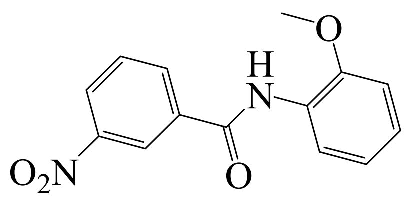
This compound was prepared from *p*-nitrobenzoyl chloride (3.66 g, 20 mmol) and 3-methylaniline (1.2 g, 10 mmol) to yield **157** as yellow crystal (1.05 g, 39%); mp 148-152 °C; IR (KBr): ν_{max} = 3280, 1660, 1580, 1540-1520 cm^{-1}, ^{1}H NMR (300 MHz, DMSO-d6): δ = 2.3 (s, 3H, CH_3), 6.9 (d, J= 7.49, 2H), 7.2 (t, 1H), 7.5 (t, 1H), 8.1 (m, 2H), 8.3 (m, 2H), 10.5 (s, 1H, CONH) ppm.^{13}C NMR (75 MHz, DMSO-d6): δ = 21.47 (CH_3), 118.14 (CH), 121.48 (CH), 124.05 (CH), 125.37 (CH), 129.06 (CH), 129.68 (CH), 138.40 (C), 139.116 (C), 141.16(C), 149.60 (C), 164.3 (CO) ppm. HRMS-FAB m/z [M + H]$^+$ calcd for $C_{14}H_{11}N_2O_3$: 255.07697 found 255.07751. Anal. Calcd for $C_{14}H_{12}N_2O_3$: C: 65.62, H: 4.72, N: 10.93 found: C: 64.93, H: 4.467, N: 10.709.

4-Nitro-N-*o*-tolyl-benzamide (158)



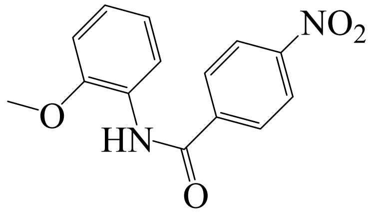
This compound was prepared from *p*-nitrobenzoyl chloride (3.66 g, 20 mmol) and 2-methylaniline (1.2 g, 10 mmol) to yield **158** as yellow crystals (0.46 g, 17%); mp 158-163 ^{o}C; IR (KBr): ν_{max} = 3250, 1660, 1580, 1540-1520 cm^{-1},^{1}H NMR (300 MHz, DMSO-d6): δ = 3.3 (s, 3H), 7.2 (m, 4H), 8.2 (d, *J* = 8.75, 2H), 8.3 (d, *J* = 8.86 , 2H), 10.2 (s, 1H, CONH) ppm.;^{13}C NMR (75 MHz, DMSO-d6): δ = 18.36 (CH_3), 124.11 (CH), 126.60 (CH), 126.88 (CH), 127.09 (CH), 129.66 (CH), 130.92 (CH), 134.27 (C), 136.37 (C), 140.73 (C), 149.73 (C), 164.26 (CO) ppm. HRMS-FAB m/z $[M + H]^+$ calcd for $C_{14}H_{11}N_2O_3$: 255.07697 found 255.07752. Anal. Calcd for $C_{14}H_{12}N_2O_3$: C: 65.62, H: 4.72, N: 10.93 found: C: 65.97, H: 4.58, N: 10.11.

N-(2-Methoxy-phenyl)-3-nitro-benzamide (159)



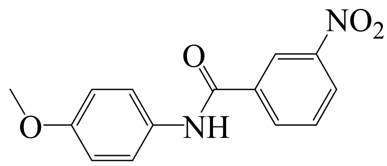
This compound was prepared from *m*-nitrobenzoyl chloride (3.66 g, 20 mmol) and 2-methoxyaniline (1.2 g, 10 mmol) to yield **159** as white crystals (2.13 g, 79.96%); Mp 140-149 ^{o}C. IR (KBr): ν_{max} = 3315, 1660, 1620-1580, 1520-1510 cm^{-1}, ^{1}H-NMR (DMSO-d_6): δ = 3.80 (s, 3H, OCH_3), 6.95 (t, 1H), 7.08 (dd, J_1 = 1.20, J_2 = 1.16 Hz, 1H), 7.20 (t, 1H), 7.63 (dd, J_1 = 1.48, J_2 = 1.48 Hz, 1H), 7.79 (t, 1H), 8.39 (t, 2H), 8.73 (t, 1H), 9.92 (s, 1H, CONH). ^{13}C-NMR (DMSO-d_6): δ = 56.18 (OCH_3), 112.13 (CH), 120.69 (CH), 122.97 (CH), 125.98 (CH), 126.60 (CH), 126.71 (CH), 127.03 (C), 130.70 (CH), 134.47 (CH), 136.49 (C), 148.29 (C), 152.74 (C), 163.71 (C). HRMS (EIMS) *m/z*: calcd. for $C_{14}H_{11}N_2O_4$ $[M - H]^+$ 271.07188, found 271.07243. Anal. Calcd. for $C_{14}H_{12}N_2O_4$: C, 61.76; H, 4.44; N, 10.29, O, 23.51. Found: C, 61.33; H, 4.22; N, 10.11%

N-(2-Methoxy-phenyl)-4-nitro-benzamide (160)



This compound was prepared from *p*-nitrobenzoyl chloride (3.66 g, 20 mmol) and 2-methoxyaniline (1.2 g, 10 mmol) to yield **160** as yellow crystals (2.09g, 78.33%); Mp 146-149 ^{o}C (Lit. 146-148).IR (KBr): ν_{max} = 3280, 1660, 1590, 1520 cm^{-1}, ^{1}H-NMR (DMSO-d$_6$): δ = 3.80 (s, 3H, OCH$_3$), 6.95 (t, 1H), 7.08 (d, *J* = 7.64 Hz, 1H), 7.19 (t, 1H), 7.68 (d, *J* = 7.17 Hz, 1H), 8.15 (d, *J* = 8.71 Hz, 2H), 8.32 (d, *J* = 8.76 Hz, 2H), 9.82 (s, 1H, CONH). ^{13}C-NMR (DMSO-d$_6$): δ = 56.19 (OCH$_3$), 112.07 (CH), 120.70 (CH), 124.08 (CH), 125.54 (CH), 126.74 (C), 126.93 (CH), 129.61 (CH), 140.73 (C), 149.64 (C), 152. 47 (C), 164.12 (C). HRMS (EIMS) *m/z*: calcd. for $C_{14}H_{11}N_2O_4$ [M - H]$^+$ 271.07188, found 271.07243. Anal. Calcd. for $C_{14}H_{12}N_2O_4$: C, 61.76; H, 4.44; N, 10.29, O, 23.51. Found: C, 60.79; H, 4.22; N, 10.07%.

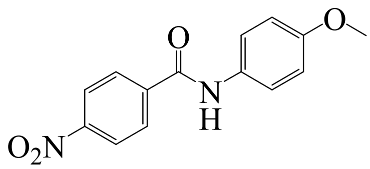
N-(4-Methoxy-phenyl)-3-nitro-benzamide (161)



This compound was prepared from *m*-nitrobenzoyl chloride (3.66 g, 20 mmol) and 4-methoxyaniline (1.2 g, 10 mmol) to yield **161** as white crystals (2.01 g, 77.96%); Mp 175-179 ^{o}C (Lit. 200 ^{o}C). IR (KBr): ν_{max} = 3300, 1670, 1520 cm^{-1}, ^{1}H-NMR (DMSO-d$_6$): δ = 3.72 (s, 3H, OCH$_3$), 6.92 (d, *J* = 8.98 Hz, 2H), 7.65 (d, *J* = 8.96 Hz, 2H), 7.80 (t, 1H), 8.39 (dd, J_1 = 7.78, J_2 = 2.18 Hz, 2H), 8.75 (s, 1H), 10.44 (s, 1H, CONH). ^{13}C-NMR (DMSO-

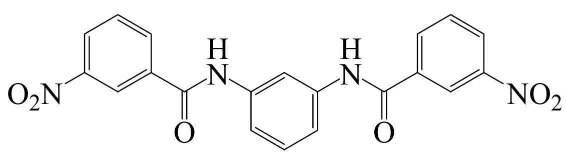
d6): δ = 55.69 (OCH_3), 114.33 (CH), 122.69 (CH), 122.80 (CH), 126.51 (CH), 130.66 (CH), 132.19 (C), 134.56 (CH), 136.87 (C), 148.25 (C), 156.37 (C), 163.36 (C). HRMS (EIMS) *m/z*: calcd. for $C_{14}H_{11}N_2O_4$ $[M-H]^+$ 271.07188, found 271.07243. Anal. Calcd. for $C_{14}H_{12}N_2O_4$: C, 61.76; H, 4.44; N, 10.29, O, 23.51. Found: C, 60.59; H, 4.22; N, 10.14%

N-(4-Methoxy-phenyl)-4-nitro-benzamide (162)



This compound was prepared from *p*-nitrobenzoyl chloride (3.66 g, 20 mmol) and 4-methoxyaniline (1.2 g, 10 mmol) to yield **162** as yellow crystals (1.98g, 74.21%); Mp 185-192 ^oC (Lit. 173). IR (KBr): ν_{max} = 3280, 1660, 1620, 1540, 1520 cm^{-1}, ^1H-NMR (DMSO-d6): δ = 3.72 (s, 3H, OCH_3), 6.91 (m, 2H), 7.63 (d, *J* = 7.64 Hz, 2H), 8.14 (d, *J* = 8.73 Hz, 2H), 7.68 (d, *J* = 8.73 Hz, 1H), 8.15 (d, *J* = 8.71 Hz, 2H), 8.32 (d, *J* = 8.76 Hz, 2H), 9.82 (s, 1H, CONH). ^{13}C-NMR (DMSO-d6): δ = 55.74 (OCH_3), 114.37 (CH), 122.63 (CH), 123.99 (CH), 129.58 (CH), 132.26 (C), 141.25 (C), 149.50 (C), 156.45 (C), 163.59 (C), 152. 47(C), 164.12 (C). HRMS (EIMS) *m/z*: calcd. for $C_{14}H_{11}N_2O_4$ $[M - H]^+$ 271.07188, found 271.07243. Anal. Calcd. for $C_{14}H_{12}N_2O_4$: C, 61.03; H, 4.44; N, 10.29, O, 23.51. Found: C, 61.03; H, 4.32; N, 10.16%

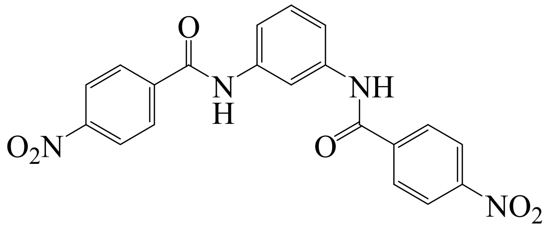
Bis-3-Nitro-N-phenyl-benzamide (163)



This compound was prepared from *m*-nitrobenzoyl chloride (7.32 g, 40 mmol) and 1,3-phenylene diamine (1.05 g, 10 mmol) to yield **163** as white crystal (0.37 g, 9.3%); mp 245-

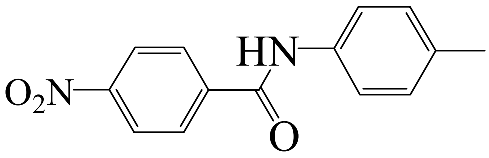
250^{o}C; IR (KBr): ν_{max} = 3350, 1680, 1550, 1510 cm^{-1}, ^{1}H-NMR (DMSO-d_6): δ = 7.35 (t, *J* = 8.45, 1H), 7.52 (dd, J_1 = 1.91, J_2 = 1.76 Hz, 2H), 7.81 (t, *J* = 7.98, 2H), 8.38 (m, 5H), 8.78 (t, *J* = 1.89, 2H), 10.65 (s, 2H, CONH); ^{13}C-NMR (DMSO-d_6): δ = 113.52 (CH), 117.03 (CH), 122.99 (CH), 126.70 (CH), 129.34 (CH), 130.69 (CH), 134.75 (CH), 136.76 (C), 139.49 (C), 148.25 (C), 163.91 (C). HRMS (EIMS) *m/z*: calcd. for $C_{20}H_{13}N_4O_6$ [M - H]$^{+}$ 405.08351, found 405.08406. Anal. Calcd for $C_{20}H_{14}N_4O_6$: C: 59.12, H: 3.47, N: 13.79 found: C: 57.67, H: 3.32, N: 13.02.

Bis-4-Nitro-N-phenyl-benzamide (164)



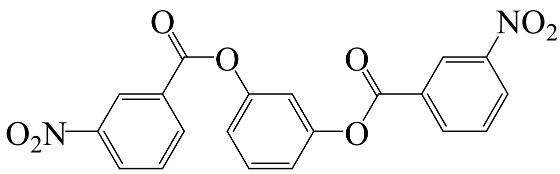
This compound was prepared from *p*-nitrobenzoyl chloride (7.32 g, 40 mmol) and 1,3-phenylene diamine (1.05 g, 10 mmol) to yield **164** as white crystal (0.9 g, 15%); mp 218-222^{o}C; IR (KBr): ν_{max} = 3315, 1660, 1620-1580, 1520-1510 cm^{-1}, ^{1}H-NMR (DMSO-d_6): δ = 7.34 (t, *J* = 8.09 Hz,1H), 7.50 (d, *J* = 7.93 Hz, 2H), 8.16 (d, *J* = 8.13Hz, 4H), 8.34 (d, *J* = 7.55 Hz, 5H), 10.62 (s, 2H, CONH). ^{13}C-NMR (DMSO-d_6): δ = 113.34 (CH), 116.97 (CH), 124.04 (CH), 129.36 (CH), 129.77 (CH), 139.50 (C), 141.09 (C), 149.67 (C), 164.47 (C). HRMS (EIMS) *m/z*: calcd. for $C_{20}H_{14}N_4NaO_6$ [M + Na]$^{+}$ 429.08110, found 429.08056. Anal. Calcd for $C_{20}H_{14}N_4O_6$: C: 59.12, H: 3.47, N: 13.79 found: C: 59.87, H: 3.68, N: 14.00.

4-Nitro-N-*p*-tolyl-benzamide (166)



This compound was prepared from *p*-nitrobenzoyl chloride (3.66 g, 20 mmol) 4-methylaniline (1.2 g, 10 mmol) to yield **166** as yellow crystal (2.13 g, 79%); mp 182-184 ^oC; IR (KBr): ν_{max} = 3320, 1660, 1590, 1540 cm^{-1}, ^1H-NMR (DMSO-d_6): δ = 2.22 (s, 3H, CH_3), δ = 7.23 (m, 4H), 8.17 (d, J = 8.71 Hz, 2H), 8.34 (d, J = 8.85 Hz, 2H), 10.19 (s, 1H, CONH). ^{13}C-NMR (DMSO-d_6): δ = 18.37 (CH_3), 124.11 (CH), 126.61 (CH), 126.89 (CH), 127.09 (CH), 129.66(CH), 130.92(CH), 134.27 (C), 136.37 (C), 140.74 (C), 149.68 (C), 164.27 (C). ^{13}C NMR (75 MHz, DMSO-d6): δ = 55.68 (CH_3), 114.32 (CH), 122.55 (CH), 124.04 (CH), 129.59 (CH), 132.22 (C), 141.19 (C), 149.53 (C), 156.35 (C), 163.87 (CO) ppm. HRMS-FAB m/z $[M + H]^+$ calcd for $C_{14}H_{11}N_2O_3$: 255.07697 found 255.07752. Anal. Calcd for $C_{14}H_{12}N_2O_3$: C: 65.62, H: 4.72, N: 10.93 found: C: 64.93, H: 4.467, N: 10.709.

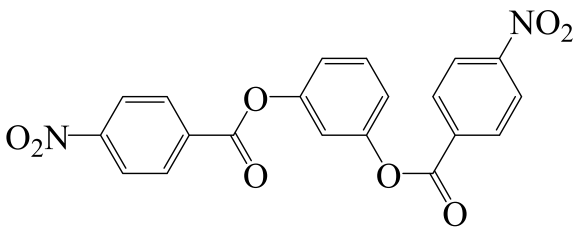
1,3-phenylene bis(3-nitrobenzoate) (167)



This compound was prepared from *m*-nitrobenzoyl chloride (7.32 g, 40 mmol) and resorcinol (1.07 g, 10 mmol) to yield **167** as white crystal (1.1 g, 27%); mp 102-107 ^oC; IR (KBr): ν_{max} = 1740, 1500 cm^{-1}, ^1H-NMR (DMSO-d_6): δ = 7.35 (t, J = 8.45, 1H), 7.52 (dd, J_1 = 1.91, J_2 = 1.76 Hz, 2H), 7.81 (t, J = 7.98, 2H), 8.38 (m, 5H), 8.78 (t, J = 1.89, 2H), 10.65 (s, 2H). ^{13}C NMR (75 MHz, DMSO-d6): δ = 117.76 (CH), 122.57 (CH), 122.838

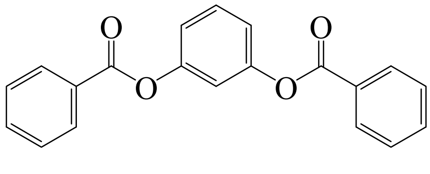
(CH), 123.57 (CH), 130.35 (CH), 132.06 (CH), 132.56 (CH), 134.35 (CH), 135.39 (CH), 148.36 (C), 149.23 (C), 170.00 (C=O) ppm. Anal. Calcd for $C_{20}H_{11}N_2O_{8.}$ H_2O: C: 56.34, H: 3.31 N: 6.57 found: C: 56.34, H: 3.31, N: 6.85.

1,3-phenylene bis(4-nitrobenzoate) (168)



This compound was prepared from *p*-nitrobenzoyl chloride (7.32 g, 40 mmol) and resorcinol (1.07 g, 10 mmol) to yield **168** as white crystal (0.98 g, 22%); mp 184-187 ^oC; IR (KBr): ν_{max} = 1620, 1540-1520 cm^{-1}, ^1H NMR (300 MHz, DMSO-d6): δ = 7.3 (m, 1H), 7.4 (t, 1H), 7.5-7.6 (t, 1H), 8.3-8.4 (m, 9H) ppm.; ^{13}C NMR (75 MHz, DMSO-d6): δ = 116.53 (CH), 120.40 (CH), 124.49 (CH), 130.80 (CH), 131.82 (CH) ppm. Anal. Calcd for $C_{20}H_{11}N_2O_{8.}$ H_2O: C: 58.83, H: 2.96 N: 6.86 found: C: 57.72, H: 3.42, N: 6.85.

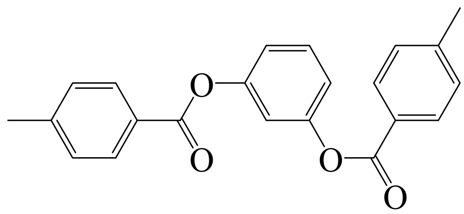
1,3-phenylene-bis-benzoate (169)



This compound was prepared from benzoyl chloride (7.32 g, 40 mmol) and resorcinol (1.07 g, 10 mmol) to yield **169** as white crystal (2.2 g, 61.78%); mp 122-1324 ^oC (Lit 117 ^oC);IR (KBr): ν_{max} = 1740 cm^{-1}, ^1H NMR (300 MHz, DMSO-d6): δ = 7.25 (d, J_1= 1.33 , J_2= 6.87 Hz, 2H), 7.33 (s, 1H), 7.55 (m, 5H), 7.73 (t, J_1= 7.0 , J_2= 7.1 Hz, 2H), 8.10 (d, J= 7.9 Hz, 4H) ppm.; ^{13}C NMR (75 MHz, DMSO-d6): δ = 116.80 (CH), 120.28 (CH), 129.21

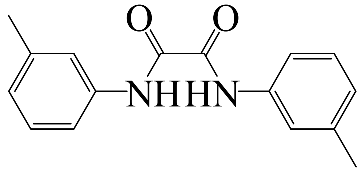
(C), 129.53 (CH), 130.35 (CH), 130.63 (C), 134.69 (CH), 151.62 (CH), 164.89 (C=O) ppm. HRMS-FAB m/z $[M + Na]^+$ calcd for $C_{20}H_{14}NaO_4$.: 341.07898, found: 341.07843. Anal. Calcd for $C_{20}H_{14}O_4$: C: 75.46, H: 4.43 found: C: 73.83, H: 4.35.

1,3-phenylene-bis-(4-methylbenzoate) (170)



This compound was prepared from *p*-methylbenzoyl chloride (7.32 g, 40 mmol) and resorcinol (1.07 g, 10 mmol) to yield **170** as white crystal (2.4 g, 67.41%); mp 125-130 °C; IR (KBr): ν_{max} = 1740, 1520 cm^{-1}, ^{1}H NMR (300 MHz, DMSO-d6): δ = 7.19-7.27 (m, 1H), 7.33-7.40 (m, 2H), 7.4 (m, 1H), 7.49-7.54 (t, 1H), 7.96-8.00 (m, 1H) ppm.; ^{13}C NMR (75 MHz, DMSO-d6): δ = 117.76 (CH), 122.57 (CH), 122.838 (CH), 123.57 (CH), 130.35 (CH), 132.06 (CH), 132.56 (CH), 134.35 (CH), 135.39 (CH), 148.36 (C), 149.23 (C), 170.00 (C=O) ppm. HRMS-FAB m/z $[M + Na]^+$ calcd for $C_{22}H_{18}NaO_4$.: 369.11028, found: 369.10973. Anal. Calcd for $C_{22}H_{18}O_4$: C: 76.29, H: 5.24 found: C: 78.16, H: 5.22.

N,N'-Di-*m*-tolyl-oxalamide (171)

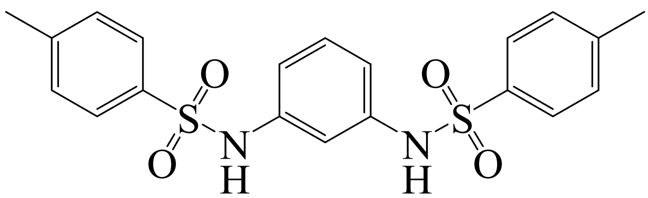


This compound was prepared from oxalyl chloride (1.27 g, 10 mmol) and 3-methylaniline (1.2 g, 10 mmol) to yield **171** as white crystals (1.51 g, 56.34%); Mp 253-266°C. IR (KBr): ν_{max} = 1700, 1540 cm^{-1}, ^{1}H-NMR (DMSO-d$_6$): δ = 2.25 (s, 6H, CH_3), 6.95 (d, J = 7.49 Hz,

2H), 7.22 (t, 2H), 7.62 (dd, J_1 = 7.78, J_2 = 1.80 Hz, 4H), 10.66 (s, 2H, CONH). ;^{13}C-NMR (DMSO-d_6): δ = 21.71 (CH_3), 118.13 (CH), 121.46 (CH), 125.83 (CH), 129.08 (CH), 138.03 (C), 138.46 (C), 159.08 (C=O). Anal. Calcd. for $C_{16}H_{16}N_2O_2$: C, 71.62; H,6.01; N, 10.44, Found: C, 68.95; H, 5.67; N, 9.94%

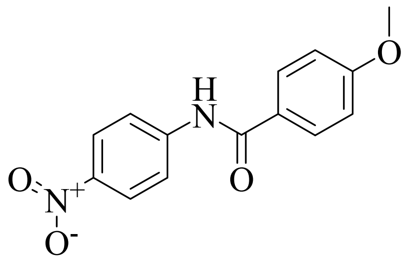
The following compounds were synthesized by Scheme 2:

4-Methyl-N-3-Amino-bisbenzenesulfonamide (165)



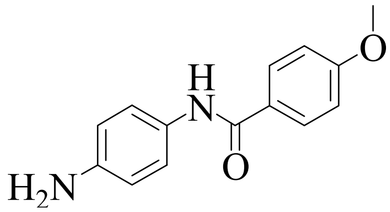
This compound was prepared from *p*-toluenesulfonyl chloride (4 g, 20 mmol) and 1,3-phenylene diamine (1.05 g, 10 mmol) to yield **165** as white crystal (1.2 g, 32%); mp decomposes at 150 °C (Let 133-134°C); IR (KBr): ν_{max} = 3340, 1590-1570, 1540-1520 cm^{-1}, ^{1}H NMR (300 MHz, DMSO-d6): δ = 2.3 (s, 6H), 6.6 (dd, J_1=2.02, J_2= 2.02 Hz, 2H), 6.9 (t, *J*=8.11 Hz, 1H), 7.0 (t, *J*=1.94 Hz, 1H), 7.2 (d, *J* = 8.17 Hz, 4H), 7.55 (m, *J* = 8.26 Hz, 4H), 10.1 (s, 2H, CONH) ppm.;^{13}C NMR (75 MHz, DMSO-d6): δ = 21.46 (CH_3), 117.83 (CH), 115.28 (CH), 127.19 (CH), 130.09 (CH), 130.17 (CH), 137.01 (C), 139.08 (C), 143.73 (C) ppm. HRMS-FAB m/z $[M + H]^+$ calcd for $C_{20}H_{19}N_2O_4S_2$: 415.07862 found 415.07917. Anal. Calcd for $C_{20}H_{20}N_2O_4S_2$: C: 57.67, H: 4.84, N: 6.73 found: C: 56.63, H: 4.641, N: 6.37.

4-Methoxy-N-(4-nitro-phenyl)-benzamide (172-a)



172-a

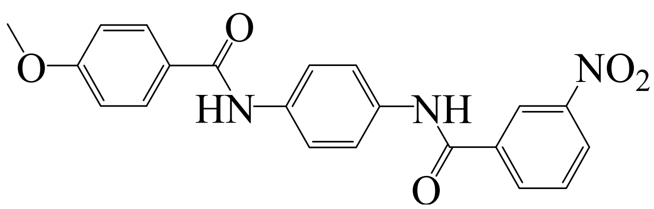
This compound was prepared from *p*-methoxy-benzoyl chloride (8.3 g, 50 mmol) and 4-nitroaniline (4.5 g, 30 mmol) to yield **172-a** as white crystal (6.3 g, 71%); HRMS (EIMS) *m/z*: calcd. for $C_{14}H_{11}N_2O_4$ $[M + H]^+$ 271.07188, found 271.07243.



172-b

This compound was prepared from reduction of **172-a** (2.1 g) by $SnCl_2$ (5 g) in acidic conditions to yield **172-b** as white-pinkish crystal (1.87 g, 82%); ^{1}H-NMR ($CDCl_3$): δ = 3.80 (s, 3H, OCH_3), δ = 4.87 (s, 2H, NH_2), 6.50 (d, J = 8.55 Hz, 2H), 6.98 (d, J = 8.60 Hz, 2H), 7.31 (d, J = 8.35 Hz, 2H), 8.87 (d, J = 8.58 Hz, 2H), 9.69 (s, 1H, CONH). ^{13}C-NMR ($CDCl_3$): δ = 55.85 (OCH_3), 113.96 (CH), 114.16 (CH), 122.78 (CH), 127.83 (C), 128.71(C), 129.76 (C), 145.54 (C), 162.01 (C), 164.62 (C). HRMS (EIMS) *m/z*: calcd. for $C_{14}H_{14}N_7NaO_2$ $[M + Na]^+$ 265.09530, found 265.09475.

N-(4-(4-methoxybenzamido)phenyl)-3-nitrobenzamide (172)

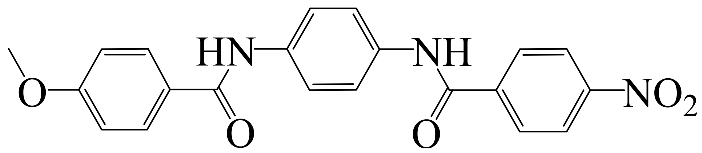


172

This compound was prepared from **172-b** (0.7 g, 3 mmol) and *m*-nitrobenzoyl chloride (1 g, 5 mmol) to yield **172** as yellow crystal (0.98 g, 86%); mp 296-297^{o}C.; IR (KBr): ν_{max} = 3350, 1622-1605, 1535-1500 cm^{-1}; ^{1}H-NMR ($CDCl_3$): δ = 3.81 (s, 3H, OCH_3), 7.03 (d, J =

8.88 Hz, 2H), 7.69-7.76 (m, 4H), 7.81 (t, J = 8.00 Hz, 1H), 7.94 (d, J = 8.85 Hz, 2H), 8.40 (dd, J_1 = 7.76, J_2 = 7.80 Hz, 2H), 8.76 (s, 1H), 10.08 (s, 1H, CONH), 10.54 (s, 1H, CONH). ^{13}C-NMR ($CDCl_3$): δ = 55.93 (OCH_3), 114.05 (CH), 121.07 (CH), 121.31 (CH), 122.82 (CH), 126.56(CH), 127.44 (C), 130.04 (CH), 130.70 (CH), 134.67 (CH), 136.09 (C), 136.83 (C), 148.27 (C), 162.36 (C), 163.55 (C), 165.22 (C). HRMS (EIMS) *m/z*: calcd. for $C_{21}H_{17}N_3NaO_5$ $[M + Na]^+$ 414.10659, found 414.10604. Anal. Calcd for $C_{21}H_{17}N_3O_5$: C: 64.45, H: 4.38, N: 10.74 found: C: 62.32, H: 3.64, N: 9.38

4-methoxy-N-(4-(-nitrobenzamido)phenyl)benzamide (173)



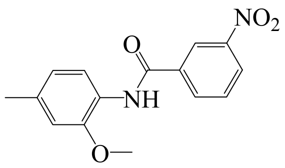
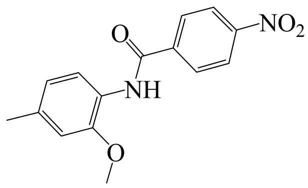
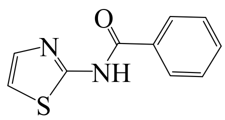
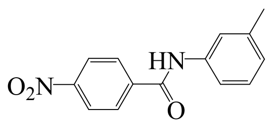
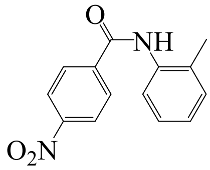
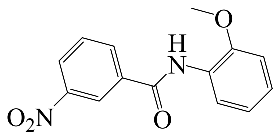
173

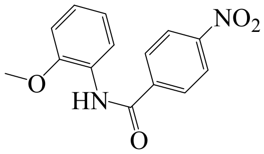
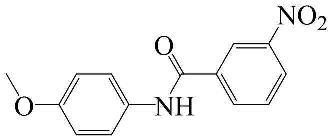
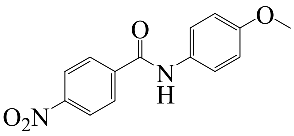
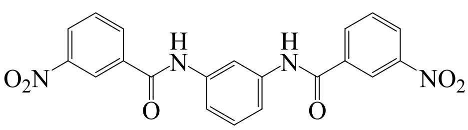
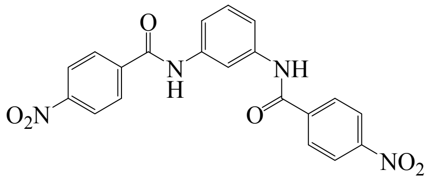
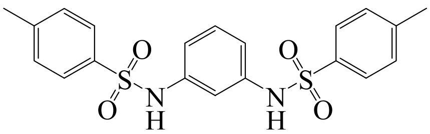
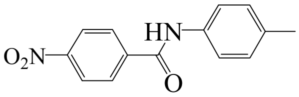
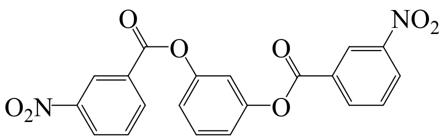
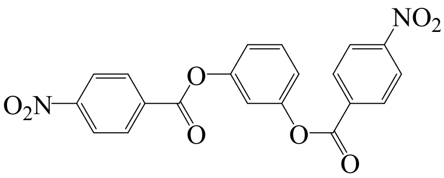
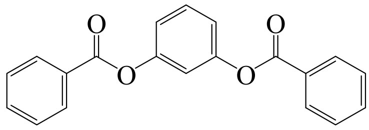
This compound was prepared from **172-b** (0.7 g, 3 mmol) and *p*-nitrobenzoyl chloride (1 g, 5 mmol) to yield **173** as white crystal (0.56 g, 50%); Mp 345-347 ^{o}C, IR (KBr): ν_{max} = 3280, 1660-1650, 1540-1520 cm^{-1} ; ^{1}H-NMR ($CDCl_3$): δ = 3.81 (s, 3H, OCH_3), 7.03 (d, J = 8.36 Hz, 2H), 7.69-7.75 (m, 4H), 7.93 (d, J = 8.06 Hz, 2H), 8.16 (d, J = 8.30 Hz, 2H), 8.34 (d, J = 8.340 Hz, 2H), 10.08 (s, 1H, CONH), 10.52 (s, 1H, CONH). ^{13}C-NMR ($CDCl_3$): δ = 55.93 (OCH_3), 114.10 (CH), 121.12 (CH), 121.26 (CH), 124.06 (CH), 127.44 (C), 129.66 (CH), 130.04 (CH), 134.73 (C), 136.11 (C), 141.16 (C), 149.60 (C), 162.37 (C), 164.09 (C), 165.21 (C). HRMS (EIMS) *m/z*: calcd. for $C_{21}H_{17}N_3NaO_5$ $[M + Na]^+$ 414.10659, found 414.10604. Anal. Calcd for $C_{21}H_{17}N_3O_5$: C: 64.45, H: 4.38, N: 10.74 found: C: 63.08, H: 3.81, N: 10.21.

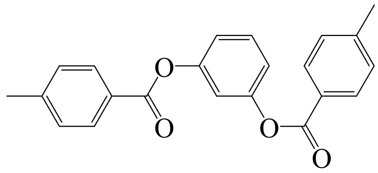
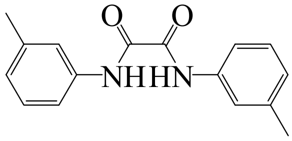
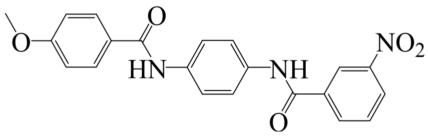
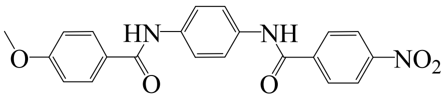
3.8 Bioassy results for synthesized FBPase inhibitors

The synthesized compounds were bioassayed employing coupled enzyme assay. Table 11 shows the prepared compounds and their corresponding experimental bioactivities.

Table 11: Experimental bioactivities of high-ranking synthetic molecules

Compound	Compound[a]	Best Fit values[b,c]		Experimental IC_{50} [d,e,f]
		Hypo1/7	Hypo2-1/2-6	
154		5.27	5.31	NA[g]
155		5.36	5.87	NA[g]
156		4.59	0.00	3.16 mM (0.99)
157		4.42	2.93	70.57 μM (0.86)
158		5.61	5.03	NA[g]
159		5.57	5.45	500 μM (0.92)

Compound	Compound[a]	Best Fit values[b,c]		Experimental IC_{50} [d,e,f]
		Hypo1/7	Hypo2-1/2-6	
160		`5.11	5.83	NA[g]
161		4.52	5.51	500 μM (0.92)
162		4.68	3.13	NA[g]
163		5.13	8.57	NA[g]
164		3.80	6.62	1.16 μM (0.99)
165		5.21	7.91	34.9 μM (0.97)
166		4.24	1.60	NA[g]
167		5.21	8.71	1.12 mM (0.99)
168		4.88	7.27	29.6 mM (0.93)
169		4.88	5.90	NA[g]

Compound	Compound[a]	Best Fit values[b,c]		Experimental IC_{50} [d,e,f]
		Hypo1/7	Hypo2-1/2-6	
170		5.46	7.52	NA[g]
171		3.77	0.00	NA[g]
172		5.13	6.48	NA[g]
173		4.65	3.62	NA[g]

[a]Chemical structures of synthetic molecules. [b]Fit values calculated against respective hypotheses using equation (D, [c]Experimental IC_{50} values determined at 10, 1, and 0.1 μM inhibitor concentrations, [d]Values in brackets represent the correlation coefficients of the corresponding dose-response curve, [e]dose-response data were against linear function. [f]Fitting was performed using Graph Pad Prism (version5.04) via fitting against sigmoidal dose-inhibition model, [g]not active (NA),

Figure 10 shows the dose-response curves of synthetic derivatives.

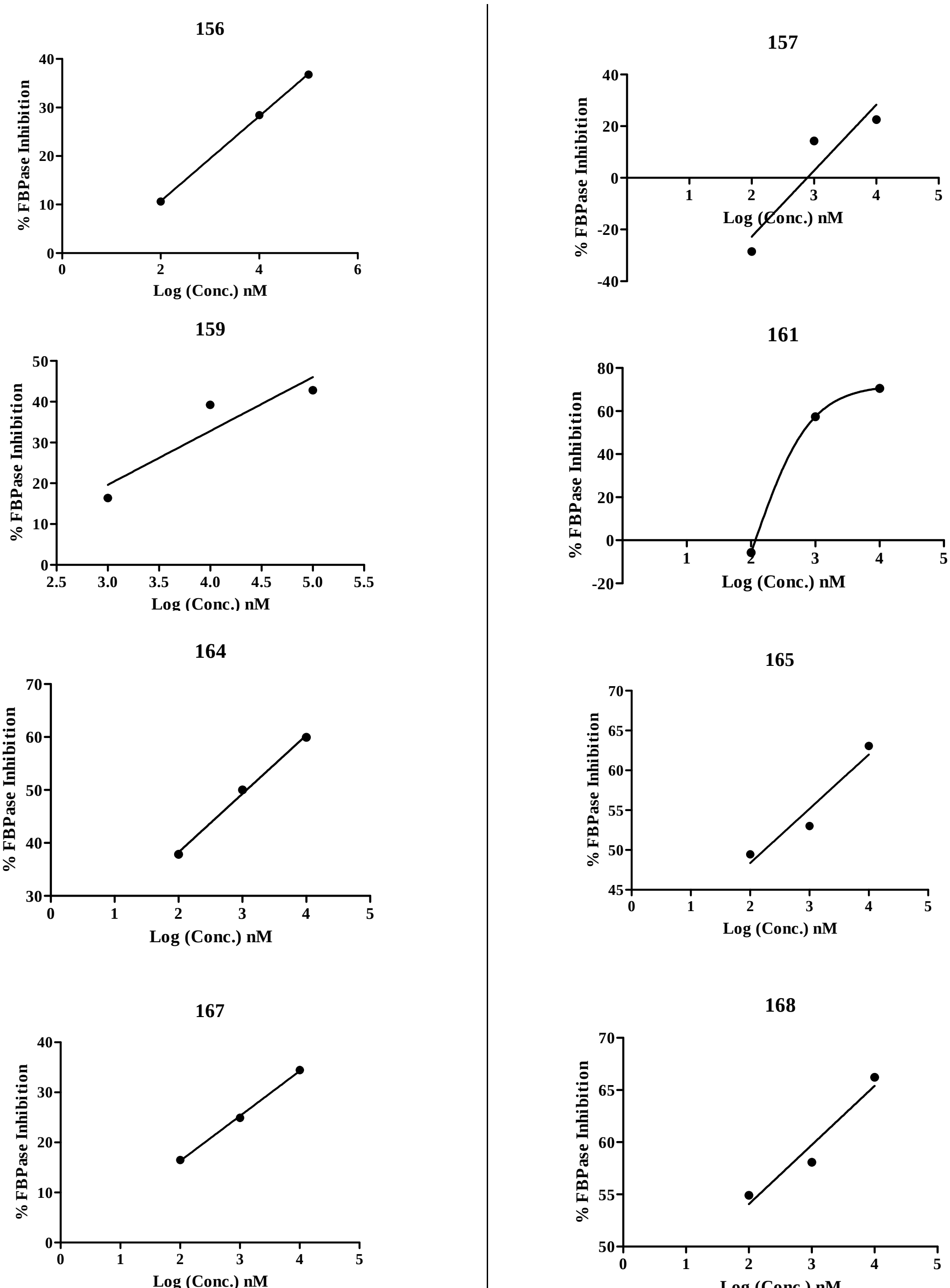


Figure 10: Dose-response plots of synthetic molecules: **156**, **157**, **159**, **161**, **164**, **165**, **167** and **168**. Data fitting was performed using GraphPad Prism (version 5.04) via fitting against linear and sigmoidal dose-inhibition model.

4. Conclusions

FBPase inhibitors are currently considered as potential treatments for diabetes. Recently, a potent derivative was reported to attenuate hyperglycemia in Zucker diabetic fatty rats (van Poelje *et al.*, 2007). The pharmacophoric space of FBPase inhibitors was explored via three diverse sets of inhibitors and using CATALYST-HYPOGEN to identify high quality binding model(s). Two orthogonal pharmacophoric models suggest the existence of at least two distinct binding modes accessible to ligands within FBPase binding pocket The selected pharmacophoric models were experimentally validated by the identification of several FBPase inhibitors retrieved via *in silico* screening. Synthetic modification guided by pharmacophoric features revealed new active compounds, the most potent of them revealed submicromolar activity. Our results suggest that the combination of pharmacophoric exploration and ROC analyses can be useful tool for finding new diverse FBPase inhibitors.

5. Future work

1- Exploring more potent amides and sulfonamides as FBPase inhibitors.

2- Toxicological studies.

3- Human studies on the hits as potential hypoglycemic agents.

4- Screening and evaluation of other hits captured by the optimal pharmacophore.

REFERENCES

Al-Nadaf, A., Abu Sheikha, Gh., Taha, M. (2010). Elaborate ligand-based pharmacophore exploration and QSAR analysis guide the synthesis of novel pyridinium-based potent β-secretase inhibitory leads. **Bioorganic & Medicinal Chemistry**,18, 3088-3115.

Beeley, Nigel, R., Sage, C. (2003). GPCRs: An update on structural approaches to drug discovery. **Targets**, 2, 19-25

Bersuker, I., Bahçeci, S. and Boggs, J. (2000), In: Güner O. F. (Ed), **Pharmacophore Perception, Development, and Use in Drug Design**. (pp. 457-473), California: International University Line.

Catalyst, version 4.11 Users' Manual, Accelrys Software Inc., San Diego, 2005.

Clement, O., and Mehl, A. (2000), In: Güner O. F. (Ed), **Pharmacophore Perception, Development, and Use in Drug Design**. (pp. 71-84), California: International University Line.

Dang, Q., Kasibhatla, S., Reddy, K., Jiang, T., Reddy, M., Potter, S., Fujitaki, J., van Poelje, P., Huang, J., Lipscomb, W. and Erion, M. (2007), Discovery of potent and specific fructose-1,6-bisphosphatase inhibitors and a series of orally-bioavailable phosphoramidase-sensitive prodrugs for the treatment of type 2 diabetes. **Journal Of The American Chemical Society**, 129,50,15491-15502

Dang. Q., Kasibhatla, S., Xiao, W., Liu, Y., Dare, J., Taplin, F., Reddy, K., Scarlato, G., Gibson, T., van Poelje, P., Potter, S. and Erion, M. (2010), Fructose-1,6-bisphosphatase Inhibitors: Design, Synthesis, and Structure-Activity Relationship of a Series of Phosphonic Acid Containing Benzimidazoles that Function as 5 '-Adenosinemonophosphate (AMP) Mimics. **Journal Of Medicinal Chemistry**, 53,1, 441-451

Dang, Q., Reddy, K., Kasibthatla, S., Jiang, T., Taplin, F., Gibson, T., Potter, S., van Poelje, P., Reddy, m. and Erion, M. (2010) Discovery of Phosphonic Acid-Containing Desaminobenzimidazoles as Fructose 1,6-Bisphosphatase Inhibitors that are Suitable for Oral Delivery via Prodrugs. **Journal Diabetes & Metabolism**, 1, 105-109

DePristo, M., de Bakker, P. and Blundell, T. (2004), Heterogeneity and inaccuracy in protein structures solved by X-ray crystallography. **Structure**, 12, 831-838.

Fisher, R. (1966), **The Principle of Experimentation Illustrated by a Psycho-Physical ExpeHafner Publishing Co**, (8^{th} ed.). New York: Hafner Publishing.

Hengming K., Zhang Y., Lipscomb W. (1990). Crystal structure of fructose-1,6-bisphosphatase complexed with fructose 6-phosphate, AMP, and magnesium. **Biochemistry**, 87, 5243-5247

Heng, S., Harris, K. and Kantrowitz E. (2010), Designing inhibitors against fructose 1,6-bisphosphatase: Exploring natural products for novel inhibitor scaffolds**. European Journal Of Medicinal Chemistry**, 45, 4,1478-1484.

Irwin, J. and Shoichet, B. (2005), ZINC - A Free Database of Commercially Available Compounds for Virtual Screening. **Journal of Chemical Information and Computer Science**, 45, 177-182.

Iversen, L., Brzozowski, M., Hastrup, S., Hubbard, R., Kastrup. J., Larsen I., Naerum, L., Norskov-Lauridsen, L., Rasmussen, P., Thim, L., Wiberg, F. and Lundgren, K. (1997) Characterization of the allosteric binding pocket of human liver fructose- 1,6-bisphosphatase by protein crystallography and inhibitor activity studies. **Protein Sciences**, 6, 971-982.

Klebe, G. (2006). **Drug Discovery Today**, 11, 580.

Kurukulasuriya R., Link J., Madar D., Pei Z., Richards S., Rohde J., Souers A., Szczepankiewicz B. (2003), Potential Drug Targets and Progress Towards Pharmacologic Inhibition of Hepatic Glucose Production. **Current Medicinal Chemistry**, 10, 123-153

Lan, P., Xie, M., Yao, Y., Chen, W.N. and Chen W.M. (2010). 3D-QSAR studies and molecular docking on [5-(4-amino-1H-benzoimidazol-2-yl)-furan-2-yl]-phosphonic acid derivatives as fructose-1,6-biphophatase inhibitors. **Journal Of Computer-Aided Molecular Design.** 24**,** 12**,** 993-1008

Van Drie, J., (2003), Pharmacophore discovery-lessons learned, Current Pharmaceutical Design, 9, 1649–1664.

Rashid, N., Imanaka, H., Kanai T.; Fukui, T., Atomi, H. and Imanaka, T. (2002). A Novel Candidate for the True Fructose-1,6-bisphosphatase in Archaea. **Journal of Biological Chemistry**, 277, 34, 30649–30655

Sutter, J., Güner, O., Hoffmann, R., Li, H. and Waldman, M. (2000), In: Güner O. F. (Ed), **Pharmacophore Perception, Development, and Use in Drug Design.** (pp. 501-511), California: International University Line.

Shaikh, M., Mittal, A. and Bharatam, P. (2008), Design of fructose-2,6-bisphosphatase inhibitors: A novel virtual screening approach. **Journal Of Molecular Graphics & Modelling**, 26, 6, 900-906.

Steuber, H., Zentgraf, M., Gerlach, C., Sotriffer, C. A., Heine, A. and Klebe, G. (2006), Expect the Unexpected or Caveat for Drug Designers: Multiple Structure Determinations Using Aldose Reductase Crystals Treated under Varying Soaking and Co-crystallisation Conditions. **Molecular Biology**,363, 174-187.

Stubbs, M., Reyda, S., Dullweber, F., Moller, M., Klebe, G., Dorsch, D., Mederski, W. and Wurziger, H. (2002), pH-dependent binding modes observed in trypsin crystals: lessons for structure-based drug design, **Biochemistry (Chemical Biology)**,3, 246-249

Triballeau, N., Acher, F., Brabet, I., Pin, J-P. and Bertrand, H-O. (2005), Virtual Screening Workflow Development Guided by the "Receiver Operating Characteristic" Curve Approach. Application to High-Throughput Docking on Metabotropic Glutamate Receptor Subtype 4. **Journal of Medicinal Chemistry**, 48, 2534-2547.

Tsukada, T., Kanno, O., Yamane, T., Tanaka, J., Yoshida, T., Okuno, A,, Shiiki, T., Takahashi, M. and Nishi, T. (2010), Discovery of potent and orally active tricyclic-based FBPase inhibitors. **Bioorganic & Medicinal Chemistry**,18,14, 5346-5351.

Tsukada, T., Takahashi, M., Takemoto, T., Kanno, O., Yamane, T., Kawamura, S., Nishi, T. (2010). Structure-based drug design of tricyclic 8H-indeno[1,2-d][1,3]thiazoles as potent FBPase inhibitors. **Bioorganic & Medicinal Chemistry Letters**, 20, 3, 1004-1007

Tsukada, T., Tamaki, K., Tanaka, J., Takagi, T., Yoshida, T., Okuno, A., Shiiki, T., Takahashi, M. and Nishi, T. (2010), A prodrug approach towards the development of tricyclic-based FBPase inhibitors. **Bioorganic & Medicinal Chemistry Letters,** 20,9,2938-2941

Van Poelje, P., Potter, S., Topczewski, E., Linemeyer, D. and Erion, M. (2005). MB06322, a potent inhibitor of gluconeogenesis, attenuates hyperglycemia without causing weight gain or hypoglycemia in female zucker diabetic fatty rats. **Diabetes,** 54, A124-A124

van Poelje, P., Dang, Q. and Erion, M. (2007). Discovery of fructose-1,6-bisphosphatase inhibitors for the treatment of type 2 diabetes. **Current Opinion In Drug Discovery & Development**, 10, 4,430-437

Veber, D., Johnson, S., Cheng, H., Smith, B., Ward, K. and Kopple, K. (2002), Molecular properties that influence the oral bioavailability of drug candidates. **Journal of Medicinal Chemistry**, 45, 2615-2623.

Verdonk, M., Marcel L., Berdini, V., Hartshorn, M., Mooij, W., Murray, C., Taylor, R., and Watson, P. (2004), Virtual screening using protein- ligand docking: Avoiding artificial enrichment. **Journal of Chemical Information and Computer Science**, 44, 793-806.

Wright, S., Hageman, D., McClure, D., Carlo, A., Treadway, J., Mathiowetz, A., Withka, J., Bauer, P. (2001), Allosteric inhibition of fructose-1,6-bisphosphatase by anilinoquinazolines. **Bioorganic and Medicinal Chemistry Letters**,11, 17-21

Wright, S., Carlo, A., Carty, M., Danley, D., Hageman, D., Karam, G., Levy, C., Mansour, M., Mathiowetz, A., McClure, L., Nestor, N., McPherson, R., Pandit, J., Pustilnik, L., Schulte, G., Soeller, W., Treadway, J., Wang, I. and Bauer, P. (2002), Anilinoquinazoline inhibitors of fructose 1,6-bisphosphatase bind at a novel allosteric

site: Synthesis, in vitro characterization, and X-ray crystallography. **Journal of Medicinal Chemistry**, 45, 3865-3877

Wright, S., Carlo, a., Danley, D., Hageman, D., Karam, G., Mansour, M., McClure, L., Pandit, J., Schulte, G., Treadway, J., Wang, I., Bauer, P. (2003) 3-(2-Carboxy-ethyl)-4,6-dichloro-1H-indole-2-carboxylic Acid: An Allosteric Inhibitor of Fructose-1,6-bisphosphatase at the AMP Site, **Bioorganic and Medicinal Chemistry Letters** , 13, 2055–2058

Xie, Y., Zhou, Z., Zhang, G., Lu J. and Zhang, W. (2010), Fructose-1,6-Bisphosphatase Regulates Glucose-Stimulated Insulin Secretion of Mouse Pancreatic beta-Cells. **Endocrinology**, 151, 10, 4688-4695

اكتشاف وتحسين مثبطات جديدة للانزيم الناقل لجزئي الفوسفات لسكر الفركتوز كعوامل محتملة ضد السكري.

إعــداد
رباب فايز تيم

المــشــرف
الاستاذ الدكتور معتصم طه

المــشــرف المـشــارك
الاستاذ الدكتور محمد مبارك

ملـــخــص

لقد تم اثبات ارتباط مرض السكري بوجود خلل في الانزيم الناقل لجزئي الفوسفات لسكر الفركتوز (FBPase Fructose-1,6-Bisphosphatase) ، والذي استحثنا الى محاولة اكتشاف وتحسين مثبطات جديدة لهذا الانزيم. وحتى هذه النهاية استطعنا اكتشاف المساحة الحاملة للخواص الدوائية (الفارماكوفية) ل 136 مركب يعمل على تثبيط هذا الانزيم باستعمال ثلاثة مجموعات متنوعة من هذه المثبطات. لقد عمدت آلية هذا البحث الى بناء 520 حامل للخاصة الدوائية (فارماكوفور) واختزالها الى 104 مجموعة عنقودية ممثلة بمراكزها ليتم فيما بعد ربط العلاقة بينها وبين الفاعلية الحيوية الناشئة عن هذه المركبات المشكلة لكل مجموعة ، و بواسطة طريقة احصائية لأنتخاب الاداء وتمييزه (receiver operating characteristic) ، نتج عن هذه المعالجة الاحصائية انتخاب فرضيات لحوامل للخواص الدوائية (فارماكوفور) وهم:

- فرض7/1 (Hypo1/7): والذي تميز باحسن اداء مقترن مع قوة الفاعلية الحيوية
- وفرضين 1/2 و6/2 ،(Hypo2/1,Hypo2/6): واللذان تميزا بتشابه كبير في الملامح الخاصة بالشكل الفارماكوفوري والذي اوحى بامكانية دمج كلا الفرضيتين لينتج فرضية جديدة باداء محسن فرض 6-2/1/2 (Hypo2-1/2-6) .

لقد تم استخدام الفرضيتين فرض7/1 (Hypo1/7) وفرض6-2/1-2 المدمج (Hypo2-1/2-6) لمسح قاعدة البيانات الخاصة بالمعهد الوطني الامريكي للسرطان (NCI) وتمكنا من الحصول على 18 مركب يمتلك فاعلية لتثبط الانزيم الناقل لجزئي الفوسفات لسكر الفركتوز(FBPase Fructose-1,6-Bisphosphatase. وكان لهذا الفضل في الاسترشاد بتصنيع 20 مركب ، كان لدى مركب واحد منها فاعلية مضاهية لما تم الحصول عليه.